Stony Brook University

Detailed Heterogeneous Chemistry Implemented in a Particle-Resolved Aerosol Model

A Thesis Presented

by

Jan Christopher Kaiser

to

The Graduate School

in Partial Fulfillment of the

Requirements

for the Degree of

Master of Arts

in

Physics

Stony Brook University

August 2010

Stony Brook University

The Graduate School

Jan Christopher Kaiser

We, the thesis committee for the above candidate for the

Master of Arts degree, hereby recommend

acceptance of this thesis.

Daniel A. Knopf – Thesis Advisor
Assistant Professor, School of Marine and Atmospheric Sciences

Axel K. Drees – Chairperson of Defense
Professor, Department of Physics and Astronomy

Philip B. Allen
Professor, Department of Physics and Astronomy

Nicole Riemer
Assistant Professor, Atmospheric Science
Department of Atmospheric Sciences,
University of Illinois at Urbana-Champaign

This thesis is accepted by the Graduate School

Lawrence Martin

Dean of the Graduate School

Abstract of the Thesis

Detailed Heterogeneous Chemistry Implemented in a Particle-Resolved Aerosol Model

by

Jan Christopher Kaiser

Master of Arts

in

Physics

Stony Brook University

2010

In this study, heterogeneous chemical reactions between trace gases and atmospheric soot particles are investigated using a particle-resolved aerosol model. The model accounts for physical and chemical processes in the atmosphere that change both particulate and gas phase composition. Four reactive gases, namely the major atmospheric oxidants O_3, NO_2, OH, and NO_3, are considered to compete with non-reactive water vapor for active surface sites on the soot particles coated with polycyclic aromatic hydrocarbons (PAHs). For this purpose, the state-of-the-art particle-resolved aerosol model PartMC-MOSAIC (Particle Monte Carlo model, coupled to the MOdel for Simulating Aerosol Interactions and Chemistry) has been extended to include heterogeneous chemical kinetics based on the recently developed Pöschl-Rudich-Ammann (PRA) framework. PartMC-MOSAIC enables us to model continuous soot emissions with a realistic particle size distribution and to track each particle's composition individually over the course of a 24 hour simulation. The flux-based approach of the PRA framework accounts for dynamic changes in the uptake of gas species on particle surfaces, which are caused by changes of gas phase and particle composition and associated modification of surface properties. Thus, it is possible to assess in detail the effects of heterogeneous reactions between major atmospheric oxidants and PAH coated soot surfaces on gas

phase composition, on uptake kinetics, and on degradation of particle-bound PAHs in atmospherically relevant scenarios. In contrast to previous modeling results we find no significant impact of these reactions on gas phase composition, regardless of the magnitude of soot emissions. Reactive uptake of O_3 and NO_2 is found to decrease by several orders of magnitude in the first minute of a particle's atmospheric lifetime but to stay relatively constant thereafter. This is in agreement with the results of previous applications of the PRA framework and experimental data. In case of OH and NO_3, uptake coefficients vary with the degree of PAH degradation. They are higher than those for O_3 and NO_2 during day ($\sim 10^{-1}$ to $\sim 10^{-4}$ vs. $\sim 10^{-7}$ to $\sim 10^{-5}$), but may be significantly lower at night (as low as $\sim 10^{-9}$), when particle-bound PAHs are very efficiently depleted by reaction with NO_3. PAH lifetime is on the order of minutes during day, when it is determined mainly by O_3, which is about an order of magnitude lower than other laboratory and modeling studies suggested. During night, when NO_3 levels are high, the PAH coating is oxidized within seconds, in agreement with experimental results. This study is the first to assess heterogeneous kinetics in atmospheric systems employing a particle-resolved aerosol model, and the complexity of the considered scenarios exceeds that of previous laboratory experiments and modeling studies. The results presented here allow for a much improved evaluation of the role of soot, one of the most ubiquitous types of atmospheric particles, on atmospheric gas phase composition and of its impact on health related issues and climate.

Contents

List of Tables

List of Figures

Acknowledgments

First and foremost, I would like to thank Daniel A. Knopf and Nicole Riemer for friendly guidance, fruitful discussions, great patience, nearly 24/7 availability and especially for the encouragement in times when I learned about the tough sides of scientific work. You are demanding advisors but working with you has been a pleasant experience. The same is true for the entire Knopf group: You are very special people and I am happy that I met all of you.

I also want to express my gratitude to the Physics Department, especially to professors Axel K. Drees and Philip B. Allen for serving on my defense committee as well as to the graduate program director, Jacobus Verbaarschot, who made it possible for me to pursue this interdisciplinary project and to Pat Peiliker, the assistant director of the graduate program, for helping me to get all the paperwork and procedures straight.

On the personal side, I cannot say how grateful I am to my fiancée for letting me go and spend this enriching year in the United States while she had to stay behind and to my family and friends for supporting me in every way they could. Without your support I could not have done this!

1. Introduction

The Earth's atmosphere consists of several layers of which the lowest two, the *troposphere* and *stratosphere*, can be directly influenced by natural processes as well as human activities on the surface of the Earth. The troposphere has a height of about $10 - 15$ km and contains roughly 80% of the entire atmospheric mass. The stratosphere extends from the top of the troposphere to about 50 km. Both these layers are composed mainly of molecular nitrogen (N_2, 78% by volume) and molecular oxygen (O_2, 21%). However, the important players in terms of effects on human health and climate are particulate matter suspended in air (e.g., Pöschl, 2005; Finlayson-Pitts and Pitts, 1997), termed *aerosols*, and so-called *trace gases* (e.g., Bernstein et al., 2004; Finlayson-Pitts and Pitts, 1997), which make up only a minor fraction of the total atmospheric composition. Both these classes of constituents are constantly changing in composition and concentration due to physical factors such as radiation, winds, and cloud formation, as well as a vast array of interdependent chemical reactions. In this thesis the focus is on the interface and interactions between atmospheric particles and trace gases.

The term *photochemistry* broadly describes all the reactions triggered by sunlight and the species involved therein. Consider ozone (O_3), for example: it is a secondary pollutant, i.e., it is only produced *in situ* following photolysis of nitrogen dioxide (NO_2) and there are no direct emissions into the atmosphere. However, the gas is well-known for its adverse effects on human health at the comparatively high concentrations found in urban polluted areas (e.g., U.S. EPA, 2009b) that can reach peak values of $100 - 200$ ppb (parts per billion of air molecules) or more. Also, even in remote locations, O_3 exists in amounts of a few tens of ppb due to background concentrations and natural emissions of ozone precursor substances (Finlayson-Pitts and Pitts, 2000; Seinfeld and Pandis, 2006). O_3 reacts readily with other atmospheric species in a process called *oxidation* which, in the context of atmospheric chemistry, usually means the addition of oxygen atoms (e.g., Kanakidou et al., 2005). A detailed description of the O_3 photochemical cycle will be given in Chapter 2.

Particulate matter is emitted into the atmosphere by natural processes such as sandstorms, volcanic eruptions, and wave-breaking, and by human activities, e.g., in transportation and industry due to burning of fuels and biomass

and in agriculture due to the cultivation of land (Colbeck and Lazaridis, 2010). It can also be formed *in situ* through nucleation of low-vapor-pressure trace gases, i.e., transition to the condensed phase without the need for a pre-existing particle (Rudich, 2003; Kanakidou et al., 2005; Seinfeld and Pandis, 2006). Depending on their size, particles may affect human health upon inhalation (Finlayson-Pitts and Pitts, 2000; Colbeck and Lazaridis, 2010). For this reason the U.S. Environmental Protection Agency (EPA) has set standards for PM_{10} and $PM_{2.5}$, referring to particulate matter of sizes $\leq 10\,\mu$m and $\leq 2.5\,\mu$m, respectively (U.S. EPA, 2009a). Moreover, large uncertainties in determining changes of local, regional and global climate are due to aerosol particles (e.g., Ramanathan et al., 2001; Colbeck and Lazaridis, 2010). Absorption and scattering of solar and terrestrial radiation and their effects on the radiative budget are collectively called the direct (aerosol) effect. The indirect (aerosol) effect considers the ability of particles to act as cloud condensation nuclei (CCN) and ice nuclei (IN) whose concentrations determine cloud lifetimes, cloud reflectivities and the formation of precipitation. Clouds, in turn, can also absorb and irradiate energy. Thus, the influence of aerosols on global climate is very complex and among the least understood and least well-quantified contributions to climate change (Forster et al., 2007).

An ubiquitous type of aerosol particles is soot, the solid product of incomplete combustion of biomass and fossil fuels, e.g., emitted by diesel engines. Fresh diesel soot particles have sizes of only up to a few hundred nanometers (Homann, 1998; Seinfeld and Pandis, 2006) and can therefore penetrate deep into human lungs (Finlayson-Pitts and Pitts, 2000). The same processes in which soot particles are produced also generate a host of reactive organic gases some of which partition to a significant fraction to the condensed phase under atmospheric conditions and thus cover the particles' surfaces (e.g., Bedjanian et al., 2010). One important group of such species are *polycyclic aromatic hydrocarbons* (PAHs) such as pyrene or benzo[*a*]pyrene, the latter of which is known to be carcinogenic (Phillips, 1983). In the present study we simulate soot particles coated with a monolayer of condensed PAHs as an idealized model system of atmospheric soot aerosol.

Particle surfaces can serve as reaction sites for adsorbing gases, similar to catalysts (Finlayson-Pitts, 2009). They can also react with atmospheric oxidants such as the hydroxyl (OH) and nitrate (NO_3) radicals or O_3 (Rudich et al., 2007). These processes are subsumed under the term *heterogeneous chemistry* because the participating chemicals are in different phases. A well-known example is the formation of the Antarctic ozone hole. During Southern hemispheric winter heterogeneous reactions on the ice crystals of polar stratospheric clouds form species that lead to rapid depletion of ozone when the sun

rises again (Crutzen and Arnold, 1986; Solomon et al., 1986; Molina et al., 1987).

Heterogeneous reactions in the troposphere can influence the composition of aerosol particles, which affects their radiative properties and ability to act as CCN or IN (Rudich et al., 2007). Moreover, their toxicity can be changed, e.g., PAHs may become mutagenic upon oxidation by nitrogen containing compounds (Finlayson-Pitts and Pitts, 2000). Lastly, some studies indicated that trace gas concentrations may be significantly influenced by heterogeneous reactions (e.g., Arens et al., 2001; Evans and Jacob, 2005; Springmann et al., 2009).

Numerous laboratory studies have been carried out in order to quantify the impacts of the above named effects by determining reaction mechanisms and measuring physicochemical parameters (Rudich, 2003). Specific focus has been on organic compounds because they are known to have a significant influence on aerosol properties (Rudich et al., 2007) and make up $20 - 90\%$ of fine particulate mass in the atmosphere (Kanakidou et al., 2005). However, due to the sheer complexity of organic aerosol particle composition and interactions, they still remain poorly characterized (Andreae, 2009). Hence, many experimental and modeling studies use proxies to determine the implications of organic aerosols, e.g. benzo[a]pyrene as a representative for PAHs exposed to O_3 (Pöschl et al., 2001; Kwamena et al., 2004).

One of the most frequently reported quantities is the *uptake coefficient*, i.e., the ratio of net uptake to collision flux, for a specific gas on a surface of a specific chemical composition. Initial uptake coefficients can be close to unity, i.e., almost all colliding molecules are irreversibly taken up (e.g., the hydroxyl radical (OH) on a fresh soot surface (Bertram et al., 2001)). Recent modeling studies, however, have shown that uptake coefficients may drop by several orders of magnitude during the first day of a particle's atmospheric lifetime (Ammann and Pöschl, 2007; Springmann et al., 2009; Shiraiwa et al., 2009). Nonetheless, in large-scale models uptake coefficients are often assumed to be constant at their initial values, i.e., the removal of trace gases by uptake on particles is essentially treated as linearly proportional to the respective gas phase concentrations (Bey et al., 2001; Tie et al., 2001; Matthias et al., 2009) and may therefore be largely overestimated.

Recently, Pöschl, Rudich and Ammann developed a theoretical framework for gas-particle interactions, termed the PRA framework (Pöschl et al., 2007; Ammann and Pöschl, 2007). It is based on species fluxes and thus allows to treat all the processes involved in heterogeneous chemistry — adsorption, desorption, and surface reactions — dynamically, so that uptake coefficients can be diagnosed rather than used as input parameters. We implemented this

framework into PartMC-MOSAIC (Particle Monte Carlo (Riemer et al., 2009) and MOdel for Simulating Aerosol Interactions and Chemistry (Zaveri and Peters, 1999; Zaveri et al., 2005b,a, 2008)), a state-of-the-art particle-resolved aerosol model that includes 77 gas species plus water vapor and more than 100 chemical reactions. This allows us for the first time to model heterogeneous chemistry under consideration of continuous particulate emissions with realistic size distributions in an atmospherically relevant context. Our model particles react with all major atmospheric oxidants (OH, NO_3, O_3, and NO_2) which compete with nonreacting water vapor for reactive surface sites. Because of the single-particle resolution we are able to track surface composition, PAH half-life, and uptake coefficients for each modeled particle individually over the 24 hour period of our simulations. Hence, we can also average these quantities over the whole population of particles with different ages. Application of this method to different photochemical regimes and environmental conditions can improve the accuracy of parameterizations, e.g., for uptake coefficients or PAH oxidation state, used in large-scale models.

This thesis is structured as follows: the second chapter will provide an overview of the relevant aspects of photochemistry and particulate matter in the atmosphere. It also covers the description of heterogeneous chemistry within the PRA framework and describes previous modeling approaches. Chapter 3 describes our model system and introduces the various parts of the computer model we used. Results of the simulations are presented and discussed in Chapter 4. Subsequently, these results are summarized and implications of our findings discussed. A brief outlook on the direction of future research is given in the last chapter.

2. Background

This chapter introduces basic concepts concerning atmospheric chemistry and aerosols, and their representation in atmospheric models. It also provides an overview of the experimental studies that form the basis for our choice of parameters.

2.1 Atmospheric chemistry

2.1.1 Fundamentals of chemical kinetics

In general, chemical reactions between reagents A and B are represented in the form

$$a\,\mathrm{A} + b\,\mathrm{B} \xrightarrow{k} c\,\mathrm{C} + d\,\mathrm{D}\ , \tag{2.1}$$

where C and D represent reaction products and a, b, c, d are integer numbers, called stoichiometric coefficients. k, the proportionality factor between reaction rate and reagent concentrations (see, e.g., Eq. (2.6)), is called the rate constant but may depend on temperature. The most commonly used expression for its temperature dependence is the Arrhenius form

$$k = A \exp\left(-\frac{E}{k_B T}\right) \tag{2.2}$$

with a temperature-independent preexponential factor A describing the collision frequency between reagent molecules and a Boltzmann factor, i.e., an exponential function that measures the fraction of colliding molecules having enough thermal energy $k_B T$ to overcome the reaction energy barrier E. Often, k is omitted from the notation 2.1.

The number of reacting molecules in an elementary reaction can range from one to three and the number of products also varies. The probability for collisions of more than three molecules is essentially zero (Finlayson-Pitts and Pitts, 2000). Reactions involving one, two, and three reagent molecules are called first-, second-, and third-order reactions, respectively.

If the reagents are in different phases, i.e., in case of heterogeneous reactions, this is indicated in parentheses behind the chemical formulas of the

species. For instance,

$$\mathrm{A(g) + B(s) \rightarrow C(s)} \tag{2.3}$$

would indicate that species A is in the gas phase (g) whereas B and C are present as solids (s). Liquid reagents are designated by the letter 'l', or, if the respective molecule is dissolved in water by 'aq'.

Photolysis reactions are written

$$\mathrm{A + h\nu \xrightarrow{\mathit{j}} C + D} \tag{2.4}$$

and sometimes the threshold wavelength λ of the incident light necessary for photodissociation is given in parentheses. The rate j here includes radiation flux, the photolyzed molecule's absorption cross section, and quantum yield, i.e., the number of molecules of one product generated per collision of a photon with a reagent molecule.

Differential equations of the form

$$\frac{d[\mathrm{A}](t)}{dt} = -j[\mathrm{A}](t) \tag{2.5}$$

are used to describe loss rates in first-order reactions (e.g., radioactive decay or photolysis). Square brackets denote concentrations and may have an index (g, s) to distinguish between gas phase and surface concentrations. The time dependence of concentrations is usually assumed even if it is not explicitly written out as in Eq. (2.5), a convention we will also follow here unless stated otherwise. For second-order reactions the expression corresponding to Eq. 2.5 is

$$\frac{1}{a}\frac{d[\mathrm{A}]}{dt} = -k[\mathrm{A}]^a[\mathrm{B}]^b \,, \tag{2.6}$$

while for third-order reactions the concentration of the third reagent will also be included. Production rates of species generated in a reaction are written analogously.

The e-folding time τ, also termed *lifetime*, of a species against a specific reaction is defined as the time it takes for [A] to reach e^{-1} of its initial value if the species is only depleted by that reaction. In Eq. (2.5), the lifetime of A against the reaction that is described by rate coefficient j can be obtained by integration. It is the inverse of j because of the reaction's first-order nature. In case of second- or third-order reactions the lifetime will also depend on concentrations of the other reagents, e.g., for Eq. (2.6), if [B] is not a function of time and $a = b = 1$:

$$\tau = \frac{1}{k[\mathrm{B}]} \,. \tag{2.7}$$

The assumption $[\mathrm{B}] \neq [\mathrm{B}](t)$ is justified if $[\mathrm{B}] \gg [\mathrm{A}]$ and there is no other parallel process that significantly depletes [B]. In all other cases, τ will also depend on the precise evolution of [B]. As atmospherically relevant systems can contain hundreds of reactions going on in parallel one soon reaches the limit where analytic solutions can no longer be obtained and numerical integration schemes become necessary to find approximate solutions.

Sometimes, instead of lifetime, the so-called half-life of a species is reported. The concept is completely analogous to that of lifetime. Instead of e-folding time, the time required for halving the concentration is given.

In studies of heterogeneous chemistry (see Sect. 2.3) loss processes of a certain species are often described by their pseudo-first-order rate coefficients k'. Generally, in such a formulation, k' includes all concentrations of species involved in a reaction other than the one that is depleted. For example, if one was interested only in the loss of B in reaction 2.1, its pseudo-first-order decay rate coefficient would be

$$k' = k \cdot [\mathrm{A}] \,, \tag{2.8}$$

according to Eq. (2.6), and again under the assumption $a = b = 1$. Moreover, in heterogeneous reactions, a pseudo-first-order rate coefficient also contains information on the actual reaction mechanism as will be described in detail in Sect. 2.3.

From expressions (2.5) and (2.6) it is evident that reaction rate constants have different units for different orders of reactions. In atmospheric chemistry, it is common to use cm^{-3} as a unit for concentrations instead of the SI unit m^{-3} (or cm^{-2} instead of m^{-2} for surface concentrations when describing surface reactions which will be discussed later). Hence, reaction rates have units of s^{-1} in case of first-order reactions, $\mathrm{cm}^3\,\mathrm{s}^{-1}$ or $\mathrm{cm}^2\,\mathrm{s}^{-1}$ for second-order reactions and $\mathrm{cm}^6\,\mathrm{s}^{-1}$ or $\mathrm{cm}^4\,\mathrm{s}^{-1}$ for third-order reactions.

Note also that concentrations of atmospheric trace gases are often given in relative units, the most commonly used being ppm, ppb, and ppt. Usually, this is understood as the relative number concentration, or relative concentration by volume, compared to air. Sometimes an additional 'v' is appended, e.g., ppmv, to make a clear distinction between relative number concentration and relative mass concentration. To obtain a sense of orders of magnitude, consider the most abundant trace gas in the atmosphere, carbon dioxide (CO_2), with a global annual average concentration of currently 388 ppm (Dr. Pieter Tans, NOAA/ESRL (`www.esrl.noaa.gov/gmd/ccgg/trends`)), and the U.S. Environmental Protection Agency's air quality standard for O_3 which is 75 ppb for an eight-hour average and 120 ppb for a one-hour average (`http://www.epa.gov/air/criteria.html`).

2.1.2 Photochemistry

The term photochemistry is used to describe the branch of chemistry that deals with the effects of electromagnetic radiation on chemical reactions. In the atmosphere, this radiation includes visible and ultraviolet light that comes from the sun.

One of the most important photochemically generated species is O_3, a colorless gas that acts as an atmospheric oxidant and can cause inflammatory responses and decrements in lung function at elevated concentration levels in polluted regions (U.S. EPA, 2006). It is produced by photolysis of nitrogen dioxide (NO_2)

$$NO_2 + h\nu \rightarrow NO + O(^3P) \qquad (\lambda > 424 \text{ nm}) \tag{2.9}$$

forming nitric oxide (NO) and an oxygen atom in the ground state ($O(^3P)$) that subsequently reacts with O_2:

$$O(^3P) + O_2 + M \rightarrow O_3 + M\,. \tag{2.10}$$

M denotes a third body (mostly N_2 or O_2) that does not react chemically but absorbs excess energy and momentum to fulfill conservation laws. Most of the NO_2 in the troposphere comes from oxidation of NO. The major fraction of emissions of the latter is due to fossil fuel combustion (Müller, 1992; Tabor et al., 1994) which, e.g., in car and truck engines, generates sufficiently high temperatures to enable the reaction of N_2 and O_2 in the air-fuel mixture. Smaller amounts are also produced from nitrogen in the fuel. On the part of natural emissions the two significant sources are biomass burning and microbial conversion of nitrogen containing compounds. Average background NO_x ($= NO + NO_2$) concentrations in rural areas are on the order of 1 ppb or less (Parrish et al., 1990; Zhang et al., 2008) whereas in urban polluted environments they can reach peak values of 100 ppb or more (Pandey et al., 2008; Azri et al., 2009).

The produced ozone quickly oxidizes NO back to NO_2 by way of the reaction

$$O_3 + NO \rightarrow NO_2 + O_2 \tag{2.11}$$

creating a cycle of generation and depletion of O_3 that would eventually reach a stationary state if reactions (2.9) - (2.11) were the only ones in which atmospheric NO_2, NO, $O(^3P)$, and O_3 are involved. However, this cycle underpredicts O_3 concentrations, even in remote locations where anthropogenic influences are negligible. Reaction (2.10) is essentially the only O_3-producing

reaction in the atmosphere and there are no O_3 emission sources (Finlayson-Pitts and Pitts, 2000). Since there are also no other significant sources of $O(^3P)$ in the troposphere other than reaction (2.9), the explanation for higher $[O_3]$, especially in urban areas, has to be oxidation of NO by other pathways that do not deplete O_3.

The additional oxidation is mainly due to the presence of so-called volatile organic compounds (VOCs), i.e., gas phase hydrocarbons such as alkanes, alkenes, aldehydes, and aromatics. They are emitted by plants as well as during combustion of fossil fuels or other organic matter and their lifetime is determined by breakdown and oxidation, especially through interaction with the hydroxyl radical (OH) which is the strongest oxidizing agent in the atmosphere. It reacts with a VOC

$$\mathrm{VOC} + \mathrm{OH} \rightarrow \mathrm{R} + \mathrm{H_2O} \tag{2.12}$$

to form an alkyl radical (R) which is highly reactive and thus quickly binds an oxygen molecule, forming an alkyl peroxy radical (RO_2) which then oxidizes NO to NO_2 without consuming O_3:

$$\mathrm{R} + \mathrm{O_2} \rightarrow \mathrm{RO_2} \tag{2.13}$$

$$\mathrm{NO} + \mathrm{RO_2} \rightarrow \mathrm{NO_2} + \mathrm{RO}\ . \tag{2.14}$$

The NO_2 produced via this mechanism is then available to form additional O_3.

The alkoxy radical (RO) subsequently also reacts with an oxygen molecule to form a carbonyl ($R'CHO$) and a hydroperoxy radical (HO_2) which also oxidizes NO and thereby regenerates the OH initially consumed in reaction (2.12):

$$\mathrm{RO} + \mathrm{O_2} \rightarrow \mathrm{R'CHO} + \mathrm{HO_2} \tag{2.15}$$

$$\mathrm{NO} + \mathrm{HO_2} \rightarrow \mathrm{NO_2} + \mathrm{OH}\ . \tag{2.16}$$

OH is produced in the background atmosphere following photolysis of O_3 which can generate excited oxygen atoms ($O(^1D)$), some of which react with water vapor (H_2O) to form two OH radicals:

$$\mathrm{O_3} + \mathrm{h}\nu \rightarrow \mathrm{O_2} + \mathrm{O}(^1\mathrm{D}) \tag{2.17}$$

$$\mathrm{H_2O} + \mathrm{O}(^1\mathrm{D}) \rightarrow 2\mathrm{OH}\ . \tag{2.18}$$

In urban polluted air, however, several additional pathways involving photolysis of nitrous acid (HONO) and aldehydes contribute to OH formation. Many

of these precursor species originate as by-products of fossil fuel combustion. Typical daytime peak concentrations of OH in urban areas are $10^6 - 10^7\,\mathrm{cm}^{-3}$ (Emmerson et al., 2005; Dusanter et al., 2009), or about $0.04 - 0.4\,\mathrm{ppt}$. These values are very small in comparison to concentrations of most other important trace gases. They are due to the hydroxyl radical's extremely high reactivity and thus very short lifetime in the atmosphere on the order of seconds. Hence, despite this low concentration it is still one of the most important photochemical species.

Now we can put all the ingredients of urban photochemistry together to explain the typical diurnal $[O_3]$ cycle with its high peak values during the afternoon (Fig. 2.1). NO, HONO and aldehydes are emitted in significant amounts mainly by cars and trucks during heavy early-morning traffic. As soon as the sun rises, OH is formed by photochemical reactions and contributes to the oxidation of NO to NO_2. NO_2 is subsequently photolyzed, providing $O(^3P)$ atoms that combine with molecular O_2 to produce O_3 which usually reaches its peak concentration in the afternoon. When the sun sets and [NO] is sufficiently high, O_3 is depleted at night via reaction (2.11).

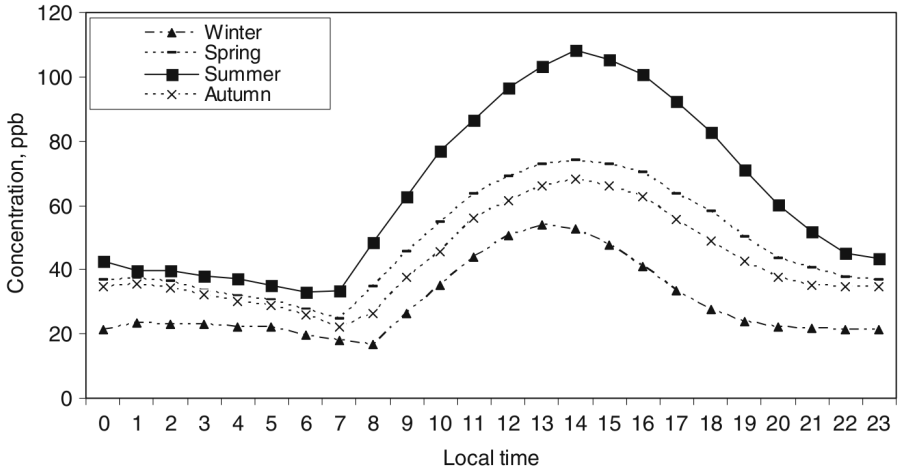

Figure 2.1: Typical diurnal cycle of O_3 concentration in an urban area, measured at a location in Giza, Egypt (taken from Khoder (2009)).

Note, however, that this chemistry-only explanation is strictly speaking only applicable to a plume that moves downwind from an urban center. Within the urban area itself turbulent mixing of the boundary layer, i.e., the lowest $1 - 3\,\mathrm{km}$ of the troposphere, with the residual layer above, must also be taken into account to explain peak O_3 concentrations (Vogel et al., 1994).

As OH also reacts with NO_2 to form nitric acid (HNO_3),

$$NO_2 + OH \rightarrow HNO_3 \ , \tag{2.19}$$

two basic regimes of the O_3 cycle exist, divided by a ratio of [VOC]:[NO_x] at which maximum O_3 production occurs. In the so-called VOC limited or *high NO_x regime*, i.e., if [VOC]:[NO_x] is smaller than the ratio of maximum O_3 production, reaction (2.19) is the main sink for OH. Hence, less NO is oxidized to NO_2 via the VOC pathway and O_3 production decreases if even more NO_x is added. Conversely, in the NO_x limited or *low NO_x regime*, O_3 production increases with increasing NO_x concentrations because more OH is produced by reaction (2.16). This behavior is illustrated in Fig. 2.2, a so-called O_3 isopleth plot.

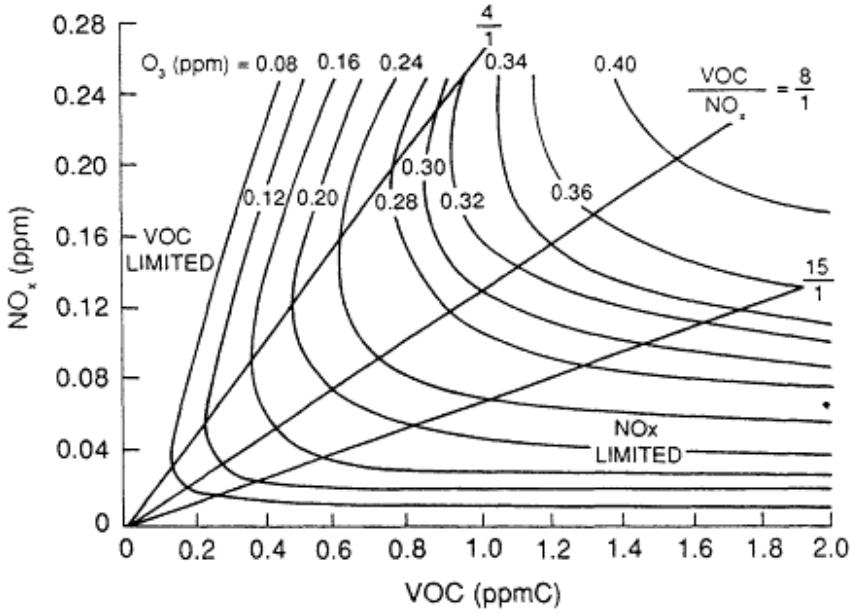

Figure 2.2: Peak [O_3] as contours (called isopleths) vs. [VOC] and [NO_x] (taken from National Research Council, Committee on Tropospheric Ozone (1991)). This plot shows the results of a box model calculation in which [VOC] and [NO_x] were kept constant. The notation "ppmC" means that the concentration of VOCs is measured by their constituent carbon atoms.

High levels of photochemical pollutant concentrations occur where emissions of NO_x and VOCs are high and mixing of the polluted air with the background troposphere is hindered. This is the case if a so-called inversion

layer is present, a layer of air in which the temperature does not decrease with increasing height, as it usually does within the troposphere, but rather increases with height. Such an inversion acts as a cap for the layer below, effectively forming a "reactor" whose effects on tropospheric composition can be further enhanced by orographic features such as mountains, e.g., around the Los Angeles basin. If such conditions coincide with fair weather, i.e., clear sky, sunshine, and high temperatures to fuel the photochemical reactions, and persist over several days, the associated episodes of very high pollutant concentrations are termed photochemical smog.

2.1.3 Nighttime chemistry

At night, OH is no longer regenerated due to the lack of sunlight. Because of its extremely high reactivity it is rapidly depleted and the nitrate radical (NO_3) takes over as the major atmospheric oxidant. NO_3 is formed through oxidation of NO_2 by O_3:

$$NO_2 + O_3 \rightarrow NO_3 + O_2 \ . \tag{2.20}$$

However, during day, NO_3 photodissociates very quickly so that it is only present in the atmosphere in significant amounts of a few tens to hundreds of ppt during night. In gas phase reactions it is considerably less reactive than OH, but its much greater abundance at nighttime has to be taken into account when considering its overall importance as an oxidant.

NO_3 also reacts with NO_2 to form dinitrogen pentoxide (N_2O_5):

$$NO_2 + NO_3 + M \leftrightarrow N_2O_5 + M \ . \tag{2.21}$$

N_2O_5 thermally decomposes back into those two species and an equilibrium is established on the order of minutes. The significance of N_2O_5 is mainly due to its reaction with liquid water in the atmosphere,

$$N_2O_5(g) + H_2O(l) \rightarrow HNO_3(aq) \ , \tag{2.22}$$

forming HNO_3 which can either evaporate or remain in the liquid phase. Gaseous HNO_3 is removed from the atmosphere efficiently by dry deposition, i.e., transfer to the Earth's surface without prior adsorption or absorption into precipitating particles. Aqueous HNO_3 will undergo wet deposition, i.e., removal by rain, fog, or snow. In summary, (2.22) constitutes a major pathway of removal of NO_x from the atmosphere. Reaction (2.22) points to the importance of heterogeneous reactions which will be addressed in the next section.

2.2 Aerosols

2.2.1 Definition, significance, and basic properties

Aerosols are technically defined as suspensions of solid or liquid particles in a gas or mixture of gases, e.g., in air. However, the term is commonly used to refer to the particle phase only. This thesis adheres to the actual definition as far as possible.

Particles are ubiquitous in the atmosphere and have to be considered for a wide range of phenomena. We give a summary of the most important points here.

Scattering and absorption of radiation. Highly concentrated, particles reduce visibility. Even if they cannot be detected by the naked eye, particles scatter and absorb solar as well as terrestrial radiation. Thus, on the one hand, efficient scatterers and absorbers influence climate by preventing solar radiation from reaching the ground, thereby exerting a cooling effect on the Earth's surface (Ramanathan et al., 2001). On the other hand, efficient absorbers lead to heating of the planetary boundary layer by trapping the energy of the incident radiation (Ramanathan et al., 2001). For instance, the term "black carbon" (BC), which is frequently used for elemental carbon in atmospheric particles such as soot, is due to its strong absorption of light which may place it among the top three global anthropogenic climate forcing agents (Hansen et al., 2005).

Cloud Condensation nuclei (CCN). Particles are necessary to maintain the hydrologic cycle, i.e., the interplay of precipitation, processing of water through the ground and evaporation, by providing nuclei for water condensation. For water to nucleate droplets in particle-free air the H_2O vapor pressure would have to attain several times its saturation value (i.e., the equilibrium H_2O vapor pressure over a flat surface of water). In contrast, CCN initiate cloud formation in the atmosphere and the supersaturation reaches at most a few percent (Pruppacher and Klett, 1997).

Health effects. The major fraction of coarse particles in the air that we breathe is removed within nose, mouth, and throat. Fine particles ($PM_{2.5}$, referring to particles with sizes $\leq 2.5\,\mu$m), however, can penetrate deeper into the lung where there is no efficient removal mechanism. These particles have been associated with increases in pulmonary diseases and mortality at

locations where their concentrations are elevated (e.g., Atkinson et al., 2001; Zanobetti and Schwartz, 2009). Additionally, particles can be coated with toxic chemicals which further increase their adverse health effects (Finlayson-Pitts and Pitts, 2000, and references therein).

When referring to the size of atmospheric particles, one usually assigns them an equivalent or effective diameter d_p. One of the most common definitions is the aerodynamic diameter d_p (Finlayson-Pitts and Pitts, 2000):

$$d_\mathrm{p} = d_\mathrm{g} k \sqrt{\frac{\rho_\mathrm{p}}{\rho_0}} \,, \tag{2.23}$$

which is the diameter of a sphere of the reference density $\rho_0 = 1\,\mathrm{g\,cm^{-3}}$ that would exhibit the same terminal fall speed, i.e., constant fall speed after equilibration of gravitational and frictional forces, as the considered particle. d_g stands for the geometric diameter and the parameter k is used to account for the particle's shape; a value of $k = 1.0$ describes a sphere.

Atmospheric particles span about five orders of magnitude in size, from the nanometer scale up to $\sim$100 μm. Bigger particles can also be carried into the air but their gravitational settling is so fast that they do not contribute a significant fraction to the atmospheric load. Due to this wide range, size distributions are usually expressed in, and plotted against, the logarithm of d_p. As one cannot take the logarithm of a unit, the numerical value of d_p in μm is usually used for that purpose.

Most measurements are carried out using sequential filtering, so that they can only yield binned results and these bins most times are neither linearly nor logarithmically spaced. Hence, the measured quantity — number, surface, volume, or mass concentration — is normalized to the bin width and then fitted with a continuous function, effectively yielding the derivative of the actual distribution ($\frac{dN}{d\log d_\mathrm{p}}$, $\frac{dS}{d\log d_\mathrm{p}}$, $\frac{dV}{d\log d_\mathrm{p}}$, and $\frac{dm}{d\log d_\mathrm{p}}$, respectively). Three of these functions are shown in Fig. 2.3 for a typical urban aerosol particle sample. The area under the curves between two diameters then gives the actual number, surface, or volume concentration of particles in that size range.

Fig. 2.3 shows the characteristic modes of atmospheric aersol particle size distributions, which shall be described briefly here.

Aitken mode. In the upper panel it is evident that by far most particles are found in the so-called Aitken mode ($\sim$0.01 μm to $\sim$0.1 μm). Particles in this mode are mostly due to direct emissions from combustion sources and biomass

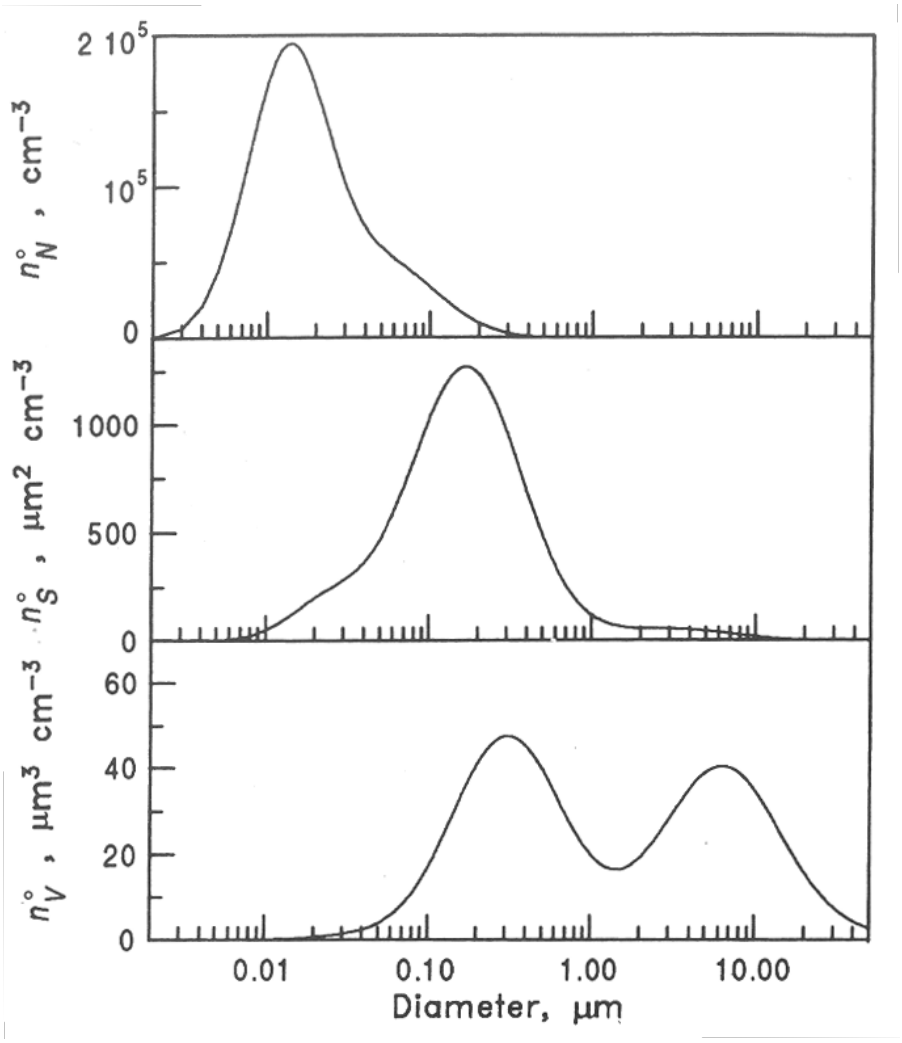

Figure 2.3: Typical size distributions with respect to number, surface and volume concentrations for an urban aerosol particle sample. ($n_N^\circ = \frac{dN}{d\log d_\mathrm{p}}$, $n_S^\circ = \frac{dS}{d\log d_\mathrm{p}}$, $n_V^\circ = \frac{dV}{d\log d_\mathrm{p}}$, taken from Seinfeld and Pandis (2006))

burning. During their subsequent processing in the atmosphere, also termed *aging*, semivolatile species can condense on them. Also, particles from the Aitken mode will coagulate, preferentially with bigger ones in the accumulation mode. Both processes move them to the accumulation mode within hours after their emission or formation.

Accumulation mode. This mode is characterized by the peak in the surface distribution and also evident in the first peak of the volume distribution in Fig. 2.3. The accumulation mode ($\sim$0.1 μm to $\sim$1 μm) is formed by direct emissions as well as condensation of trace gases such as sulfuric acid (H_2SO_4), HNO_3 and semivolatile organics. Moreover, coagulation with Aitken mode particles adds mass and surface to this mode. Essentially all the interface area between gas and particulate phases, which is available for condensation and surface reactions, is provided by the accumulation mode. The only significant removal process from this mode is precipitation, or wet deposition of particles, which explains their comparatively long atmospheric lifetime of typically $1-2$ weeks.

Coarse mode. Fig. 2.3 also shows the coarse mode ($\sim$1 μm to $>$ 10 μm) which consists mainly of seasalt, biogenic particles such as pollens, and wind-blown dust, e.g., from tilled land, roads, or deserts. Even though the coarse mode contributes a negligible number of particles to the atmospheric load it carries a large fraction of the particulate mass which scales with volume. The major sink for these relatively big particles is sedimentation, i.e., gravitational settling which occurs on time scales of hours to days.

Nucleation mode. Depending on gas phase composition and atmospheric conditions, a fourth mode, namely the nucleation mode, may exist at the far left end of the aerosol particle number distribution ($\sim$1 nm to $\sim$10 nm). These very small particles are formed by nucleation of atmospheric trace gases, mainly by the binary nucleation of H_2SO_4 and water vapor, for which nucleation occurs at much lower levels above saturation than for both species separately (Finlayson-Pitts and Pitts, 2000, and references therein). Nucleation mode particles have similar fates to Aitken mode particles.

Any of these modes can be fit with reasonable accuracy by a lognormal size distribution, i.e., a normal distribution of the respective derivative ($\frac{dN}{d\log d_\mathrm{p}}$, etc.) with respect to $\log d_\mathrm{p}$ or $\ln d_\mathrm{p}$ instead of d_p itself:

$$\frac{dN}{d\log d_\mathrm{p}} = \frac{N_\mathrm{tot}}{\sqrt{2\pi}\log\sigma} e^{-\frac{\left(\log d_\mathrm{p} - \log \overline{d_\mathrm{p}}\right)^2}{2(\log\sigma)^2}} \quad . \tag{2.24}$$

Here, N_tot denotes the total number concentration in the respective mode, $\log\sigma$ the width of the distribution and $\overline{d_\mathrm{p}}$ the median diameter. As mentioned above, the numerical values of d_p and $\overline{d_\mathrm{p}}$ in μm are usually used here.

Overall concentrations of particulate matter in air range from a few $10\,\mathrm{cm}^{-3}$ in polar regions to some $10^6\,\mathrm{cm}^{-3}$ in polluted cities. This translates to mass concentrations of particles with diameters $\leq 10\,\mu\mathrm{m}$ (PM_{10}) of a few $\mu\mathrm{g\,m}^{-3}$ to a maximum of about $300\,\mu\mathrm{g\,m}^{-3}$ (Finlayson-Pitts and Pitts, 2000; Seinfeld and Pandis, 2006).

Just like its size, a particle's composition also reflects its origin and history. The most abundant species are:

- Sulfate (SO_4^{2-}) which is mainly formed by the oxidation of gaseous sulfur dioxide (SO_2) in the aqueous phase,
- Nitrate ($\mathrm{NO}_3{}^-$) from condensation of HNO_3 on solid particles and its dissolution in liquid particles, e.g., upon formation by $\mathrm{N}_2\mathrm{O}_5$ hydrolysis (reaction (2.22)),
- Ammonium (NH_4^+) from the reaction of gaseous ammonia (NH_3) with sulfuric and nitric acids,
- Elemental carbon (EC) which only comes from direct emissions, and
- Organic carbon (OC), i.e., carbon in compounds other than elemental or carbon monoxide and dioxide.

Particles containing organics can either be emitted directly in processes such as fuel combustion or biomass burning or formed *in situ* by nucleation and gas-to-particle conversion (e.g., see Sect. 2.2.2). If formed in the atmosphere, they are commonly termed *secondary organic aerosols* (SOA). Organic compounds account for 20 to 90% of the particulate mass in the accumulation mode (Jimenez et al., 2009) and can have a variety of effects on particles' optical properties as well as on their ability to act as CCN or ice nuclei (Rudich et al., 2007; Knopf et al., 2010). However, the formation and atmospheric processing of organic aerosols are still not very well understood (Andreae, 2009; Jimenez et al., 2009) which makes more detailed studies — like the one presented here — necessary.

2.2.2 Soot

Although there is no rigorous definition of soot as a substance, there is agreement on a few characteristics in the literature. It originates as the solid by-product of incomplete fuel combustion, in particular from diesel engines, and biomass burning and can contain a large fraction of elemental carbon

(Adler et al., 2010). Soot particles are agglomerates of spherules with diameters in the tens of nm (Homann, 1998; Pósfai et al., 1999; Seinfeld and Pandis, 2006). Figure 2.4 shows a schematic illustration (left) and the graphene-like layers of the individual spherules (right). The atmospheric load of soot varies from $\mathrm{ng\,m^{-3}}$ over remote oceans to tens of $\mu\mathrm{g\,m^{-3}}$ in urban locations (Seinfeld and Pandis, 2006). Due to heterogeneous gas-to-particle processes the particles can contain nitrate, sulfate and organic compounds (El Haddad et al., 2009).

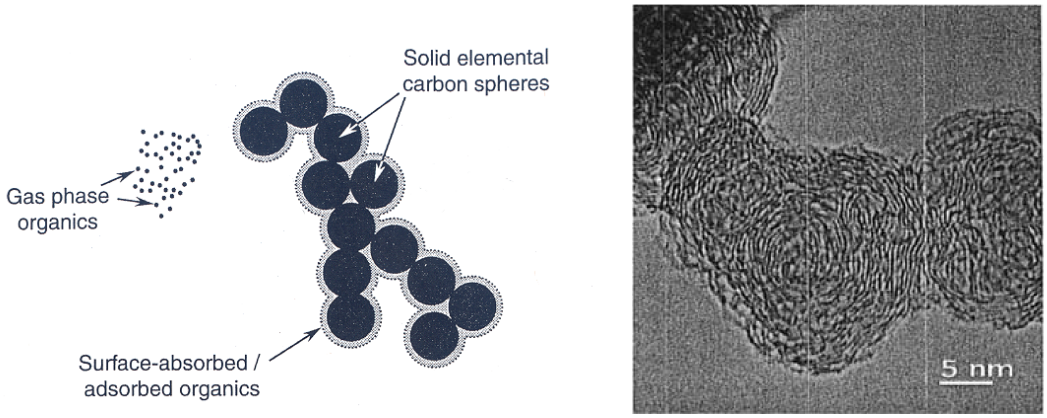

Figure 2.4: Left: schematic of a typical coated soot particle (adapted from Finlayson-Pitts and Pitts, 2000); right: high resolution transmission electron microscope image of individual spherules showing the graphene-like, layered structure of a soot particle's constituents (Vander Wal and Tomasek, 2003).

Although soot particles are initially rather hydrophobic (e.g., Kotzick et al., 1997), they generally become more hydrophilic upon oxidation in the atmosphere (e.g., Jimenez et al., 2009). This process leads to an increase in their ability to act as CCN during their atmospheric lifetime. As part of the accumulation mode, soot particles have lifetimes on the order of one week.

An important group of organics are PAHs that are produced by the same processes that also produce soot. Those with low volatility subsequently condense on the particles while the exhaust cools down (Finlayson-Pitts and Pitts, 2000). PAHs consist of two or more carbon ring structures that contain five or six carbon atoms each. Benzo[a]pyrene, one of the most prominent PAHs, was among the first atmospheric substances found to be carcinogenic in humans (Phillips, 1983). Moreover, many of the PAHs become mutagenic upon nitration, i.e., reaction with nitrogen oxides (Finlayson-Pitts and Pitts, 2000;

Pöschl, 2002). Hence, it is important to know these species' atmospheric lifetimes for health risk assessment and also for source apportionment because with that knowledge the originally emitted quantity of a compound can be inferred from the measured one.

It has been shown that PAHs have a special affinity towards soot particles (Dachs and Eisenreich, 2000). Moreover, field and experimental studies suggest that there is a certain nonexchangeable fraction of these compounds that always remains in the particulate phase under atmospheric conditions (Harner and Bidleman, 1998; Guilloteau et al., 2008, 2010). Therefore, significant amounts of PAHs are found in soot particles (e.g., Pakbin et al., 2009; Kashiwakura and Sakamoto, 2010).

2.3 Heterogeneous chemistry

Interactions between the gas and condensed phases of an aerosol play an important role in the particles' atmospheric fates. In addition to the physical processes of condensation and evaporation of gas phase species onto and from particles, chemical reactions take place simultaneously between the two phases. While gas phase molecules can also permeate the surface and react with the particle bulk, the focus of this study is on reactions with and on the surface. These processes are among the least understood contributions to chemical aging of organic aerosol particles because of the much greater complexity compared to gas phase or bulk condensed phase reactions. Not only do reactant concentrations change here but also the available area for adsorption and gas-surface reactions may be different over time. Moreover, any of the following physicochemical parameters of the surface which govern heterogeneous chemistry (and which we keep constant in our study for simplicity) can be altered during the involved processes:

- the mass accommodation coefficient α, which describes the fraction of gas molecules sticking to the surface upon collision,
- the effective molecular cross section σ, which is a surface composition dependent measure of how much space an adsorbed molecule will take up on the surface,
- the desorption lifetime τ_{d}, i.e., the time that an average molecule stays on the surface before desorbing back to the gas phase if it does not react with surface species, and

- the reaction probability, γ, i.e., the fraction of molecules colliding with a surface that instantly reacts with it.

Heterogeneous reactions may proceed via different mechanisms. In this study, most of the considered reactions (see Tab. 3.1) show a Langmuir-Hinshelwood (L-H) type behavior. This term is borrowed from catalysis where it describes a two-step process: first, molecules are adsorbed onto a surface and then, in a subsequent step, the actual reaction takes place (Rothenberg, 2008). Note that, in contrast to what we describe here as L-H type processes, the surface neither changes nor reacts in the original definition. In the following, we will call the reactions involved in these processes *surface layer reactions* (SLRs).

A second commonly observed mechanism in atmospheric heterogeneous chemistry can be described as Eley-Rideal like. Again, the term is borrowed from catalysis and originally refers to a one-step process in which a molecule from the gas phase hits another one that is adsorbed on the surface and they instantly react (Rothenberg, 2008). In what we call *gas-surface reactions* (GSRs) here, the mechanism is very similar: a certain fraction (determined by the reaction probability) of the molecules that collide with the surface-bound reactant undergoes instant reaction, i.e., there is no need for the gaseous reactant to adsorb prior to reaction.

In measurements, L-H type reactions manifest themselves in a nonlinear dependence of the condensed material's pseudo-first-order decay rate coefficient on the gas phase concentration of the second reactant (e.g., Pöschl et al., 2001; Kwamena et al., 2004). In our notation this would mean that k' in Eq. (2.8) would rise less than linearly with [A] indicating fast initial uptake due to adsorption of B and a slower surface reaction between A and B as the rate-limiting step.

2.3.1 PRA framework

To address the complex interplay of heterogeneous processes on atmospheric particles from a theoretical point of view, Pöschl, Rudich, and Ammann recently developed a model framework, termed PRA framework, that treats those processes based on fluxes across the interfaces between the various model compartments (Pöschl et al., 2007; Ammann and Pöschl, 2007). Thus, it provides a dynamic description of the phenomena governing heterogeneous chemistry, i.e., it allows to take into account changes in the underlying parameters outlined in Sect. 2.3.

The PRA framework divides aerosols into four distinct model compartments: the gas phase (g), two surface layers, and the particle bulk (Fig. 2.5). The surface consists of a sorption layer (s) that accommodates volatile species X_i and a quasi-static layer (ss) where non-volatile species Y_j reside. Moreover, gas phase and particle bulk are subdivided to account for near-surface corrections. Such corrections can be necessary if heterogeneous processes deplete bulk or gas phase concentrations near the surface faster than diffusion in the respective compartment can replenish them (see also the subsection "Feedback on gas phase" below).

This section will present those parts of the formalism that are relevant for the present study as indicated in Fig. 2.5. For instance, everything related to the bulk will be omitted because we do not consider bulk processes here.

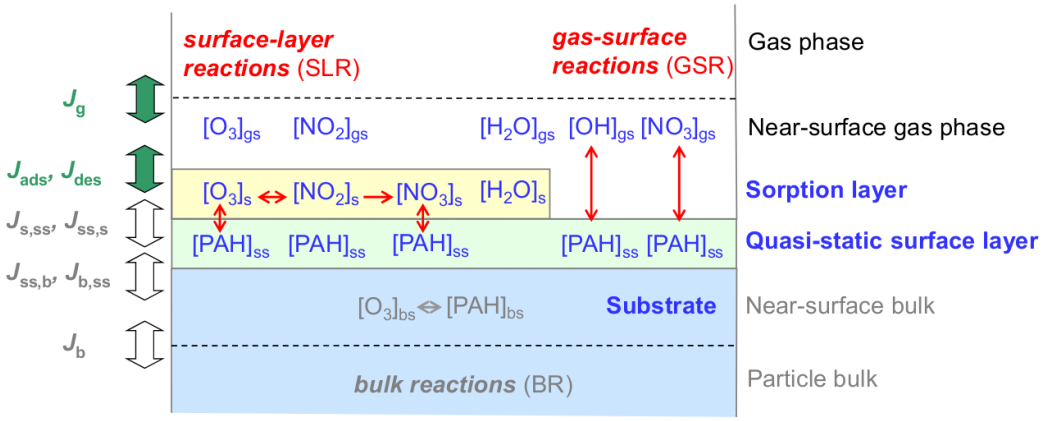

Figure 2.5: PRA model compartments with species and flux nomenclature (taken from Shiraiwa et al. (2009)). Fluxes considered here are indicated by big green arrows, reactions by thin red arrows. Grey text shows compartments not taken into account in the present study. The index 'gs' denotes gas concentration close to the surface.

Gas-particle fluxes

The overall efficiency of a reaction of a gas X_i with a surface is given by the uptake coefficient

$$\gamma_{X_i} = \frac{J_{\mathrm{net},X_i}}{J_{\mathrm{coll},X_i}} , \tag{2.25}$$

which is the ratio of net gas flux J_{net,X_i} onto the particle to the flux J_{coll,X_i} of molecules colliding with it (molecules per unit area and time). Note that this

expression is technically only valid in a system that considers only one single reactive or adsorbing gas species and for a process that does not change the underlying parameters.

For dealing with a more complex system — like the one presented here, where we consider four reactive gases and co-adsorbing water vapor — we define an effective uptake coefficient γ'_{X_i}. We deviate from the actual nomenclature of the PRA framework (Pöschl et al., 2007) here in order to make this distinction clear. The effective uptake coefficient is the proportionality factor that relates the rate of net gas uptake to the rate of gas-surface collisions per unit volume. Thus, it is a dynamic quantity and includes effects like partial coverage of reactive sites by adsorbed molecules and may also account for other changes in surface composition (see, e.g., Eq. (2.26)). Moreover, it can depend on both surface and gas phase concentration of species X_i (see, e.g., Eq. (2.34)).

In case of a GSR between X_i and Y_j and under consideration of species that adsorb into the sorption layer, the effective uptake coefficient is

$$\gamma'_{\mathrm{X}_i} = \gamma_{\mathrm{X}_i} \cdot (1 - \theta_{\mathrm{s}}) \cdot \theta_{\mathrm{ss,Y}_j} \ , \tag{2.26}$$

where

$$\theta_{\mathrm{s}} = \sum_i \theta_{\mathrm{s,X}_i} = \sum_i \sigma_{\mathrm{X}_i} [\mathrm{X}_i]_{\mathrm{s}} \tag{2.27}$$

denotes surface coverage of the sorption layer (index s), expressed by effective cross sections σ_{X_i} multiplied by surface concentrations $[\mathrm{X}_i]_{\mathrm{s}}$ of the respective species. Analogously, $\theta_{\mathrm{ss,Y}_j} = \sigma_{\mathrm{Y}_j} [\mathrm{Y}_j]_{\mathrm{ss}}$ is the coverage of the quasi-static surface layer (index 'ss') with Y_j. Equation (2.26) takes into account that the effective uptake coefficient does not only depend on the reaction probability, γ_{X_i}, which is a material constant. (Note that in the literature this quantity is also often called uptake coefficient.) γ'_{X_i} also depends on the fraction of the quasi-static surface layer that is not covered by adsorbing species $(1 - \theta_{\mathrm{s}})$ and on the fraction of reactive sites within that exposed portion $(\theta_{\mathrm{ss,Y}_j})$. Thus, net flux of X_i onto the surface becomes:

$$J_{\mathrm{net,X}_i} = \gamma'_{\mathrm{GSR}n,\mathrm{X}_i,\mathrm{Y}_j} \cdot J_{\mathrm{coll,X}_i} = \gamma_{\mathrm{GSR}n,\mathrm{X}_i,\mathrm{Y}_j} (1 - \theta_{\mathrm{s}}) \theta_{\mathrm{ss,Y}_j} \cdot J_{\mathrm{coll,X}_i} \ . \tag{2.28}$$

Index n denotes the number of the respective GSR in Tab. 3.1 and X_i in this case stands for either OH or $\mathrm{NO_3}$, the two trace gases considered here that undergo GSRs.

For the Langmuir-Hinshelwood mechanism net flux can be expressed as

the difference between adsorption and desorption flux:

$$J_{\mathrm{net,X}_i} = J_{\mathrm{ads,X}_i} - J_{\mathrm{des,X}_i} \ . \tag{2.29}$$

The accommodation coefficient $\alpha_{\mathrm{s,X}_i}$ relates adsorption to collision flux:

$$J_{\mathrm{ads,X}_i} = \alpha_{\mathrm{s,X}_i} J_{\mathrm{coll,X}_i} = \alpha_{\mathrm{s,0,X}_i}(1-\theta_{\mathrm{s}}) J_{\mathrm{coll,X}_i} \ , \tag{2.30}$$

where $\alpha_{\mathrm{s,0,X}_i}$ denotes the accomodation coefficient of an adsorbate-free surface and $\alpha_{\mathrm{s,X}_i}$ takes changes in sorption layer coverage into account. Desorption is determined by surface concentration $[\mathrm{X}_i]_{\mathrm{s}}$ and desorption lifetime $\tau_{\mathrm{d,X}_i}$:

$$J_{\mathrm{des,X}_i} = \frac{[\mathrm{X}_i]_{\mathrm{s}}}{\tau_{\mathrm{d,X}_i}} \ . \tag{2.31}$$

As desorption is not proportional to the collision flux, the latter cannot be eliminated from the expression for the effective uptake coefficient here. As it is impossible to measure the collision flux directly an expression derived from gas kinetic theory is used to replace it by measurable parameters:

$$J_{\mathrm{coll,X}_i} = \frac{\omega_{\mathrm{X}_i}}{4}[\mathrm{X}_i]_{\mathrm{g}} \ , \tag{2.32}$$

where

$$\omega_{\mathrm{X}_i} = \sqrt{\frac{8RT}{\pi M_{\mathrm{X}_i}}} \tag{2.33}$$

stands for the thermal speed of a gas molecule. R is the universal gas constant, T temperature and M_{X_i} the molar mass of species X_i. Hence, the effective uptake coefficient for Langmuir-Hinshelwood type kinetics reads:

$$\gamma'_{\mathrm{X}_i} = \alpha_{\mathrm{s,0,X}_i}\left(1 - \sum_i \sigma_{\mathrm{X}_i}[\mathrm{X}_i]_{\mathrm{s}}\right) - \frac{4}{\tau_{\mathrm{d,X}_i}}\sqrt{\frac{\pi M_{\mathrm{X}_i}}{8RT}}\frac{[\mathrm{X}_i]_{\mathrm{s}}}{[\mathrm{X}_i]_{\mathrm{g}}} \ . \tag{2.34}$$

It should be noted that expression (2.32) for the collision flux and with it Eq. (2.34) only holds if uptake is sufficiently slow compared to gas phase diffusion, so that $[\mathrm{X}_i]_{\mathrm{g}}$ is not significantly depleted close to the particle surface. Otherwise a correction factor is required to account for this depletion (see below, in the discussion of gas phase feedback). The correction factor can be ignored without compromising accuracy if $\gamma'_{\mathrm{X}_i} \leq 10^{-3}$ (Ammann and Pöschl, 2007) which is true for all species considered here that follow the Langmuir-Hinshelwood mechanism, except initial NO_2 uptake. However, $\gamma'_{\mathrm{NO_2}}$ drops so

rapidly compared to the time resolution of our simulations that the correction is unnecessary in that case, too (see Fig. 4.4 in Chapter 4).

Chemical reactions

Chemical gain and loss terms are based on concentrations of the reagents and on reaction rate constants in case of SLRs, or reaction probabilities for GSRs. The reactions considered in this study are given in Tab. 3.1.

Net chemical production and loss of volatile species in and from the sorption layer ($P_{\mathrm{s,X}_i} - L_{\mathrm{s,X}_i}$) are due to both reactions within that layer and reactions with species in the quasi-static surface layer:

$$P_{\mathrm{s,s,X}_i} - L_{\mathrm{s,s,X}_i} = \sum_n \sum_p \sum_q c_{\mathrm{SLR}n,\mathrm{s,X}_i} k_{\mathrm{SLR}n,\mathrm{X}_p,\mathrm{X}_q} [\mathrm{X}_p]_\mathrm{s} [\mathrm{X}_q]_\mathrm{s} \tag{2.35}$$

$$P_{\mathrm{s,ss,X}_i} - L_{\mathrm{s,ss,X}_i} = \sum_n \sum_p \sum_q c_{\mathrm{SLR}n,\mathrm{s,X}_i} k_{\mathrm{SLR}n,\mathrm{X}_p,\mathrm{Y}_q} [\mathrm{X}_p]_\mathrm{s} [\mathrm{Y}_q]_\mathrm{ss} \ . \tag{2.36}$$

Here, $c_{\mathrm{SLR}n,\mathrm{s,X}_i}$ represent stoichiometric coefficients of X_i in the respective reaction equations. They are positive if X_i is produced in a reaction and negative if it is consumed. n is the number of the SLR as given in Tab. 3.1, and p and q run over all sorption layer and quasi-static surface layer species involved in production and loss of X_i. The second equation can be written analogously for production and loss of species in the quasi-static surface layer ($P_{\mathrm{ss,s,Y}_j} - L_{\mathrm{ss,s,Y}_j}$).

The gas-surface reactions considered in this study lead to production and loss of species in the quasi-static layer:

$$P_{\mathrm{ss,g,Y}_j} - L_{\mathrm{ss,g,Y}_j} = \sum_n \sum_p \sum_q c_{\mathrm{GSR}n,\mathrm{ss,Y}_j} \gamma_{\mathrm{GSR}n,\mathrm{X}_p,\mathrm{Y}_q} (1 - \theta_\mathrm{s}) J_{\mathrm{coll,X}_p} \theta_{\mathrm{ss,Y}_q} \ . \tag{2.37}$$

Time evolution of surface species concentrations

The general forms of the ordinary differential equations describing time evolution of surface species concentrations are

- for species with Langmuir-Hinshelwood kinetics:

$$\frac{d[\mathrm{X}_i]_\mathrm{s}}{dt} = J_{\mathrm{ads,X}_i} - J_{\mathrm{des,X}_i} + P_{\mathrm{s,s,X}_i} - L_{\mathrm{s,s,X}_i} + P_{\mathrm{s,ss,X}_i} - L_{\mathrm{s,ss,X}_i} \ , \tag{2.38}$$

- and for species in the quasi-static surface layer:

$$\frac{d[\mathrm{Y}_j]_{\mathrm{ss}}}{dt} = P_{\mathrm{ss,s,Y}_j} - L_{\mathrm{ss,s,Y}_j} + P_{\mathrm{ss,g,Y}_j} - L_{\mathrm{ss,g,Y}_j} \ . \tag{2.39}$$

Equations (2.30) - (2.32), and (2.35) - (2.37) are then used to replace the right hand side terms. The system of ordinary differential equations that arises from writing out Eqs. (2.38) and (2.39) explicitly for all involved species is the basis for modeling the aerosol particles' surface composition. In our computer model it is solved for each particle at discrete time steps by a numerical integration routine.

Feedback on gas phase

The net effect of heterogeneous reactions on the gas phase is expressed by the uptake coefficient:

$$\frac{d[\mathrm{X}_i]_{\mathrm{g}}}{dt} = \sum_n \gamma'_{n,\mathrm{X}_i} J_{\mathrm{coll,X}_i} \cdot \frac{S_n}{V} \ , \tag{2.40}$$

where n runs over all particles in the population and $\frac{S_n}{V}$ is the amount of surface area per volume of air for an individual particle. The model described in Sect. 3.1 uses this equation to determine gas phase changes caused by heterogeneous chemistry.

As the reaction probabilities γ_{X_i} for the GSRs considered here are higher than the formerly mentioned threshold of 10^{-3}, it is necessary to apply a correction factor for the calculation of their gas phase feedback. Hence, the collision flux becomes

$$J_{\mathrm{coll,X}_i} = \frac{\omega_{\mathrm{X}_i}}{4}[\mathrm{X}_i]_{\mathrm{gs}} \ , \tag{2.41}$$

with the near-surface gas phase concentration $[\mathrm{X}_i]_{\mathrm{gs}} = C_{\mathrm{g,X}_i}[\mathrm{X}_i]_{\mathrm{g}}$ and the gas phase diffusion correction factor $C_{\mathrm{g,X}_i}$, which is given in the PRA framework as

$$C_{\mathrm{g,X}_i} = \frac{1}{1 + \gamma_{\mathrm{X}_i} \frac{0.75+0.28Kn_{\mathrm{X}_i}}{Kn_{\mathrm{X}_i}(1+Kn_{\mathrm{X}_i})}} \ , \tag{2.42}$$

based on work by Fuchs and Sutugin (1971). The Knudsen number Kn_{X_i} is calculated from the gas phase diffusion coefficient $D_{\mathrm{g,X}_i}$ in air, air pressure p, thermal speed ω_{X_i} of the gas molecules and particle diameter d_{p}:

$$Kn_{\mathrm{X}_i} = \frac{6D_{\mathrm{g,X}_i}}{p\omega_{\mathrm{X}_i}d_{\mathrm{p}}} \ . \tag{2.43}$$

2.3.2 Heterogeneous reactions on soot

Numerous studies have been conducted to measure the effects related to various atmospheric trace gases reacting with or on soot surfaces. For a review of this field see, e.g., Nienow and Roberts (2006). The soot particles' PAH coating assumed here has a similar molecular structure to bare soot (see Fig. 2.4 for the structure and Pöschl, 2005; Cain et al., 2010, for reference) and can therefore be assumed to have similar physical properties such as accommodation coefficients.

The following paragraphs will briefly describe the findings of the studies that form the basis for our parameter choices. A compilation of various measurements relevant to the system of surface-bound PAHs interacting with O_3, NO_2, and H_2O can be found in Shiraiwa et al. (2009). The latter is also the source of a major fraction of parameter values assumed in this study.

Refer to Tables 3.1 and 3.2 for the numerical values of the parameters discussed here.

Ozone and water vapor

Rogaski et al. (1997) measured gas phase loss to uncoated soot particles of O_3 and H_2O among others and calculated uptake coefficients from their data. Since the reported values are from measurements at low pressure and not averaged over more than a few minutes we interpret these coefficients as accommodation coefficients. Moreover, Rogaski et al. showed that water uptake is not influenced by pre-treatment of the particles with O_3 or NO_2, which supports our assumption that accommodation coefficients do not change.

Similar experiments were conducted with benzo[a]pyrene (BaP) coated soot particles by Pöschl et al. (2001). They found a nonlinear dependence of k'_{BaP} on gas phase O_3 concentration. As explained above, this indicates a Langmuir-Hinshelwood type reaction of O_3 with the surface-bound BaP. From their measurements a second-order rate constant $k_{\mathrm{O_3,BaP}}$ for the reaction between adsorbed O_3 and BaP was derived. According to Shiraiwa et al. (2009), the value of this reaction rate constant is supported by the results of a study performed by Schauer (2004). Pöschl et al. also found that the presence of water vapor slowed down the overall reaction of gaseous O_3 with BaP on the surface. This can be explained by competitive co-adsorption of O_3 and H_2O on the reactive surface sites (Springmann et al., 2009).

In contrast to O_3, H_2O does not react chemically with soot surfaces but also adsorbs on the particles. As we will see in Chapter 4, its influence on heterogeneous oxidation of soot-bound PAHs cannot be neglected.

Desorption lifetimes were also determined in the studies cited above. We follow the assumption for τ_{d,O_3} by Shiraiwa et al. (2009) and use the data cited in their paper to calculate an average τ_{d,H_2O}.

Nitrogen dioxide and surface-produced nitrate radical

By measuring gas phase loss of NO_2, Tabor et al. (1994) determined initial uptake coefficients on different types of soot and showed them to be identical. As can be seen from Eq. (2.34), the initial uptake coefficient is equivalent to the accommodation coefficient. Thus, we employ the values reported by Tabor et al. as accommodation coefficients in our study.

NO_2 does not significantly degrade PAHs on soot particles by itself (Pöschl, 2002; Nguyen et al., 2009). However, its co-adsorption can increase the depletion by O_3 which may be due to formation of reactive intermediate species such as the NO_3 radical (Pöschl, 2002; Shiraiwa et al., 2009). A range of possible combinations for rates of the O_3-NO_2 surface reaction forming NO_3, the subsequent NO_3-PAH reaction, and NO_3 desorption lifetime are presented by Shiraiwa et al. (2009), based on the measured enhancement of the apparent O_3-PAH reaction. For our study we choose average values from their suggestions.

We also use the desorption lifetime τ_{d,NO_2} as assumed in Shiraiwa et al. (2009).

Specific attention has been given to the system soot-NO_2-H_2O because of the possible formation of HONO, one of the important OH precursors (e.g., Rogaski et al., 1997; Ammann et al., 1998; Gerecke et al., 1998; Kleffmann et al., 1999; Arens et al., 2001; Aubin and Abbatt, 2007; Khalizov et al., 2010). However, so far the results have not been conclusive in determining the significance of this effect.

Hydroxyl radical

Bertram et al. (2001) investigated OH uptake on soot and various other solid organic surfaces. Their measurements of heterogeneous loss from the gas phase show very efficient uptake of OH by these substrates. This finding in conjunction with the high reactivity of OH towards gas phase organics justifies treatment of the heterogeneous reaction as a one-step process, i.e., as Eley-Rideal like, in our study.

For the OH-PAH reaction probability we choose a value reported by Bertram et al. (2001) for the reaction of OH with pyrene because the latter is the compound we use as a representative for soot-bound PAHs as will

be explained in detail in Sect. 3.2.

The gas phase diffusion coefficient of OH in air was measured by Ivanov et al. (2007). The experimental approach was analogous to the measurements of uptake coefficients discussed above. Deconvoluting the observed first-order loss of gaseous OH into a reactive and a diffusive contribution they were able to extract the diffusion coefficient.

Gas phase nitrate radical

Gross and Bertram (2008) showed that the heterogeneous reaction with gaseous NO_3 may be a major sink of particle-bound PAHs because of the NO_3 radical's extremely high reactivity in these reactions. They measured reaction probabilities for NO_3 and other atmospheric oxidants on different solid PAHs and compared their oxidizing potentials by multiplying uptake coefficients with typical gas phase concentrations of the oxidants. Values of this efficiency measure were about two orders of magnitude higher for NO_3 than for any other oxidant they investigated, including N_2O_5, NO_2, HNO_3, and O_3. However, OH radicals were not considered in that study.

These findings lead us to assume an Eley-Rideal type mechanism for the NO_3-PAH reaction for the purpose of our study. We use the value of $\gamma_{NO_3,PAH}$ for a pyrene surface reported by Gross and Bertram (2008).

The diffusion coefficient for NO_3 in air assumed here is drawn from measurements by Rudich et al. (1996). Employing an analogous technique to that of Ivanov et al. (2007) described briefly above, they determined gas phase diffusion coefficients of NO_3 in N_2 and in O_2. The obtained values were identical and can be regarded as representative for NO_3 in air since, together, N_2 and O_2 make up about 99% of the air by volume (see Chapter 1).

2.4 Modeling atmospheric chemistry

Atmospheric chemistry models, usually called chemistry transport models, are used to simulate the composition of the atmosphere at regional or global scales. Both, health effects and climate forcings depend crucially on concentrations of trace gases and suspended particles and on the composition of particulate matter. Hence, there is a necessity to accurately predict atmospheric composition based on current and past measurements and observations. Before new model schemes are employed they are evaluated against laboratory experiments or field studies, or both.

The most basic form of chemistry transport models is the box model which

simulates chemistry in an air parcel or air mass that is considered to be representative of the atmospheric conditions at the time and location for which the simulation is carried out. It calculates the time evolution of gas phase and particle phase species due to physical and chemical transformations and can also include additional processes such as dilution with background air, emissions, and deposition.

The rate of change of the chemical species is expressed as ordinary differential equations (ODEs), and the system of ODEs is solved by a time-integration method at discrete time steps. The length of these steps has to be chosen to achieve a balance between accurately resolving the time scales of involved processes and computational limitations.

Such box models can be included in three-dimensional models that also treat meteorology and terrain specific effects. Two different approaches are possible here. In an Eulerian model the part of the atmosphere in question is divided into a grid of adjacent boxes whose coordinates are fixed with respect to the ground. The boxes are interconnected by fluxes of the inventory species. In Lagrangian models, boxes follow the meteorologic flow and are thus not fixed with respect to the Earth's surface.

Usually, a similar separation or modularization as that of meteorology and atmospheric chemistry outlined above is also employed within the chemistry models. Thus, gas phase chemistry and meteorological parameters such as temperature, humidity, and pressure drive the processes governing aerosol evolution. In the following two sections we therefore briefly describe the most significant features of gas phase modules and aerosol modules separately.

2.4.1 Gas phase chemistry

Gas phase chemistry is described by rate equations such as Eqs. 2.5 or 2.6. The resulting systems of differential equations can become very extensive if systems of atmospheric relevance are to be simulated explicitly. For example, the Master Chemical Mechanism (`http://mcm.leeds.ac.uk/MCM/project.htt`) includes about 4500 chemical species undergoing around 12600 reactions for a description of the atmospheric degradation of 124 VOCs. However, even this mechanism relies on simplifying assumptions that reduce the numbers of both involved species and reactions.

It is obvious that mechanisms of this kind cannot efficiently be implemented into the dynamic context of large-scale 3D models that also consider other relevant parameters such as meteorological conditions and emissions. Hence, for these kinds of models, simplified schemes of atmospheric chemistry exist that lump groups of chemically similar compounds into single computational

species. Examples of such schemes are the Second Generation Regional Acid Deposition Model (RADM2) (Stockwell et al., 1990) with 63 chemical species and 157 reactions and the Carbon Bond Mechanism (CBM-Z) by Zaveri and Peters (1999) including 67 species and 164 reactions (Zaveri et al., 2008).

2.4.2 Aerosol chemistry and physics

For aerosol particles, concentrations have to be predicted with respect to both particle size and composition. Two basic approaches for simulating the condensed phase are commonly used in atmospheric models. In sectional models (e.g., Jacobson, 1997; Adams et al., 1999; Zaveri et al., 2008) particles are assigned to bins depending on their size. All particles in one bin are assumed to behave in the same way and have the same composition. These models can predict either mass or number of particles per bin, or both. Similarly, in modal models (e.g., Binkowski and Shankar, 1995; Wilson et al., 2001; Stier et al., 2005) all particles in one mode have the same composition although they can be of different sizes. Such modes are typically assumed to have lognormal size distributions whose moments are predicted by the simulation. Three moments, e.g., mean particle diameter, width of the distribution, and total mass of that mode, are sufficient for a full characterization. In sum, the different modes considered in a model should reproduce distributions as shown in Fig. 2.3.

Aerosol models simulate gas-particle partitioning, which is determined by condensation and evaporation of water vapor and trace gases as well as by nucleation of new particles from low-volatility vapors. Some models also treat internal chemical and physical processes such as phase changes inside the particles (cf. Sect. 3.1.2). Coagulation routines are often also implemented.

In both modal and sectional models rules have to be defined when to move particles from one bin to another or from one mode to another. Thus, the total number or mass of particles per bin or per mode can be predicted by the models.

However, the assumption of completely internal mixing, i.e., the same composition for all particles in one bin or mode, is not a realistic representation of particles actually found in the atmosphere. Advances in numerical methods and computational resources have made it possible in recent years to apply particle-resolved models to atmospheric aerosols to address this deficiency. With that approach it is possible to track continuous changes in composition of individual particles, allowing for a much more accurate representation of atmospheric conditions. Such a model is used for this study and described in more detail in Sect. 3.1.

2.4.3 Previous studies of heterogeneous chemistry

Previous modeling studies of heterogeneous chemistry mainly focused on its effects on trace gas concentrations. For example, the effect of the NO_2-soot reaction yielding HONO described in Sect. 2.3.2 was investigated by Aumont et al. (1999) and Kotamarthi et al. (2001). Due to substantial variability in laboratory measurement results which were used as input parameters, however, their results also showed a large uncertainty in terms of the possible effect on daytime O_3 and NO_x concentrations.

Effects on the latter were also investigated with box model simulations by Saathoff et al. (2001) who considered reactions of soot with O_3, NO_2, HNO_3, NO_3/N_2O_5, and $HO_2/HOONO_2$ and by Aklilu and Michelangeli (2004) who took into account reactions with O_3, HNO_3, NO_2, N_2O_5, and NO_3. Their results showed different degrees of influence that heterogeneous chemistry may have on these pollutants. Reductions in O_3 concentration of up to about 25% were obtained for certain scenarios but both groups cautioned not to overestimate the atmospheric implications of these results since they used upper limit values for the governing parameters.

None of the above studies included any treatment of the underlying physicochemical processes described by the PRA framework (Sect. 2.3.1). Instead, they relied on parameterizations that held uptake coefficients constant. However, simulations employing the PRA framework showed that effective uptake coefficients can vary by several orders of magnitude during a day (Ammann and Pöschl, 2007; Springmann et al., 2009; Shiraiwa et al., 2009).

In our study, the particle-resolved aerosol model allows us to take into account both diurnal changes in atmospheric chemical composition (which were not included by Ammann and Pöschl (2007) and Shiraiwa et al. (2009)) and realistic emissions of soot particles. Soot emissions have only been considered in a simplified way by Springmann et al. (2009), where soot surface was replenished at certain intervals in a box model simulation, and have not been modeled more realistically so far.

3. Modeling Approach

This chapter describes in detail the aerosol model used here, the simulated system consisting of PAH coated soot particles reacting with atmospheric trace gases, and the scenarios for our simulations. The aerosol model consists of two parts, the particle-resolved model PartMC and the box model MOSAIC. Coupling these two models enables us to track the composition of individual particle surfaces and the evolution of heterogeneous kinetics, expressed, e.g., in effective uptake coefficients.

3.1 Particle-resolved aerosol model

We use a particle-resolved aerosol model here because it allows us to resolve both size and composition of particles continuously, i.e., without introducing bins, and to track individual particles.

A sectional model, as outlined in Sect. 2.4.2, would not allow for coexistence of particles with the same size but different composition, and in a modal model, composition would have to be discretized. Since we consider continuous particle emissions and subsequent processes that transform the particles' composition, neither a sectional nor a modal model can be employed.

Moreover, neither the sectional nor the modal approach allow for tracking of particle evolution with time since only number or mass per bin or per mode are used to describe the particulate phase in these models. Since the quantities we are interested in, specifically effective uptake coefficients, crucially depend on the evolution of individual particles (as will be shown in the next chapter), neither approach would have been successful for the present study.

Thus, for our simulations we use PartMC-MOSAIC (Riemer et al., 2009), a sophisticated particle-resolved aerosol model. Its main parts(PartMC, or Particle Monte Carlo model, and MOSAIC, or MOdel for Simulating Aerosol Interactions and Chemistry) and the heterogeneous kinetics extension added for the purpose of this study are described in the following subsections.

3.1.1 PartMC

PartMC is a highly efficient computer model for simulating aerosol mixing state in a Lagrangian air parcel. It is based on a Monte Carlo approach, i.e., all particle-involving processes are modeled by choosing random samples of particles and treating them according to prescribed probability distributions. These processes can include emissions, coagulation, and dilution with background air as well as condensation and evaporation of trace gases and water vapor.

Each particle is represented by a composition vector $\vec{\mu}$ with components μ_a, denoting masses (in kg) of the constituent species $a = 1, \ldots, A$. The cumulative number density of particles containing less than μ_a of species a at a given time is $N(\vec{\mu}, t)$ (unit: m^{-3}), so that the number distribution with respect to constituent masses can be written as

$$n(\vec{\mu}, t) = \frac{\partial^A N(\vec{\mu}, t)}{\partial \mu_1 \partial \mu_2 \ldots \partial \mu_A} \,, \tag{3.1}$$

in units of $\mathrm{m}^{-3}\,\mathrm{kg}^{-\mathrm{A}}$.

The full equation for the evolution of PartMC-MOSAIC's particulate phase is:

$$\begin{aligned}
\frac{\partial n(\vec{\mu}, t)}{\partial t} = & \underbrace{\frac{1}{2} \int_0^{\mu_1} \int_0^{\mu_2} \cdots \int_0^{\mu_A} K(\vec{\mu}', \vec{\mu} - \vec{\mu}') \cdot n(\vec{\mu}', t)\, n(\vec{\mu} - \vec{\mu}', t)\, d\mu_1'\, d\mu_2' \ldots d\mu_A'}_{\text{coagulation gain}} \\
& \underbrace{- \int_0^{\infty} \int_0^{\infty} \cdots \int_0^{\infty} K(\vec{\mu}, \vec{\mu}') \cdot n(\vec{\mu}, t)\, n(\vec{\mu}', t)\, d\mu_1'\, d\mu_2' \ldots d\mu_A'}_{\text{coagulation loss}} \\
& + \underbrace{\dot{n}_{\text{emit}}(\vec{\mu}, t)}_{\text{emission}} + \underbrace{\lambda_{\text{dil}}(t) \Big(n_{\text{back}}(\vec{\mu}, t) - n(\vec{\mu}, t) \Big)}_{\text{dilution}} + \underbrace{\frac{1}{\rho_{\text{dry}}(t)} \frac{d\rho_{\text{dry}}(t)}{dt} n(\vec{\mu}, t)}_{\text{air density change}} \\
& \underbrace{- \sum_{i=1}^{C} \frac{\partial}{\partial \mu_i} \Big(c_i I_i(\vec{\mu}, \vec{g}, t)\, n(\vec{\mu}, t) \Big)}_{\text{condensation / evaporation}} \underbrace{- \frac{\partial}{\partial \mu_{C+1}} \Big(c_{\text{w}} I_{\text{w}}(\vec{\mu}, \vec{g}, t)\, n(\vec{\mu}, t) \Big)}_{\text{water transfer}} \,,
\end{aligned} \tag{3.2}$$

where $K(\vec{\mu}_1, \vec{\mu}_2)$ ($\mathrm{m}^3\,\mathrm{s}^{-1}$) is the coagulation rate between particles with constituent masses $\vec{\mu}_1$ and $\vec{\mu}_2$, $\dot{n}_{\text{emit}}(\vec{\mu}, t)$ ($\mathrm{m}^{-3}\,\mathrm{kg}^{-\mathrm{A}}\,\mathrm{s}^{-1}$) is the number distribution rate of aerosol emissions, $n_{\text{back}}(\vec{\mu}, t)$ ($\mathrm{m}^{-3}\,\mathrm{kg}^{-\mathrm{A}}$) is the background number distribution, $I_i(\vec{\mu}, \vec{g}, t)$ ($\mathrm{mol}\,\mathrm{s}^{-1}$) is the condensation or evaporation flux of gas

species i (with $I_{\mathrm{w}}(\vec{\mu}, \vec{g}, t)$ the flux for water), and c_i ($\mathrm{kg\,mol^{-1}}$) is the conversion factor from moles of gas species i to mass of aerosol species i (with c_{w} the factor for water) (Riemer et al., 2009). The components of $\vec{g}$ are the gas phase concentrations $[\mathrm{X}_i]_{\mathrm{g}}$ introduced in the PRA framework and C is the number of condensing species. $C+1$ denotes the index of water vapor in the particle composition vector. Boundary conditions for the solution of Eq. 3.2 are non-negative constituent masses and conservation of mass.

Note that, while most terms of Eq. (3.2) are computed by PartMC, the terms for condensation, evaporation, and water transfer are calculated in MOSAIC, which will be introduced in the next section.

In order to keep our focus on the analysis of heterogeneous reactions, we do not subject particles to all the processes described by Eq. (3.2) in the present study. We omit coagulation and dilution as well as condensation and evaporation of trace gases and water vapor. Air density does not change since pressure and mixing height are kept constant here (see Sect. 3.4). Instead, we use PartMC to model emissions of PAH coated soot particles with a realistic size distribution (see Sect. 3.2 for details) and add terms for heterogeneous chemistry. The equivalent of Eq. (3.2) thus reads:

$$\begin{aligned}\frac{\partial n(\vec{\mu}, t)}{\partial t} = \underbrace{\dot{n}_{\mathrm{emit}}(\vec{\mu}, t)}_{\text{emission}} + \underbrace{\sum_{i=1}^{C+1} \frac{\partial}{\partial \mu_i}\left(c_i J_{\mathrm{ads}}(\vec{\mu}, \vec{g}, t)\, S(\vec{\mu})\, n(\vec{\mu}, t)\right)}_{\text{adsorption}} \\ \underbrace{- \sum_{i=1}^{C+1} \frac{\partial}{\partial \mu_i}\left(c_i J_{\mathrm{des}}(\vec{\mu})\, S(\vec{\mu})\, n(\vec{\mu}, t)\right)}_{\text{desorption}} + \underbrace{R_{\mathrm{surf}}(\vec{\mu}, \vec{g})}_{\text{surface reactions}} \quad .\end{aligned} \tag{3.3}$$

Some subtle differences in the definitions have to be noted here: C is now the number of adsorbing gas species and water vapor is not written out explicitly anymore, c_i is now the conversion factor from molecules $\mathrm{cm^{-2}\,s^{-1}}$ to $\mathrm{kg\,cm^{-2}\,s^{-1}}$ ($\mathrm{kg\,molec.^{-1}}$), and $J_{\mathrm{ads}}(\vec{\mu}, \vec{g}, t)$ and $J_{\mathrm{des}}(\vec{\mu})$ ($\mathrm{molec.\,cm^{-2}\,s^{-1}}$) are now surface area-weighted average adsorption and desorption fluxes onto and from all particles in the population. $S(\vec{\mu})$ ($\mathrm{cm^2}$) stands for total particle surface area and $R_{\mathrm{surf}}(\vec{\mu}, \vec{g})$ ($\mathrm{m^{-3}\,kg^{-A}\,s^{-1}}$) summarizes all the heterogeneous reactions considered here (Tab. 3.1). It should also be noted that the newly introduced terms in Eq. (3.3) are actually computed within MOSAIC (see next subsection).

The emission rate $\dot{n}_{\mathrm{emit}}(\vec{\mu}, t)$ can be prescribed to change at specified times. The number of particles added to the air parcel at one time step $t_i \rightarrow t_j$ is

assumed to be Poisson distributed around a mean value of

$$\overline{N} = \int_0^\infty \int_0^\infty \dots \int_0^\infty \underbrace{\left(\int_{t_i}^{t_j} \dot{n}_{\text{emit}}(\vec{\mu}, t) dt \right)}_{\approx (t_j - t_i)\, \dot{n}_{\text{emit}}(\vec{\mu}, t_i)} d\mu_1 d\mu_2 \dots d\mu_A. \tag{3.4}$$

Hence, at every time step, a sample of S particles with a composition determined by $n_{\text{emit}}(\vec{\mu}) = (t_j - t_i)\, \dot{n}_{\text{emit}}(\vec{\mu}, t_i)$ is added with a probability

$$p(S = k) = \frac{\overline{N}^k e^{-\overline{N}}}{k!}. \tag{3.5}$$

At each time step current values of environmental parameters, gas concentrations and particle compositions are passed to MOSAIC which computes adsorption, desorption, and chemical reactions on the particles as well as in the gas phase and returns updated values to PartMC.

3.1.2 MOSAIC

MOSAIC is a deterministic aerosol model that includes treatment of internal physical and chemical processes within particles. It consists of four modules that were also designed for high computational efficiency. Even though we only use the first one here, a brief description of all four of them shall be given.

CBM-Z, a revised Carbon Bond Mechanism (Zaveri and Peters, 1999), is MOSAIC's gas phase solver. In the version we use, it includes 77 reactive gas species plus water vapor in a lumped structure. For instance, in addition to the explicitly resolved organic peroxides, CH_3OOH (methyl hydrogen peroxide) and C_2H_5OOH (ethyl hydrogen peroxide) there is another "species", ROOH (higher organic peroxides). The gases are subjected to 15 photolytic and 172 other reactions.

MTEM, the Multicomponent Taylor Expansion Method, calculates approximate activity coefficients of electrolytes in aqueous solutions that are required to determine the gas-particle partitioning of semi-volatile species (Zaveri et al., 2005b).

MESA, the Multicomponent Equilibrium Solver for Aerosols, determines the partitioning of species between solid and liquid phases within aerosol particles

which is important to accurately represent their deliquescence growth behavior (Zaveri et al., 2005a).

ASTEM, the Adaptive Step Time-Split Euler Method, is used to calculate gas-particle partitioning, i.e., condensation of non-volatile species on the aerosol particles as well as condensation and evaporation of semi-volatile species (Zaveri et al., 2008).

MOSAIC can be operated as either a sectional or a modal model. In PartMC-MOSAIC the sectional approach is used and an individual bin is assigned to each of the particles regardless of its size or composition. This is done in order to maintain the full information about every single particle while handing them back and forth between PartMC and MOSAIC.

An analogous integrodifferential equation to Eq. 3.2 underlies PartMC-MOSAIC's treatment of gas phase chemistry:

$$\begin{aligned}\frac{dg_i(t)}{dt} = &\underbrace{\dot{g}_{\mathrm{emit},i}(t)}_{\text{emission}} + \underbrace{R_{\mathrm{gas},i}(\vec{g})}_{\text{gas phase reactions}} \\ &\underbrace{- \int_0^\infty \int_0^\infty \cdots \int_0^\infty I_i(\vec{\mu},\vec{g},t)\cdot n(\vec{\mu},t)\, d\mu_1\, d\mu_2 \ldots d\mu_A}_{\text{condensation / evaporation}} \\ &\underbrace{+ \lambda_{\mathrm{dil}}(t)\Big(g_{\mathrm{back},i}(t) - g_i(t)\Big)}_{\text{dilution}} + \underbrace{\frac{1}{\rho_{\mathrm{dry}}(t)}\frac{d\rho_{\mathrm{dry}}(t)}{dt} g_i(t)}_{\text{air density change}} \ .\end{aligned} \tag{3.6}$$

Here, $\dot{g}_{\mathrm{emit},i}(t)$ ($\mathrm{mol\,m^{-3}\,s^{-1}}$) is the emission rate of gas species X_i, $g_{\mathrm{back},i}(t)$ ($\mathrm{mol\,m^{-3}}$) is the background concentration of X_i, and $R_{\mathrm{gas},i}(\vec{g})$ ($\mathrm{mol\,m^{-3}\,s^{-1}}$) is the concentration growth rate of X_i due to gas chemical reactions (Riemer et al., 2009).

In our present study we use only one of MOSAIC's modules, namely CBM-Z, for the same reasons that we neglected many of the terms in Eq. (3.2), i.e., to keep our focus on the effects of heterogeneous chemistry. For consistency we therefore omit the last three terms of Eq. (3.6) and replace them with expressions corresponding to the terms introduced in Eq. (3.3). The resulting equation is then solved by the extended CBM-Z mechanism (see next subsection) within MOSAIC.

3.1.3 Heterogeneous chemistry

As mentioned above, PartMC-MOSAIC has been extended for the present study to also treat the processes involved in the heterogeneous reactions summarized in Tab. 3.1. Although CBM-Z previously included loss of several adsorbing gases to aerosol particles, the associated changes in particle composition were not recorded. Moreover, constant uptake coefficients were assumed for these species regardless of particle composition and changes thereof. The only included surface processes were three catalytic reactions known to take place on atmospheric particles, such as the N_2O_5 hydrolysis described by reaction (2.22).

The new extension allows PartMC-MOSAIC to store the amount of adsorbed gas species and treat heterogeneous reactions within and between two surface layers based on the PRA framework (Sect. 2.3.1). Thus, uptake of trace gases is now dynamically adjusted according to the particles' surface composition.

A selection of the files in which major changes to the code of PartMC-MOSAIC were made, can be found in the appendix.

3.2 Model system

We model diesel soot particles coated with one monolayer of PAHs which we treat as one species (termed PAH in the following). For its molecular weight and cross section we use the values of pyrene ($C_{16}H_{10}$) as one of the most abundant PAHs found in the particulate phase of diesel exhaust (e.g., Pakbin et al., 2009; Kashiwakura and Sakamoto, 2010), which can serve as a representative with somewhat average values: $M_{\mathrm{PAH}} = 202.3\,\mathrm{g\,mol^{-1}}$ and $\sigma_{\mathrm{PAH}} = 8 \cdot 10^{-15}\,\mathrm{cm^2}$. The latter is an estimation based on the assumption cited in Shiraiwa et al. (2009) that each benzene ring — of which pyrene has four — contributes $2\,\mathrm{nm^2}$.

In our simulations, O_3(g), NO_2(g), and H_2O(g) compete for adsorption on reactive surface sites. Subsequently, O_3(s) and NO_2(s) undergo the surface layer reactions summarized in Tab. 3.1 where reaction rates are also given. Y_j are nonvolatile oxidation and, possibly, nitration products of PAH whose exact chemical structure is not known (Springmann et al., 2009; Shiraiwa et al., 2009). H_2O(s) does not react chemically in our scenarios.

NO_3(s) radicals produced by SLR6 between O_3(s) and NO_2(s) (Tab. 3.1) may desorb or react via SLR7 with PAH here. OH(g) and NO_3(g) radicals from the gas phase are considered to undergo gas-surface reactions which are

also given in Tab. 3.1 along with the corresponding reaction probabilities.

The values of all necessary physicochemical parameters that we use are listed in Tab. 3.2.

Table 3.1: Heterogeneous reactions considered in this study and corresponding reaction rate constants and reaction probabilities. Note that on the products side of the reactions only relevant species are given here.

Surface layer reaction		Rate constant [$\mathrm{cm^2\ s^{-1}}$]
(SLR1)	$\mathrm{O_3(s) + PAH(ss) \rightarrow Y_2(ss)}$	$k_{\mathrm{SLR1,O_3,PAH}} = 2.7 \cdot 10^{-17\,a}$
(SLR2)	$\mathrm{O_3(s) + Y_2(ss) \rightarrow Y_3(ss)}$	$k_{\mathrm{SLR2,O_3,Y_2}} = 2.7 \cdot 10^{-19\,b}$
(SLR3)	$\mathrm{O_3(s) + Y_3(ss) \rightarrow Y_4(ss)}$	$k_{\mathrm{SLR3,O_3,Y_3}} = 2.7 \cdot 10^{-21\,b}$
(SLR4)	$\mathrm{NO_2(s) + Y_2(ss) \rightarrow Y_5(ss)}$	$k_{\mathrm{SLR4,NO_2,Y_2}} = 7.0 \cdot 10^{-18\,b}$
(SLR5)	$\mathrm{NO_2(s) + Y_3(ss) \rightarrow HONO(g)}$	$k_{\mathrm{SLR5,NO_2,Y_3}} = 7.5 \cdot 10^{-21\,b}$
(SLR6)	$\mathrm{O_3(s) + NO_2(s) \rightarrow NO_3(s)}$	$k_{\mathrm{SLR6,O_3,NO_2}} = 5 \cdot 10^{-17\,a}$
(SLR7)	$\mathrm{NO_3(s) + PAH(ss) \rightarrow Y_6(ss)}$	$k_{\mathrm{SLR7,NO_3,PAH}} = 5 \cdot 10^{-15\,a}$
Gas-surface reaction		Reaction probability
(GSR1)	$\mathrm{OH(s) + PAH(ss) \rightarrow Y_7(ss)}$	$\gamma_{\mathrm{GSR1,OH,PAH}} = 0.32^{c}$
(GSR2)	$\mathrm{NO_3(s) + PAH(ss) \rightarrow Y_8(ss)}$	$\gamma_{\mathrm{GSR2,NO_3,PAH}} = 0.79^{d}$

[a] Shiraiwa et al. (2009); [b] adapted from Ammann and Pöschl (2007); [c] Bertram et al. (2001); [d] Gross and Bertram (2008)

3.3 Steady state assumption

Adsorption rates in the scenarios considered here are always at least about three orders of magnitude higher than the reaction rate of the fastest surface layer reaction. The same holds for desorption rates of these species ($\mathrm{O_3(s)}$, $\mathrm{NO_2(s)}$, $\mathrm{H_2O(s)}$). Hence, an equilibrium of the physical processes is achieved quickly compared to the time scales of the chemical reactions. We therefore assume the sorption layer concentrations of adsorbing species to be in steady state:

$$\frac{d[\mathrm{X}_i]_\mathrm{s}}{dt} = \underbrace{J_{\mathrm{ads,X}_i}}_{\text{adsorption}} - \underbrace{J_{\mathrm{des,X}_i}}_{\text{desorption}} - \underbrace{L_{\mathrm{s,s,X}_i} - L_{\mathrm{s,ss,X}_i}}_{\text{chemical loss}} = 0\ , \tag{3.7}$$

where $\mathrm{X}_i = \mathrm{O_3(s), NO_2(s), H_2O(s)}$.

Table 3.2: Physicochemical parameters used in this study.

Species (X_i)	$\alpha_{s,0,X_i}$	σ_{X_i} [cm^2]	τ_{d,X_i} [s]	D_{g,X_i} [hPa cm^2 s^{-1}]
O_3	10^{-3} [a]	$1.7 \cdot 10^{-15}$ [a]	10^a	—
NO_2	$6.4 \cdot 10^{-2}$ [b]	$3.0 \cdot 10^{-15}$ [c]	$5 \cdot 10^{-2}$ [a]	—
H_2O	$4 \cdot 10^{-4}$ [d]	$1.08 \cdot 10^{-15}$ [e]	$3.6 \cdot 10^{-4}$ [a]	—
OH	—	—	—	217 [f]
NO_3	—	$1.7 \cdot 10^{-15}$ [g]	10^a	107 [h]

[a] Shiraiwa et al. (2009); [b] Tabor et al. (1994); [c] Ammann and Pöschl (2007); [d] Rogaski et al. (1997); [e] Nishino (2001); [f] Ivanov et al. (2007); [g] as in Shiraiwa et al. (2009), personal communication; [h] Rudich et al. (1996)

Additionally, NO_3(s) production, desorption and chemical loss equilibrate quickly compared to the time scales on which quasi-static surface layer species concentrations ($[Y_j]_{ss}$) change so that we can also assume steady state for $[NO_3]_s$:

$$\frac{d[NO_3]_s}{dt} = \underbrace{P_{s,s,NO_3}}_{\text{chemical production}} - \underbrace{J_{des,NO_3}}_{\text{desorption}} - \underbrace{L_{s,ss,NO_3}}_{\text{chemical loss}} = 0 \tag{3.8}$$

The three equations (3.7), together with Eq. (3.8), allow us to determine $[X_i]_s$ ($X_i = O_3(s), NO_2(s), H_2O(s), NO_3(s)$) from the $[Y_j]_{ss}$, which define the production and loss terms. Thus, we can set the time step for our simulations according to reaction time scales which greatly reduces computation time since the very fast process of adsorption would otherwise require a much higher temporal resolution.

Control runs without steady state assumptions and four to five orders of magnitude shorter time steps showed very good agreement with the steady state calculations after one simulated minute. Thus, while accuracy of our results is not significantly influenced by this assumption, it greatly reduces computational cost.

3.4 Scenario setups

Our modeling approach can be pictured as an air parcel floating into and over a region of urban pollution where it is followed for 24 hours. The prescribed mixing height of $h = 400$ m is used to convert the emission rates in Tab. 3.3 from values per unit area to values per unit volume. Background trace gas concentrations used for initialization of the air parcel's gas phase composition

are taken from Riemer et al. (2009) and also given in Tab. 3.3.

Table 3.3: Initial trace gas concentrations and emissions applied in this study (table adapted from Riemer et al. (2009)).

Species	Symbol	Initial concentration [ppb]	Emissions [$\mathrm{nmol\,m^{-2}\,s^{-1}}$]
Nitric oxide	NO	0.1	31.8[a]
Nitrogen dioxide	NO_2	1.0	1.67[a]
Nitric acid	HNO_3	1.0	-
Ozone	O_3	50.0	-
Hydrogen peroxide	H_2O_2	1.1	-
Carbon monoxide	CO	21	291.3
Sulfur dioxide	SO_2	0.8	2.51
Ammonia	NH_3	0.5	6.11
Hydrogen chloride	HCl	0.7	-
Methane	CH_4	2200	-
Ethane	C_2H_6	1.0	-
Formaldehyde	HCHO	1.2	1.68
Methanol	CH_3OH	0.12	0.28
Methyl hydrogen peroxide	CH_3OOH	0.5	-
Acetaldehyde	ALD2	1.0	0.68
Paraffin carbon	PAR	2.0	96
Acetone	AONE	1.0	1.23
Ethene	ETH	0.2	7.2
Terminal olefin carbons	OLET	$2.3 \cdot 10^{-2}$	2.42
Internal olefin carbons	OLEI	$3.1 \cdot 10^{-4}$	2.42
Toluene	TOL	0.1	4.04
Xylene	XYL	0.1	2.41
Lumped organic nitrate	ONIT	0.1	-
Peroxyacetyl nitrate	PAN	0.8	-
Higher organic acid	RCOOH	0.2	-
Higher organic peroxide	ROOH	$2.5 \cdot 10^{-2}$	-
Isoprene	ISOP	0.5	0.23
Alcohols	ANOL	-	3.45

[a] We actually use different rates for NO_x emissions as explained in the text.

For the geographical location of the modeling site, whose latitude along with the time of year determines the diurnal pattern of insolation, and thus photochemistry, we choose representative midlatitude coordinates. All simulations are conducted for a summer day because photochemical pollution attains

its highest levels during that season. We begin the simulations at both 6:00 am and 6:00 pm to assess the different effects of the gas phase on particles emitted during day and during night. Environmental parameters are kept constant at $T = 293\,\mathrm{K}$ and $p = 1013.25\,\mathrm{hPa}$.

Soot particles in our model have spherical shape and are emitted with a lognormal size distribution. Its median diameter of $d_\mathrm{p} = 50\,\mathrm{nm}$ (or $\log d_\mathrm{p} = -1.3$) together with a width of $\log \sigma = 0.24$ are representative of diesel soot (Riemer et al., 2009), and place the particles in the accumulation mode. The particles are emitted at a "constant" rate (one Poisson sample at every time step, as explained in Section 3.1.1) during the 24 simulated hours. For each of our scenarios (S1 - S4, see Tab. 3.4) we use a low and a high soot emission rate chosen in such a way to yield final concentrations of $0.1\,\mu\mathrm{g\,m^{-3}}$ and $10\,\mu\mathrm{g\,m^{-3}}$, respectively. Thus, we are able to determine the effect of different emission rates on both trace gas concentrations and average particle properties.

Table 3.4: Definition of scenarios (S1 - S4) considered in this study and simulation specifiers ('-am/-pm' for simulations started at 6:00 am and 6:00 pm, respectively, and '-lo/-hi' for simulations with low and high soot emissions, respectively).

Simulation	RH [%]	NO_x emission level	start time	soot emission level
S1-am-lo	30	low	6:00 am	low
S1-am-hi	30	low	6:00 am	high
S1-pm-lo	30	low	6:00 pm	low
S1-pm-hi	30	low	6:00 pm	high
S2-am-lo	30	high	6:00 am	low
S2-am-hi	30	high	6:00 am	high
S2-pm-lo	30	high	6:00 pm	low
S2-pm-hi	30	high	6:00 pm	high
S3-am-lo	80	low	6:00 am	low
S3-am-hi	80	low	6:00 am	high
S3-pm-lo	80	low	6:00 pm	low
S3-pm-hi	80	low	6:00 pm	high
S4-am-lo	80	high	6:00 am	low
S4-am-hi	80	high	6:00 am	high
S4-pm-lo	80	high	6:00 pm	low
S4-pm-hi	80	high	6:00 pm	high

Concerning the gas phase we distinguish between scenarios with a low relative humidity (RH) of 30% (scenarios S1 and S2, see Tab. 3.4) and a high RH of 80% (S3 and S4, Tab. 3.4), i.e., $6.9 \cdot 10^3$ ppm and $1.8 \cdot 10^4$ ppm of water vapor in the air. We consider different RH levels because competitive co-adsorption of H_2O was shown by Springmann et al. (2009) to make a profound difference in PAH degradation. Emission rates of trace gases given in Tab. 3.3 are based on measurements during the Southern California Air Quality Study in 1988. These emissions lead to a high NO_x regime, where peak $[O_3]_g$ decreases with increasing NO_x emissions. In order to obtain a low NO_x scenario, too, we multiply the corresponding rates by 0.1. This is done to examine the effects of different oxidant levels in general and also because simulations by Saathoff et al. (2001) for the two different photochemical regimes yielded considerably different results. Together, RH and NO_x emission levels define the four scenarios S1 - S4 (Tab. 3.4) that we simulated.

All simulations were conducted using 300 particles on average. As particles are constantly added through emissions and we do not consider any particle loss processes, this number would continuously rise. However, memory limitations inhibit simulations of more than about 700 particles at the same time on an ordinary desktop computer. Thus, half of the particles are selected randomly and discarded once their total number exceeds 600, so that we cannot keep track of every single emitted particle. In order to reduce the errors introduced by the combination of relatively small particle numbers and deletion of random samples, we conducted each of the 16 simulations (Tab. 3.4) at least eleven times and averaged over all these runs for determination of population-related quantities. Note that the removal of particles does not lead to a difference in soot concentrations because the computational volume is reduced at the same time.

To keep computation time reasonable we used a time step of one minute for all our simulations. Because this is not short enough to resolve the time scale of adsorption we assume steady state for sorption layer species as described in Sect. 3.3. Compared to the time scales of the chemical reactions considered in this study, one minute is short enough to reasonably resolve the chemistry. This has been verified by comparing simulation results to previously published data (Ammann and Pöschl, 2007; Springmann et al., 2009). However, there is one notable exception: SLR6 between NO_3(g) and PAH(ss) proceeds too rapidly at high (nighttime) $[NO_3]_g$ (see discussion in the next chapter). Hence, we use an approximation to determine surface species concentrations if $[PAH]_{ss}$ decreases by more than 80% of its initial value during the first time step of a particle's lifetime.

4. Results and Discussion

Heterogeneous chemical reactions on PAH coated soot surfaces are simulated to determine corresponding changes in surface composition and to assess their feedback on the gas phase. These simulations primarily serve as a tool to determine the specific effects of different water vapor and oxidant concentrations on the efficiency of the modeled reactions. The secondary goal is to give a sense of the orders of magnitude to be expected for degradation of particle-bound PAHs and removal of trace gases from the gas phase by surface reactions. This study is the first to assess the importance of heterogeneous reactions in an urban polluted area on a particle-resolved basis.

In the first two sections of this chapter background information on the gas phase chemistry and composition in our scenarios is provided and individual particles' fates are discussed. Insight gained on this particle-by-particle level is then applied in the discussion of soot population properties in sections 4.5 - 4.7. Throughout this analysis it should be kept in mind that, even though our simulation scenarios represent realistic conditions, the model still uses highly idealized assumptions.

4.1 Gas phase without particles

Since the concentrations of heterogeneously reacting gases in scenarios S1 and S3 evolve almost identically over the course of the simulated time and since S2 resembles S4, too, we only discuss results for the two extreme scenarios S1 and S4 here (Figs. 4.1 and 4.2, respectively). The most important difference between these two scenarios is in the absolute concentration levels of O_3(g), NO_2(g), OH(g) and NO_3(g). Qualitatively, the behavior of the species' concentrations is similar in both scenarios while $[O_3]_g$ is higher in the morning in S1 but does not rise as high as in S4 and $[NO_2]_g$ shows a more pronounced overall upward trend in S4-pm than in S1-pm. Note that identifiers '-lo' and '-hi' are omitted here because no soot emissions are considered in this discussion of the reference gas phase.

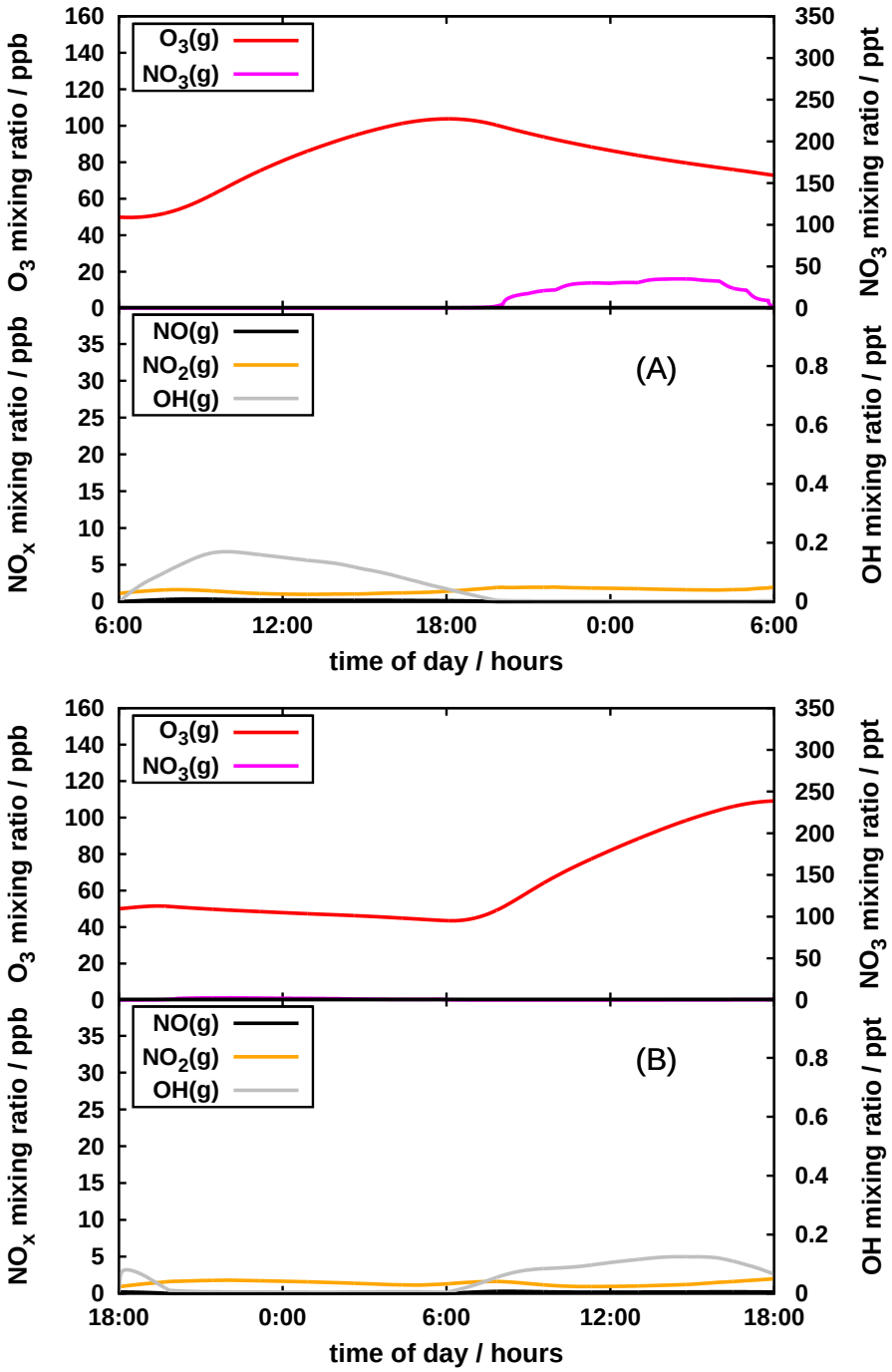

Figure 4.1: Gas phase evolution in scenario S1 (low RH and low NO_x emissions) without soot emissions. Simulations were started at 6:00 am (S1-am, panel A) and 6:00 pm (S1-pm, panel B).

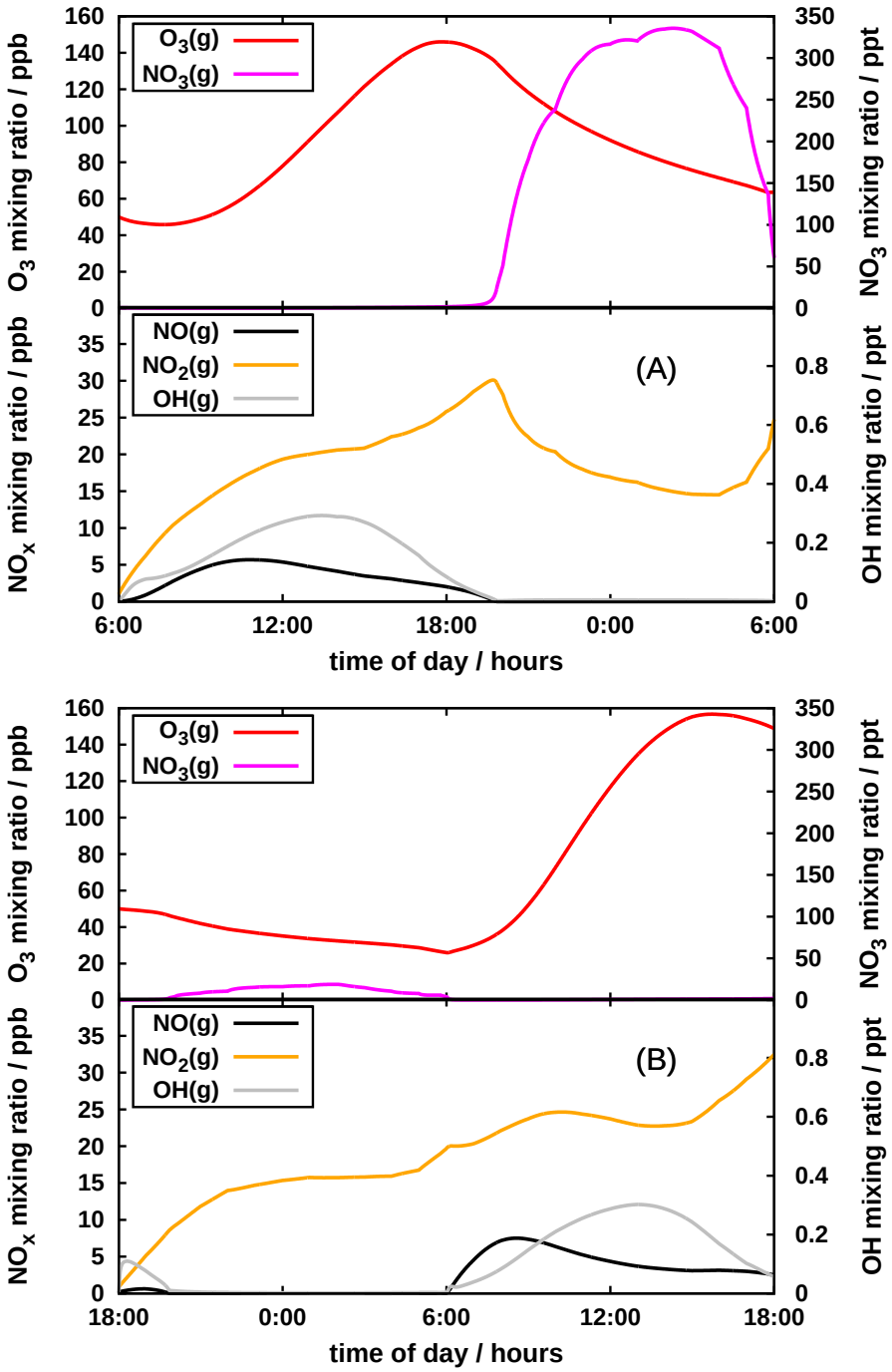

Figure 4.2: Gas phase evolution in scenario S4 (high RH and high NO_x emissions) without soot emissions. Simulations were started at 6:00 am (S4-am, panel A) and 6:00 pm (S4-pm, panel B).

Three typical diurnal cycles are clearly visible in Figs. 4.1 and 4.2.

- O_3(g) behaves as described in Sect. 2.1.2 ("Photochemistry"), with low concentrations in the early morning and concentration peaks in the late afternoon.
- OH(g) is only produced by photolytic reactions and its concentration quickly drops to very low levels at night due to its high reactivity.
- Lastly, NO_3(g) shows the complementary evolution to OH(g) because it is quickly destroyed by photolysis during day but can build up to higher concentrations during night.

Both $[NO]_g$ and $[NO_2]_g$ behave similarly in all four simulations shown in Figs. 4.1 and 4.2. Note that since $[NO]_g$ is very small throughout the simulations in scenario S1, its changes can hardly be detected in Fig. 4.1 but we kept the scale as in Fig. 4.2 to facilitate comparison of the two scenarios.

After sunset NO is depleted by reaction with O_3 and no longer replenished efficiently once photolysis of NO_2 stops and emissions decrease. The rise in $[NO_2]_g$ towards nightfall can be explained in part by a decrease in photolysis. Moreover, the highest VOC concentrations of the day (not shown) are attained during that time and therefore NO oxidation becomes most efficient. At night, however, as NO_x emissions decrease and NO_3(g) builds up, NO_2 is efficiently converted to N_2O_5 via reaction (2.21) with NO_3(g). Steps in the evolution of $[NO_3]_g$ are due to hourly changes in the emission rate of NO and the subsequent chemistry of nitrogen oxides.

Due to lower NO_x emissions at night and no prior buildup of pollutants in the air parcel in simulations started at 6:00 pm, NO_3(g) and O_3(g) concentrations are lower during night for S1-pm and S4-pm than in the corresponding scenarios started at 6:00 am. NO_2(g), however, can reach just as high concentrations at the end of these simulations as at 6:00 pm in the simulations started in the morning. The reason for this is that NO_2(g) attains higher than background levels at sunrise in the simulations that start at 6:00 pm due to nightly reaction of O_3 and NO (reaction (2.11)).

The relative magnitude of the three adsorbing species' gas phase concentrations (O_3, NO_2, and H_2O) determine their contributions to surface composition, which will be discussed in the next section. As described in Sect. 3.2, $[H_2O]_g$ is constant at $6.9 \cdot 10^3$ ppm or $1.8 \cdot 10^4$ ppm for low and high RH scenarios, respectively. Hence, adsorbate concentrations will be determined by $[O_3]_g$ and $[NO_2]_g$ as well as by reactions on the surface.

Peak $[O_3]_g$ ranges from about 100 ppb in S3-am (not shown) to about 160 ppb in S4-pm and is always attained roughly between 3:00 pm and 6:00 pm.

For $[NO_2]_g$, peak values occur around sunset and vary between about 2 ppb for any of the low NO_x emission simulations and about 40 ppb in S2-pm (not shown).

$[OH]_g$ and $[NO_3]_g$ peak roughly in the middle of the day and night, respectively, which is where we expect them to impact PAH degradation most strongly. Maximum values lie between 0.1 ppt (S1-pm) and 0.3 ppt (S4-pm) for OH and 2 ppt (S3-pm, not shown) and almost 350 ppt for NO_3 (S4-am).

Overall, our scenarios represent polluted conditions with highly elevated O_3 concentrations characteristic of photochemical smog episodes. NO_x levels do not reach extreme values but are also clearly higher than under background conditions. The typical diurnal cycle of $[O_3]_g$ is well reproduced (cf. Fig. 2.1) and OH and NO_3 concentrations also agree nicely with atmospheric measurements (e.g., Finlayson-Pitts and Pitts, 2000; Emmerson et al., 2005; Seinfeld and Pandis, 2006; Dusanter et al., 2009, and references therein).

4.2 Individual particles

4.2.1 Surface composition

To illustrate the evolution of surface composition on individual particles, Fig. 4.3 shows the results of simulations of only one particle each, emitted at 6:00 am. Subsequent soot emissions were switched off here because, as described in Sect. 3.4, they lead to removal of particles. This means that in many model runs one cannot find a single particle that was present throughout the entire simulation.

Note, however, that we do track the evolution of every individual particle emitted at any time as long as it exists in the simulation. Surface composition on particles emitted during times with different levels of adsorbing gas concentrations can differ considerably from what Fig. 4.3 shows. This has to be kept in mind during the discussion in the following sections where the soot population as a whole is considered.

We use logarithmic axes in Fig. 4.3 because surface species concentrations span several orders of magnitude and because their evolution proceeds much more quickly during the first few minutes than during the rest of the simulation. Surface species that are not shown in Fig. 4.3 are omitted because their concentrations do not yield much more insight but would instead make the plots more difficult to read.

As can be seen by comparing Fig. 4.3 with Figs. 4.1 and 4.2, surface concentrations $[O_3]_s$ and $[NO_2]_s$ closely follow the corresponding gas phase

concentrations, accompanied by a lowering of $[H_2O]_s$ where $[O_3]_s$ reaches its peak value. This is due to competitive co-adsorption of the three gases and the relative increase in $[O_3]_g$ against $[H_2O]_g$. The initial monolayer of PAH on the particles shown in Fig. 4.3 is depleted mainly by O_3 via reaction SLR1, forming Y_2, which is subsequently consumed by the slower reactions with both O_3 and NO_2. PAH half-life is roughly 9 min for all particles shown in Fig. 4.3.

Note that we report half-life here — instead of the more common lifetime — because, as mentioned above, we have to remove particles from the simulation several times when we turn on emissions. Thus, we cannot track all particles until their $[PAH]_{ss}$ reaches e^{-1} of its original value. We may still lose particles before they reach $0.5 \cdot [PAH]_{ss}(t{=}0)$ but that loss will be significantly smaller and the results correspondingly more accurate.

The particles shown in Fig. 4.3 display a similar evolution of quasi-static surface layer species (PAH and Y_j) because that evolution is mainly defined by initial PAH depletion. Since, for the first few minutes, the relevant gas phase species have very similar concentrations in all scenarios because we start out with the same background conditions, this initial depletion proceeds almost identically for all particles in Fig. 4.3. However, SLR2 with O_3 and SLR4 with NO_2 deplete Y_2 more quickly at later times in the simulations of scenarios with high NO_x emissions (S2 and S4).

Although the accommodation coefficient $\alpha_{s,0,NO_2}$ for NO_2 is an order of magnitude higher than that for O_3 (Tab. 3.2), $[NO_2]_s$ is much smaller than $[O_3]_s$ because of the combined effects of a lower NO_2 gas phase concentration and a much shorter desorption lifetime $\tau_{d,NO_2} \ll \tau_{d,O_3}$ (50 ms and 10 s, respectively, see Tab. 3.2).

The effect of higher RH can be seen by comparison of $[H_2O]_s$ in the upper two panels of Fig. 4.3 with the lower two. Clearly, higher water vapor concentrations lead to higher $[H_2O]_s$, thus offsetting $[O_3]_s$.

A striking feature of Fig. 4.3 is the relatively high concentration that Y_8, the product of reaction GSR2 between PAH and NO_3(g), reaches even on these particles which are emitted at a time where $[NO_3]_g$ is very small (about 1 ppt, see also Figs. 4.1 and 4.2). Although GSR2 does not have a significant influence on PAH degradation on the particles shown in Fig. 4.3, the buildup of relatively high $[Y_8]_{ss}$ already indicates that GSR2 is a very efficient oxidation process for particle-bound PAH. Indeed, as we will see in Sect. 4.4, PAH half-life is largely determined by the reaction with NO_3(g) when $[NO_3]_g$ reaches its peak levels. The quasi-static surface layer of particles emitted during such peak times will consist almost entirely of Y_8 within time scales on the order of a minute or less, meaning that $[Y_8]_{ss} \sim 10^{14}\,\mathrm{cm}^{-2}$ because essentially all the initially present PAH(ss) will be converted to Y_8(ss).

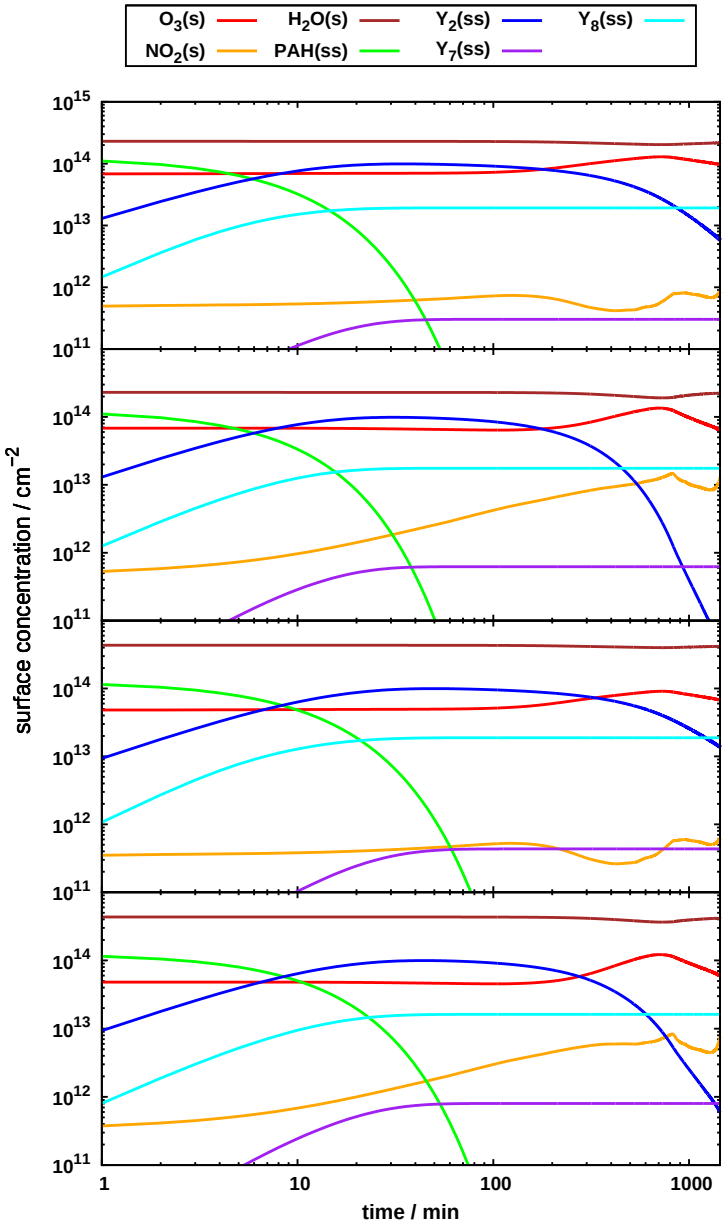

Figure 4.3: Surface composition of individual particles that are emitted at the beginning of the respective simulations. Panels represent, from top to bottom, simulations S1-am with low RH and low NO_x emissions, S2-am with low RH and high NO_x emissions, S3-am with high RH and low NO_x emissions, and S4-am with high RH and high NO_x emissions. All simulations shown were started at 6:00 am and were run without further soot emissions. Note the logarithmic time axis.

Note that the size of a particle can play a role here, too, since the diffusion correction factor C_{g,NO_3} has values as low as 0.8 for some of the particles in our size distribution. Thus, the flux of molecules hitting the surface is decreased by up to 20% on a large particle compared to a small one, which will decrease the reaction rate of GSR2 by the same fraction. This translates to a less efficient degradation of PAH by NO_3(g). However, that difference is only significant in cases where GSR2 and SLR1 proceed at roughly the same rates. For most times, this is not the case because during day SLR1 dominates GSR2 and during night GSR2 by far dominates SLR1 (as described again in Sect. 4.4).

GSR1, involving OH, does not significantly affect oxidation of surface-bound PAH although OH is the most reactive species in atmospheric gas phase chemistry. The small yield of the reaction product of GSR1, Y_7, reflects its small contribution to PAH(ss) degradation. This apparently counterintuitive result will be explained in more detail in Sect. 4.4. SLR7 is even less efficient in degrading PAH(ss) because of the very low concentrations of NO_3(s) (one to two orders of magnitude less than $[NO_2]_s$, not shown in Fig. 4.3).

Since $[O_3]_s$ and $[NO_2]_s$ follow $[O_3]_g$ and $[NO_2]_g$, respectively, their gas phase evolution can be deduced from Fig. 4.3. Thus, the similar gas phases of S1 and S3 and of S2 and S4 mentioned in the previous section are reflected in Fig. 4.3.

A straightforward comparison with previous studies is not possible here because the considered systems and choices of parameters differ. Ammann and Pöschl (2007) and Shiraiwa et al. (2009) simulated constant gas phase scenarios and Springmann et al. (2009) used considerably different desorption lifetimes for NO_2 and H_2O. Qualitatively, however, we see similar surface composition evolution on our particles as Shiraiwa et al. who considered a similar system to the one studied here. Parallels to the work of Springmann et al. are also visible, e.g., $[O_3]_s$ and $[NO_2]_s$ following the corresponding gas phase concentrations, and $[H_2O]_s$ staying relatively constant over most of the simulated time. Absolute values, however, differ strongly, because the shorter desorption lifetimes employed in our study lead to much lower surface concentrations of H_2O and NO_2 and we also consider additional heterogeneous reactions here.

4.2.2 Effective uptake coefficients

Since adsorption of O_3 and NO_2 into the sorption layer proceeds very quickly we cannot resolve the initial evolution of the corresponding uptake coefficients during the first minute of a particle's atmospheric lifetime. Thus, after the first minute, where the time axis in Fig. 4.4 starts, an equilibrium between reversible adsorption and desorption is already established, i.e., γ'_{O_3} has already

dropped from $\alpha_{s,0,O_3} = 10^{-3}$ to $\sim 10^{-5}$ and γ'_{NO_2} from $\alpha_{s,0,NO_2} = 6.4 \cdot 10^{-2}$ to $\sim 5 \cdot 10^{-6}$. These two effective uptake coefficients are therefore determined entirely by surface layer reactions on the timescales resolved in our simulations. This is evident in Fig. 4.4 where γ'_{O_3} initially tracks the evolution of $[PAH]_{ss}$ (Fig. 4.3) and later that of $[NO_2]_s$ (Fig. 4.3) when reaction SLR6 with NO_2(s) takes over from SLR1 with PAH(ss) as the major sink for O_3(s). Similarly, γ'_{NO_2} follows $[O_3]_s$ because SLR6 is also the major sink for NO_2(s).

Effective uptake coefficients for OH and NO_3 basically follow the $[PAH]_{ss}$ evolution. As total sorption layer coverage is almost constant over the entire simulated time, $\theta_{ss,PAH}$ is the only changing factor in the definition of γ'_{OH} and γ'_{NO_3} (Eq. (2.26)).

This interpretation of effective uptake coefficient evolution on individual particles is applicable to particles emitted at any time during a simulation. The qualitative behavior does not change. However, relative gas phase concentrations of O_3 and NO_2 have an influence on relative values of the corresponding effective uptake coefficients and co-adsorbing water vapor affects the absolute values of all effective uptake coefficients discussed here. It depresses γ'_{O_3} and γ'_{NO_2} by occupying more sorption sites at high RH, i.e., in S3 and S4, than at low RH (in S1 and S2). The same initially applies to effective uptake coefficients for OH and NO_3. However, at later times in the simulation, an increase in γ'_{OH} and γ'_{NO_3} with RH is observed because the blocking of sorption sites by H_2O molecules decreases the speed of PAH depletion. This enables more of the OH and NO_3 molecules colliding with the surface to react with it at later times. All these effects can be seen in Fig. 4.4.

Furthermore, in terms of quantitative changes, the time scales on which SLR6 becomes the major sink for O_3(s) and on which γ'_{OH} and γ'_{NO_3} decline differ for particles emitted during times of different gas phase composition. For instance, PAH on particles emitted during night, when $[NO_3]_g$ levels are high, can be much more rapidly depleted than during day, thus leading to much quicker decline in both γ'_{OH} and γ'_{NO_3}.

As mentioned before, large-scale models often employ constant uptake coefficients to account for heterogeneous chemistry. Our results clearly show that this assumption is not justified in all cases. Even γ'_{NO_2}, which stays rather constant throughout the course of our simulations, drops by about four orders of magnitude within the first minute as described above. γ'_{O_3} drops by roughly two orders of magnitude during the first minute and can decrease by two more over the simulated 24 hour period, depending on the gas phase evolution. Effective uptake coefficients for OH and NO_3 exhibit an even stronger decline in the simulations shown in Fig. 4.4, namely by seven orders of magnitude within only two hours.

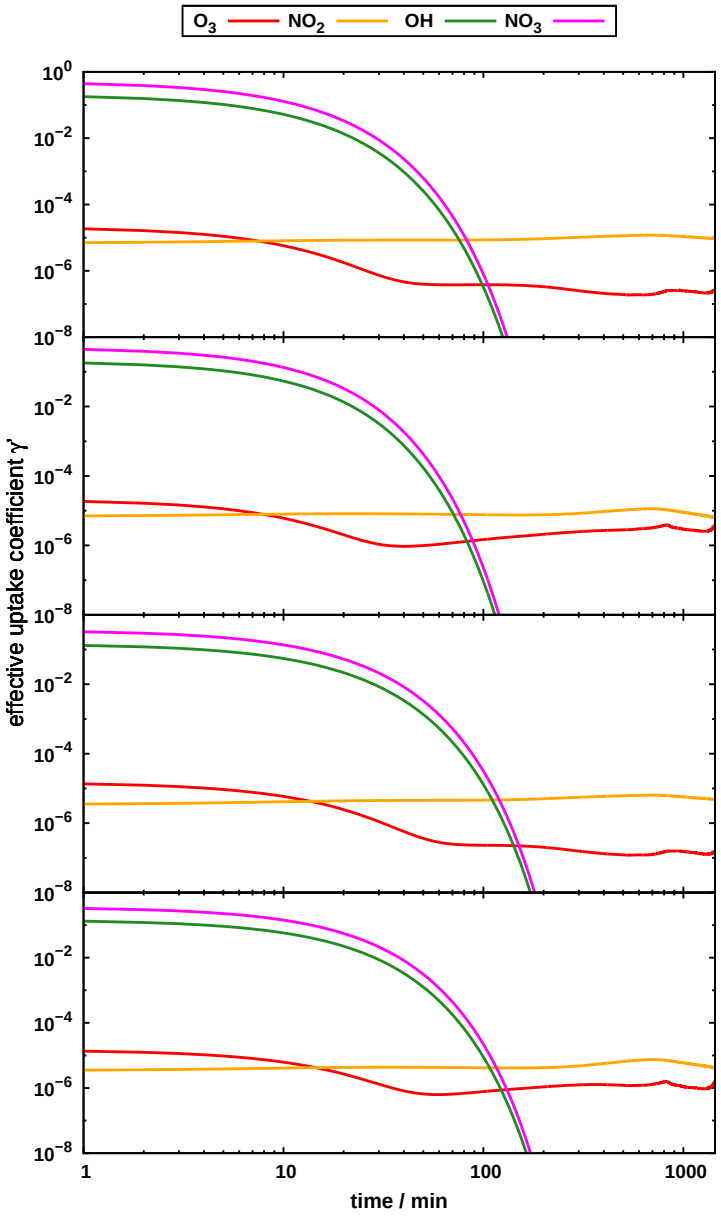

Figure 4.4: Effective uptake coefficients of individual particles that are emitted at the beginning of the respective simulations (the same particles as in Fig. 4.3). Panels represent, from top to bottom, simulations S1-am with low RH and low NO_x emissions, S2-am with low RH and high NO_x emissions, S3-am with high RH and low NO_x emissions, and S4-am with high RH and high NO_x emissions. All simulations shown were started at 6:00 am and were run without further soot emissions.

4.3 Population PAH surface coverage

Figure 4.5 shows how PAH surface coverage of the particles in the population evolves with time. Simulations that lead to the results plotted here were conducted with gas phase compositions corresponding to Figs. 4.1 and 4.2. As can be seen in Fig. 4.5, particles in various states of PAH degradation exist at any given time. However, from the large fraction of particles with very low PAH surface coverage, one can also clearly see that their transformation proceeds quickly compared to the time scale of the whole simulation. This is consistent with PAH degradation on the individual particles shown in Fig. 4.3 and with population-averaged lifetimes on the order of seconds to minutes as indicated by the results discussed in Sect. 4.4 below. At night, particle surfaces are so rapidly transformed that they reach a PAH surface coverage of $\theta_{\mathrm{ss,PAH}} \leq 0.05$ within the first minute of their atmospheric lifetime.

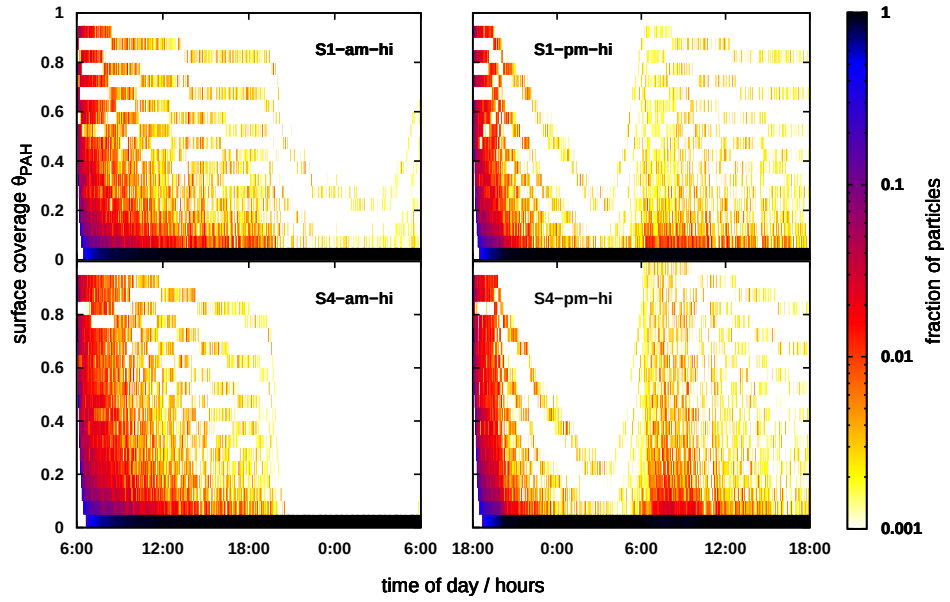

Figure 4.5: PAH surface coverage of all particles in the population for simulations of scenarios S1 (low RH and low NO_x emissions) and S4 (high RH and high NO_x emissions) with high soot emissions. The gas phase in these simulations corresponds to Figs. 4.1 for the upper panels and to 4.2 for the lower panels. On the horizontal axis time is plotted and the vertical axis measures PAH surface coverage in bins of width 0.05. The color scale shows the fraction of total particle number in each bin at each time step.

The fraction of particles with PAH surface coverage between 0.95 and 1.0 is always zero because the surface coverage is determined at the end of each time step. Hence, initial values are never plotted and one can see that surface oxidation always proceeds quickly enough to deplete PAH by more than 5% during the first minute of a particle's lifetime. The white vertical gaps also show the discrete nature of time in our simulations, i.e., particles "skip" certain bins of PAH surface coverage because the value is only calculated once per time step.

4.4 Population PAH half-life

Comparing Fig. 4.6 to Figs. 4.1 and 4.2 one can see the signature of the dominant PAH depleting species. During day, PAH half-life evolution mirrors $[O_3]_s$, which, as explained in Sect. 4.2.1, follows $[O_3]_g$ in our simulations. The more O_3 on the surface, the faster PAH can be converted to Y_2 by SLR1 and the shorter PAH half-life becomes. At night NO_3 acts as the dominant PAH oxidant. Elevated nighttime $[NO_3]_g$ levels render GSR2 much more efficient than SLR1 in depleting PAH so that its half-life falls to very low values. Note that we cannot resolve half-lives of less than 1 min but the actual values during night will be significantly lower. For example, under the assumption that GSR2 is the only efficient depletion mechanism for surface-bound PAH, $[NO_3]_g = 300\,\mathrm{ppt}$ will lead to a PAH half-life of only a few seconds.

It might come as a surprise that OH has a negligible effect on the oxidation of particle-bound PAH because of its high reactivity in homogeneous gas phase reactions. However, due to its extremely low concentration even at peak values, its collision flux with particles is also very small. As an example, consider a particle of diameter $d_p = 50\,\mathrm{nm}$ with about half of its sorption layer covered by adsorbing gases. We can calculate pseudo-first order PAH loss rate constants k', i.e., all the factors in $L_{ss,PAH}$ except $[PAH]_{ss}$, for the three reactions SLR1, GSR1, and GSR2 on such a particle:

$$k'_{SLR1,O_3,PAH} = 2.2 \cdot 10^{-3}\,\mathrm{s}^{-1}\,, \tag{4.1}$$

$$k'_{GSR1,OH,PAH} = 2.4 \cdot 10^{-4}\,\mathrm{s}^{-1}\,, \tag{4.2}$$

$$k'_{GSR2,NO_3,PAH} = 7.0 \cdot 10^{-1}\,\mathrm{s}^{-1}\,. \tag{4.3}$$

For these calculations, we assumed concentrations of $[O_3]_s = 8 \cdot 10^{13}\,\mathrm{cm}^{-2}$, $[OH]_g = 6 \cdot 10^6\,\mathrm{cm}^{-3}$ (corresponding to peak values observed in our simulations), and $[NO_3]_g = 300\,\mathrm{ppt}$. These rates show that, even at peak $[OH]_g$, its contribution to PAH depletion is at most about 10% of that of O_3, whereas

oxidation by NO_3(g) is extremely efficient at high nighttime concentrations.

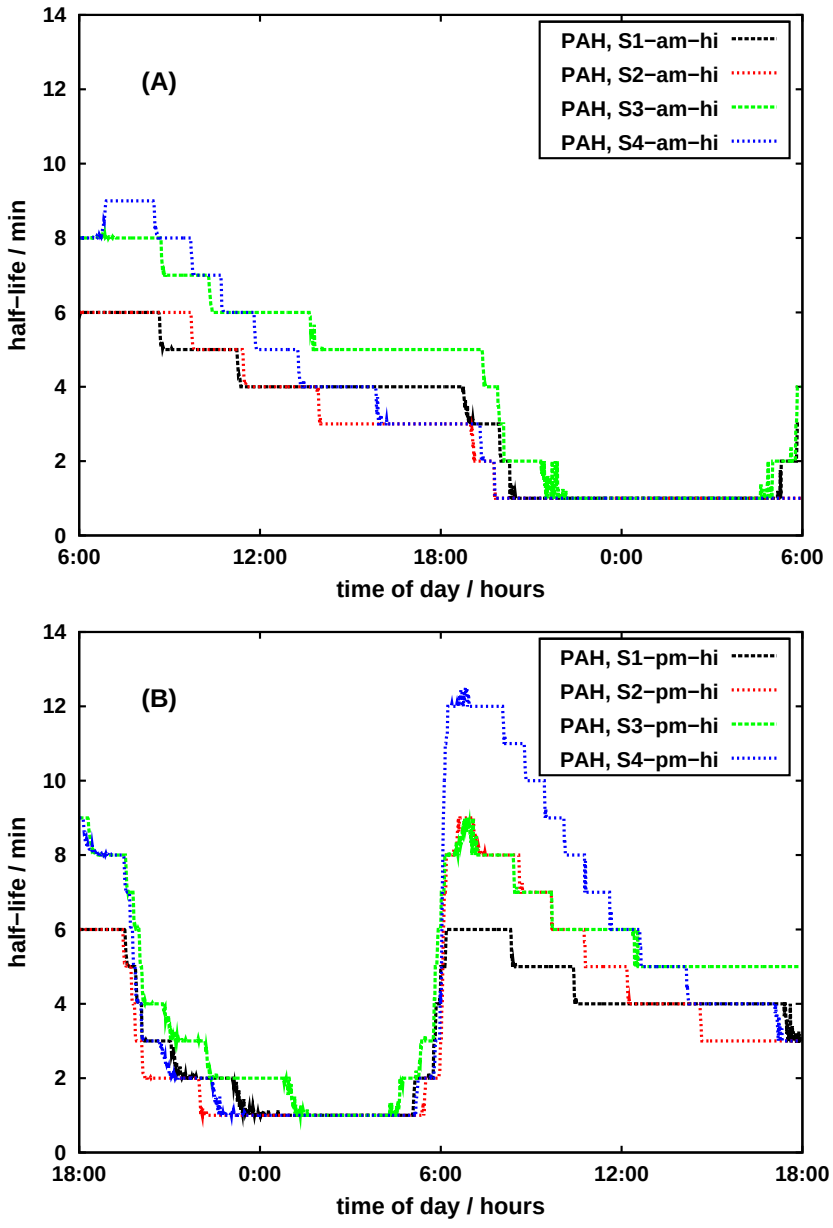

Figure 4.6: Evolution of population PAH half-life in simulations with high soot emissions for all considered scenarios. Panel (A) shows simulations started at 6:00 am, panel (B) simulations started at 6:00 pm.

Although both NO_x and H_2O have no direct effect on PAH degradation they do influence it indirectly. H_2O molecules occupy surface sites as mentioned before and thus PAH half-life is reduced by up to four minutes, or 40%, at lower RH (S1 compared to S3 and S2 vs. S4) because more of these sites are free to adsorption of reactive species. The effect of different NO_x emissions (S1 vs. S2, S3 vs. S4) is more complex.

In the simulations started at 6:00 am, $[O_3]_g$ initially decreases in the high NO_x emission scenarios (S2 and S4). During that period reaction (2.20) between O_3 and NO_2 dominates the production of new O_3 following photolysis of NO_2. Lower $[O_3]_g$ then leads to longer PAH half-life (e.g., S4-am-hi vs. S3-am-hi in Fig. 4.6). Later on, however, when VOCs build up leading to higher $[NO_2]_g$, which makes O_3 formation more and more efficient, $[O_3]_g$ attains higher values in the high NO_x scenarios, thereby reducing PAH half-life (e.g., S2-am-hi vs. S1-am-hi in Fig. 4.6).

Simulations started at 6:00 pm also show longer PAH half-life in the morning hours of high NO_x emission simulations (S2-pm-hi vs. S1-pm-hi and S4-pm-hi vs. S3-pm-hi in Fig. 4.6). The reason is again reaction (2.20) which depletes O_3 during night where no photolysis of NO_2 occurs that would replenish it. Hence, if NO_x emissions are higher, $[O_3]_g$ is more efficiently reduced during night and therefore it is lower in the morning when it takes over from NO_3(g) as the major sink for PAH(ss). This leads to a maximum of four minutes, or 40%, longer PAH half-life in the morning of simulation S4-pm-hi compared to S3-pm-hi. Later in the day we see the same effect as for the simulations started at 6:00 am: $[O_3]_g$ rises to higher levels in the high NO_x emission scenarios and thus PAH half-life becomes shorter.

In terms of nighttime effects of different NO_x emission levels on PAH half-life, start time of the simulations does not make a significant difference. Higher NO_x emissions (S2 and S4) lead to higher levels of $[NO_3]_g$ at night which shorten PAH half-life. Note, however, that the effects during peak $[NO_3]_g$ are not quantifiable because PAH half-life is less than the model's time resolution at that time in all simulations.

Compared to the benzo[*a*]pyrene half-lives on soot particles found by Springmann et al. (2009), which were on the order of tens of minutes, the PAH half-lives reported here are shorter, especially during night. Experimentally determined benzo[*a*]pyrene lifetimes reported by Pöschl et al. (2001) agreed with the results of Springmann et al.. The discrepancy with the values reported here is likely due to PAH oxidation by NO_3(g) which neither of these research groups considered. This explanation is supported by the work of Gross and Bertram (2008) who calculated atmospheric PAH lifetimes on the order of tens of seconds for solid pyrene exposed to 50 ppt of NO_3(g).

4.5 Population uptake coefficients

We define the effective population uptake coefficient $\overline{\gamma'}_{\mathrm{X}_i}$ as the surface area-weighted average over the whole population of soot particles:

$$\overline{\gamma'}_{\mathrm{X}_i} = \frac{\sum_n S_n \gamma'_{\mathrm{X}_i,n}}{\sum_n S_n} \,. \tag{4.4}$$

Here, n is an index that runs over all particles of the simulated population, S_n the corresponding surface area and $\gamma'_{\mathrm{X}_i,n}$ the effective uptake coefficient for species X_i on particle n.

An effective population uptake coefficient is useful for application in large-scale models. These models typically use the total amount of soot surface per unit volume of air to represent surface area available for heterogeneous reactions because computational limitations inhibit a more detailed treatment of particles. The total amount of soot surface per unit mass (of soot) can be determined experimentally and converted to a total surface area per unit volume (of air) by multiplying that value with the mass concentration of soot in the air, e.g., about $10\,\mu\mathrm{g\,m^{-3}}$ at the end of our simulations with the high soot emission rate.

Equation (4.4) is evaluated for O_3, NO_2, NO_3, and OH at every time step. Plots of these values for all simulations with high soot emissions that were started at 6:00 am are shown in Fig. 4.7. Note that the data for OH and NO_3 was smoothed before plotting the graphs by calculating the moving average over 20 consecutive time steps. This eliminates high frequency noise generated by the stochastic emission process in conjunction with the quick decline of γ'_{OH} and $\gamma'_{\mathrm{NO_3}}$ on individual particles (and leads to the cut-off before the end of the simulation).

Interestingly, $\overline{\gamma'}_{\mathrm{O_3}}$ and $\overline{\gamma'}_{\mathrm{NO_2}}$ are relatively constant albeit at much lower levels than the initial values of $\gamma'_{\mathrm{O_3}}$ and $\gamma'_{\mathrm{NO_2}}$ on the individual particles, namely 10^{-3} and $6.4 \cdot 10^{-2}$, respectively. After some initial adjustment these two coefficients show the same behavior as indicated in Fig. 4.4: $\overline{\gamma'}_{\mathrm{O_3}}$ follows the evolution of $[\mathrm{NO_2}]_\mathrm{s}$ and vice versa. This is difficult to see in Fig. 4.7 due to the wide plot range but in order to make the graphs easily comparable to Fig. 4.4 we kept the same scale.

The period of adjustment of $\overline{\gamma'}_{\mathrm{O_3}}$ is caused by aging of the population as a whole, i.e., an initial decrease in $\gamma'_{\mathrm{O_3}}$ on each individual particle as shown in Fig. 4.4. However, this overall decrease is delayed by emissions of fresh particles that contribute higher effective uptake coefficients due to SLR1 with PAH. If particle-bound PAH was oxidized more efficiently by other species

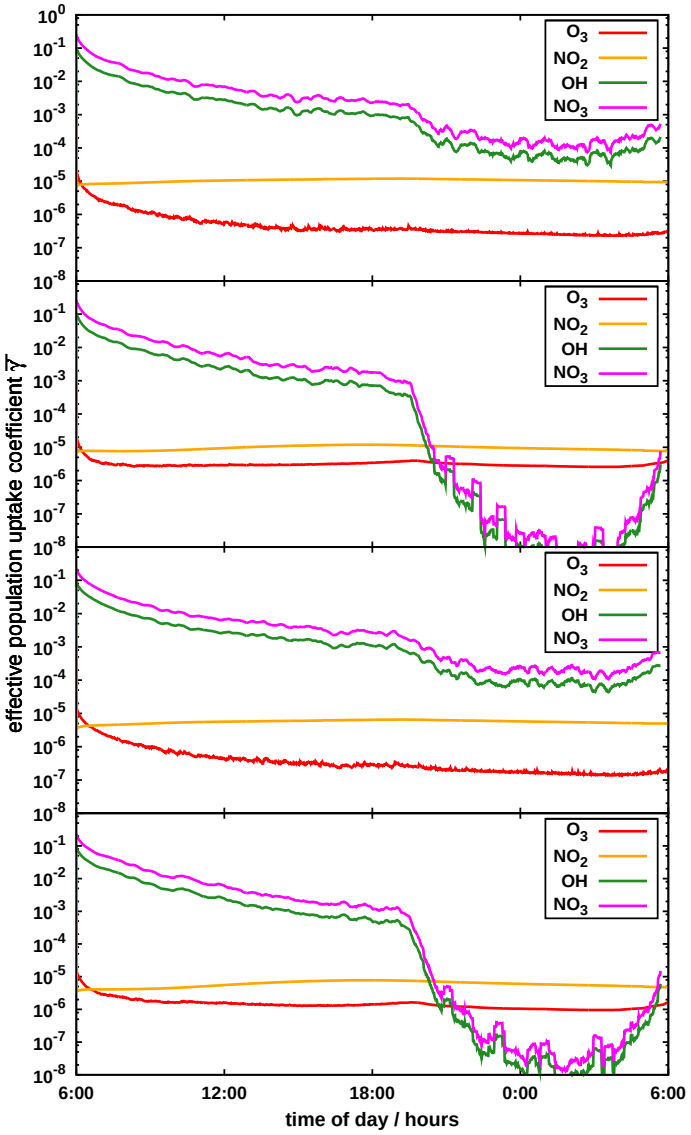

Figure 4.7: Effective population uptake coefficients in simulations with high soot emissions and started at 6:00 am for all scenarios. Panels represent, from top to bottom: S1-am-hi with low RH and low NO_x emissions, S2-am-hi with low RH and high NO_x emissions, S3-am-hi with high RH and low NO_x emissions and S4-am-hi with high RH and high NO_x emissions. The gas phase for the topmost panel corresponds to Fig. 4.1(A) and that for the lowermost panel to Fig. 4.2(A). In order to simplify comparison to Fig. 4.4 the same scales were kept even though this lead to partial cutoff of the curves.

in the atmosphere, $\overline{\gamma'}_{O_3}$ would adjust to the $[NO_2]_g$ evolution more quickly, because SLR6 would sooner become the major O_3(s) sink on the surface. For example, a particle emitted at night, when the high $[NO_3]_g$ levels lead to rapid PAH conversion, reaches the SLR6-limited regime much faster. This is also the reason for the smoother nighttime evolution of $\overline{\gamma'}_{O_3}$ compared to its daytime behavior: effective uptake coefficients on newly emitted particles are almost instantly limited by SLR6 because PAH is rapidly depleted by GSR2 with NO_3(g), and therefore they do not alter the population average much.

$\overline{\gamma'}_{OH}$ and $\overline{\gamma'}_{NO_3}$ show the same evolution because they only differ by a constant factor of $\gamma_{GSR1,OH,PAH}/\gamma_{GSR2,NO_3,PAH}$ (see Eq. (2.26)). Their initial decline in Fig. 4.7 reflects an increase in average particle age of the population and therefore less available PAH left over on an average particle. The drop during night is due to quicker PAH oxidation which entails a more rapid decline in γ'_{OH} and γ'_{NO_3} on freshly emitted particles (as explained in Sect. 4.2.2).

As discussed above for individual particles, co-adsorption of water vapor also reduces the effective population uptake coefficients for O_3 and NO_2 by occupying sorption sites. The increase in RH from 30% (S1, S2) to 80% (S3, S4) leads to a reduction in uptake by roughly a factor of two. In contrast, $\overline{\gamma'}_{OH}$ and $\overline{\gamma'}_{NO_3}$ seem to be slightly increased. This is due to the dominance of aged particles in the soot population as shown in Fig. 4.5. Therefore, the regime where higher amounts of adsorbed water vapor lead to more PAH left over on the particles (as described in Sect. 4.2.2) has to be considered. This increases γ'_{OH} and γ'_{NO_3} on the individual particles at higher RH compared to lower RH, and thus their contributions to the population average. The effect is small during day, i.e., less than a factor of two, but can be as high as roughly a factor of five during night in the high NO_x emission simulations (S2-am-hi and S4-am-hi).

Values of $\overline{\gamma'}_{NO_2}$ fall roughly between $4 \cdot 10^{-6}$ and $1.5 \cdot 10^{-5}$ in all simulations while $\overline{\gamma'}_{O_3}$ shows a significant dependence on NO_x emission level. After reaching the SLR6-limited regime it is about one order of magnitude smaller in low NO_x emission scenarios (S1, S3) than for high NO_x emissions (S2, S4) because less NO_2(s) is available for reaction with O_3(s). In contrast, $\overline{\gamma'}_{OH}$ and $\overline{\gamma'}_{NO_3}$ are higher in the low NO_x scenarios, especially during night, because of the slower depletion of PAH.

Once the soot particle population is dominated by aged particles, i.e., those whose monolayer of PAH has already been oxidized to a significant degree, effective population uptake coefficients for O_3 and NO_2 are increased by an order of magnitude or more due to SLR6 compared to control runs where the reaction was switched off (not shown). This is in line with the finding that $\overline{\gamma'}_{NO_2}$ follows $[O_3]_s$ and vice versa because of reaction SLR6 becoming the main

sink for both O_3(s) and NO_2(s).

As already indicated by the effective uptake coefficients on individual particles (Fig. 4.4), population averaged values that take into account particle aging quickly decrease by several orders of magnitude. Thus, assuming them to stay constant at their initial values in chemistry transport models may lead to erroneous predictions. Such parameterizations so far did not account for passivation of reactive sites by heterogeneous kinetics and thus ignored the underlying physicochemical processes.

4.6 Feedback on gas phase

Feedback on the gas phase is negligible, consistent with the small effective uptake coefficients. According to Eq. (2.40), γ'_{X_i} (and, analogously, $\overline{\gamma'}_{\mathrm{X}_i}$) measures the fraction of molecules colliding with a surface that is irreversibly taken up. Hence, in case of O_3 and NO_2 no more than about 10^{-5} of the molecules that collide with soot surfaces are permanently removed from the gas phase. Even though this fraction can be higher for OH and NO_3 we do not detect a significant impact on $[\mathrm{OH}]_\mathrm{g}$ and $[\mathrm{NO_3}]_\mathrm{g}$ either. This is due to the initially very small amount of available soot surface per unit volume when $\overline{\gamma'}_{\mathrm{OH}}$ and $\overline{\gamma'}_{\mathrm{NO_3}}$ are highest. One can estimate the order of magnitude of relative change in $[\mathrm{X}_i]_\mathrm{g}$ during the first few minutes by looking at the individual terms of Eq. (2.40). It reads

$$\frac{d[\mathrm{X}_i]_\mathrm{g}}{dt} = -\overline{\gamma'}_{\mathrm{X}_i} \frac{\omega_{\mathrm{X}_i}}{4} C_{\mathrm{g,X}_i} [\mathrm{X}_i]_\mathrm{g} \cdot \frac{S}{V} \,, \tag{4.5}$$

if we assume the average value $\overline{\gamma'}_{\mathrm{X}_i}$ for γ'_{X_i} and replace $J_{\mathrm{coll,X}_i}$ using Eq. (2.32). Here, initially, $\overline{\gamma'}_{\mathrm{X}_i} \sim 10^{-1}$ for $\mathrm{X}_i = \mathrm{OH}, \mathrm{NO_3}$, $\omega_{\mathrm{X}_i} \sim 10^4\,\mathrm{cm^2\,s^{-1}}$, $C_{\mathrm{g,X}_i} \sim 1$ and $\frac{S}{V} \sim 10^{-8}\,\mathrm{cm^2\,cm^{-3}}$ in the first few minutes of high soot emission simulations. Dividing both sides of Eq. (4.5) by $[\mathrm{X}_i]_\mathrm{g}$ one obtains a rate of relative change on the order of $10^{-5}\,\mathrm{s^{-1}}$ which leads to a decrease in $[\mathrm{X}_i]_\mathrm{g}$ of $\sim$0.1% over the first few minutes where the effective uptake coefficients are highest.

Heterogeneous production of HONO is also negligible in our simulations due to the relatively small surface concentrations of NO_2 and the very low reaction rate $k_{\mathrm{SLR5,NO_2,Y_3}}$.

It is difficult to assess a possible effect of NO_3(s) desorption on the gas phase because of the competing gas-surface reaction between NO_3(g) and PAH(ss). An estimation of desorption flux, similar to that for Eq. (4.5), may yield some insight. Assuming a maximum NO_3(s) concentration of $\sim 10^{11}\,\mathrm{cm^{-2}}$ reached in our simulations, one obtains a desorption flux that could be of similar

magnitude to the removal of NO_3(g) from the gas phase estimated above, if the amount of soot surface per unit area and $[NO_3]_s$ simultaneously attained their highest levels. However, this will not be the case most of the time. Hence, surface production of NO_3 is unlikely to affect gas phase composition significantly.

In summary, our results suggest that heterogeneous reactions on soot do not have a significant impact on the gas phase. However, this is in contrast to several other studies that found considerable reductions in $[O_3]_g$, for example (e.g., Aklilu and Michelangeli, 2004; Springmann et al., 2009). Such differences can possibly be explained by our novel approach to soot representation, which yields a specific surface area of $\sim 10\,m^2\,g^{-1}$ that is much lower than the upper limit estimation of $500\,m^2\,g^{-1}$, for instance, that Springmann et al. used. The finding that soot particles do not act as a significant source of HONO confirms the result of studies by Kleffmann et al. (1999), Aubin and Abbatt (2007), Springmann et al. (2009), and Nguyen et al. (2009) but disagrees with others (Ammann et al., 1998; Gerecke et al., 1998; Arens et al., 2001; Kotamarthi et al., 2001). It seems that the HONO production by reaction of NO_2 with or on soot strongly depends on the type of soot and the associated physicochemical parameters.

4.7 Influence of soot emission rate

As a consequence of the low overall effective uptake coefficients, changes in soot emission levels have a negligible impact in our scenarios. All particle-related results presented above were obtained from simulations with a high soot emission rate (except for Figs. 4.3 and 4.4 which show individual particles). They differ only marginally when looking at the low soot emissions scenarios. As an example, PAH half-life is plotted for simulations S4-am-hi and S4-am-lo in Fig. 4.8. Thus, the influence on the gas phase becomes even smaller in our low soot emission simulations since, on the one hand, effective uptake coefficients are not significantly altered, but on the other hand, available particle surface area decreases by two orders of magnitude.

Previous results by Springmann et al. (2009) showed large differences in the impact of heterogeneous reactions on gas phase composition at different soot emission levels. However, this impact was measured in terms of the reduction in $[O_3]_s$ which we do not detect here. If heterogeneous chemistry in our simulation had also affected the gas phase, other quantities such as effective population uptake coefficients or population PAH half-life would potentially also have changed between the simulations with low and high soot emissions.

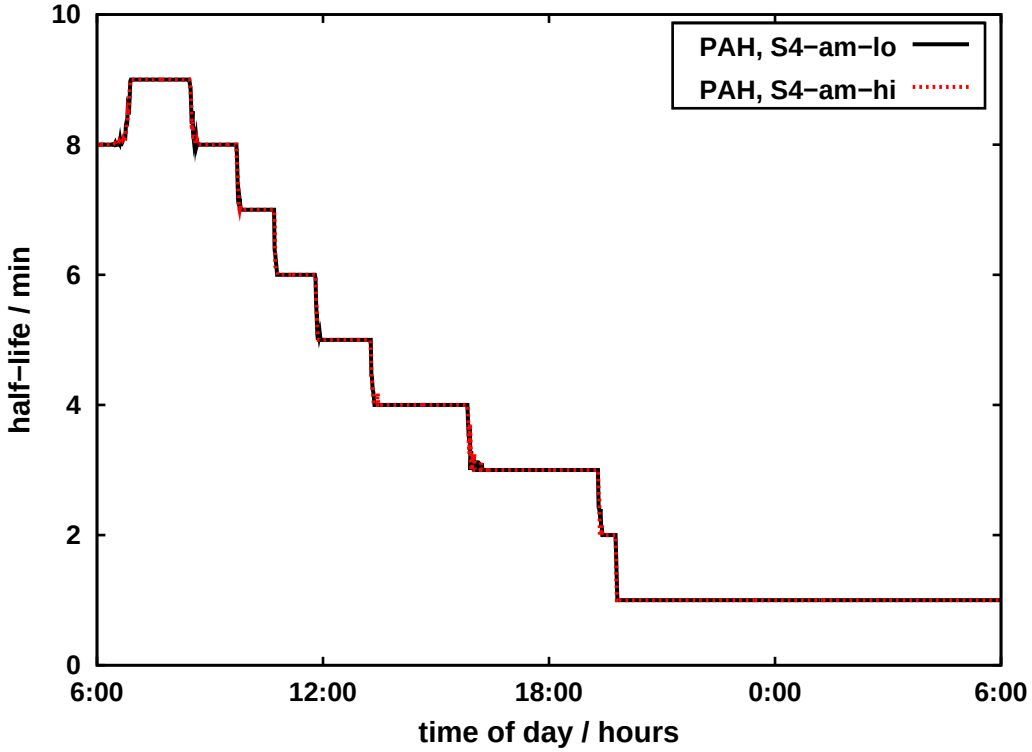

Figure 4.8: Evolution of population PAH half-life in a simulation of scenario S4 (high RH, high NO_x emissions) started at 6:00 am with both low and high soot emissions.

5. Summary and Conclusions

We applied a particle-resolved aerosol model for the first time to assess in detail the effects of heterogeneous reactions on atmospheric soot particles coated with PAHs. For this purpose, we compiled literature data from many different laboratory experiments for use in a unifying theoretical framework that takes into account the elementary processes governing heterogeneous kinetics. Laboratory measurements are not available for atmospherically relevant systems of the complexity considered here. Moreover, the particle-level insight gained in our study is useful to parameterize the influence of heterogeneous soot chemistry on the gas phase as well as the degree of oxidation of atmospheric surfaces. Health risk assessment may also benefit from such simulations since lifetimes of toxic species can be diagnosed. Our most important findings are summarized here and their atmospheric implications discussed briefly.

PAH degradation

This study shows that heterogeneous degradation of PAHs on soot particles in the atmosphere may proceed rather quickly, with lifetimes on the order of minutes or less. At night, when $[NO_3]_g$ levels are high and render the gas-surface reaction with the PAH very efficient, lifetime drops to a few seconds.

The exact structure of oxidized PAH reaction products has yet to be determined so that we cannot make predictions concerning toxicity based on our results. A study by Durant et al. (1996) indicated that oxygenation of PAHs may reduce their mutagenicity, but then again, according to Finlayson-Pitts and Pitts (2000), nitration may lead to increased mutagenicity.

As higher oxidation was shown to be well correlated with higher hygroscopicity (Jimenez et al., 2009), i.e., ability to take up water, the conclusion seems justified that soot particles could quickly become efficient cloud condensation nuclei. Thus, heterogeneous processing of soot particles may have a significant influence on their climatic impact.

The hydroperoxy radical (HO_2) may enhance heterogeneous PAH oxidation even further since it is also among the most reactive oxidants in the gas phase and available at higher concentrations than OH. However, literature on its reaction with soot or soot-bound PAHs is limited (Saathoff et al., 2001; Bedjanian et al., 2005).

When extrapolating our results to the atmosphere, it has to be kept in mind that we neglected physical processes that will certainly affect the actual evolution of particle-bound PAHs. Deposition and coagulation were not considered, neither did we include dilution of the soot particle concentration with background air. Perhaps most importantly, we did not account for condensation of water vapor or semivolatile substances, such as HNO_3 and H_2SO_4 on our particles. If the latter processes proceed on similar or shorter timescales than the heterogeneous oxidation process they may delay PAH degradation considerably. Another process that we neglected here is photolysis of particle-bound PAHs, which may lead to enhanced degradation.

Lastly, atmospheric soot particles likely contain more than one monolayer of PAHs, which may change the rate of their degradation because only the outermost layer is directly exposed to reactive gas species. Multilayer coating would also change absolute quantities of both PAHs and their oxidized products.

Effective uptake coefficients

The effective uptake coefficient γ' was defined here as the proportionality factor between the rate of change of a gas phase concentration and the rate of gas-surface collisions per unit volume. This avoids confusion with constant uptake coefficients and reaction probabilities, which have also been called uptake coefficients in the literature. Moreover, it extends the basic definition of an uptake coefficient — as the ratio between net flux onto a surface and collision flux, considering only one gas and no changes in surface properties — to a system of several co-adsorbing and reactive gas phase species that may alter surface composition and associated parameters.

Averaged over the simulated population of soot particles, we find relatively uniform values for the effective uptake coefficient of the gases following the two-step Langmuir-Hinshelwood type process, $\overline{\gamma'}_{O_3}$ and $\overline{\gamma'}_{NO_2}$. They range from $\sim 10^{-7}$ to $\sim 10^{-5}$. In case of direct gas-surface reactions, $\overline{\gamma'}$ depends strongly on the state of PAH degradation in our simulations. During day, $\overline{\gamma'}_{OH}$ and $\overline{\gamma'}_{NO_3}$ have values roughly between $\sim 10^{-2}$ and $\sim 10^{-3}$ for most of the simulated time, but at night they can become as low as $\sim 10^{-9}$.

Hence, under the assumptions made here for underlying physicochemical parameters and reaction mechanisms we find that constant effective uptake coefficients may be a useful approximation for O_3 and NO_2 if the proper values are used. However, our simulations show that these values differ considerably, i.e., about two to three orders of magnitude, from the initial uptake coefficients for fresh surfaces. The relatively constant values of $\overline{\gamma'}_{O_3}$ and $\overline{\gamma'}_{NO_2}$ are mainly

due to the surface reaction of O_3(s) and NO_2(s) that, over the atmospheric lifetime of an average particle, constitutes the most important sink for both of these adsorbed species.

The differences in $\overline{\gamma'}_{OH}$ and $\overline{\gamma'}_{NO_3}$ between daytime and nighttime can be explained by the diurnal cycle of $[NO_3]_g$. Its negligible concentrations during day do not affect PAH degradation significantly, but the buildup during night renders NO_3(g) by far the most efficient oxidant considered here. A more detailed parameterization or an appropriate averaging scheme would be necessary if gas-surface reactions with OH and NO_3 were to be considered in a large-scale model.

Again, caution has to be applied when considering the atmospheric implications of these findings. We neglected possible changes in physicochemical surface parameters that may be associated with changes in surface composition. Moreover, the assumption of homogeneous concentrations of surface-bound and surface-adsorbed species may not be correct. If, for example, molecules adsorbed in multiple layers on parts of the surface and left other sorption sites free, our results might be considerably different.

Feedback on the gas phase

In general, our results for $\overline{\gamma'}_{O_3}$, $\overline{\gamma'}_{NO_2}$, $\overline{\gamma'}_{OH}$, and $\overline{\gamma'}_{NO_3}$ suggest that it may not be necessary to consider soot particles as a sink for the corresponding trace gases. The finding that the effective uptake coefficients are independent of soot emission rate and associated soot concentration also supports this conclusion. However, it is in contrast to several other studies that found significant impacts, e.g., on O_3(g) concentrations (Aklilu and Michelangeli, 2004; Springmann et al., 2009).

Possibly, we underestimate the uptake of OH and NO_3 because these species most likely will also react with secondary species on the soot surface. If these reactions proceed at similar rates as those with the primary PAHs the influence on the radicals' gas phase concentrations may actually be more pronounced. The assumption of similar rates for oxidation of secondary species may be supported by a study of the HO_2 reaction with soot by Bedjanian et al. (2005). They found no significant dependence of this reaction on particle age, which is related to the degree of oxidation.

In contrast, if particle deposition or condensation of other atmospheric species onto soot lead to a decrease in the efficiency of heterogeneous removal of gas phase species, an even smaller feedback would be the result. Since this seems likely, our results suggest that atmospheric soot particles have no significant direct effect on either O_3 or NO_2 concentrations. Indirect effects,

e.g., by consumption of oxidants necessary for O_3 generation or by formation of O_3 precursor substances, may still play a role here.

However, for HONO, one important representative of O_3 precursor species, this study also indicates no major contribution. Soot particles in our simulations do not act as a significant source of HONO. This agrees with results of laboratory measurements by Kleffmann et al. (1999) and Nguyen et al. (2009), and with modeling studies by Aubin and Abbatt (2007), Springmann et al. (2009). However, several experimental studies (Ammann et al., 1998; Gerecke et al., 1998; Arens et al., 2001) as well as a box model calculation by Kotamarthi et al. (2001) found formation of considerable amounts of HONO by heterogeneous reactions on soot.

Consideration of reactions of soot or soot-bound PAHs with HO_2 might alter our findings for gas phase feedback. A combined laboratory and box model study by Saathoff et al. (2001) suggested that they may have a measurable influence on peak O_3 concentrations. This finding was supported by experimental results for the reaction of soot particles with HO_2 (Bedjanian et al., 2005).

Limitations and applicability

Our study relies on a number of idealizing assumptions, e.g., perfectly spherical soot particles for the calculation of available surface area, to mention only one. Moreover, some of the physicochemical parameters cited here vary considerably from one laboratory experiment to the other, different PAHs exhibit largely different reaction rates, and the specific type of soot used in an experiment also has a significant effect on the precise values of its parameters. Accommodation coefficients, effective molecular cross sections of adsorbing gases, desorption lifetimes, and reaction probabilities may also change with the changes in surface composition induced by heterogeneous reactions. Additionally, we neglected a number of physical processes such as coagulation of particles and condensation of semi-volatile species upon them.

That said, our study demonstrated that it is possible to account for detailed heterogeneous kinetics within a particle-resolved aerosol model. The results obtained in this study yield insight into the possible significance of heterogeneous reactions on atmospheric soot particles and can be regarded as a best estimate according to currently available data.

6. Outlook

Based on the results of our study, we make a few suggestions concerning the direction of future research here.

Clearly, more experimental research in terms of physicochemical parameters is required for more accurate predictions employing the model presented here. Field studies may lead to formulation of a soot-and-coating system that better represents actual atmospheric particles, so that laboratory measurements could subsequently focus on such a system. The reaction between HO_2 and soot or soot-bound PAH may be an important factor here. Hence, if more detailed studies of such reactions become available it will be worthwile to implement them in PartMC-MOSAIC.

Considering future applications of this model, it would certainly be interesting to include the physical processes of deposition, coagulation, and condensation of semi-volatile species as well as water vapor. This would allow to assess the relative influences of physical and chemical aging of atmospheric particles.

Additionally, other scenarios and systems of atmospheric relevance can be investigated. Especially, test cases might be designed that can also be realized in laboratory measurements. Thus, modeling results could be evaluated directly against corresponding experiments to gain more insight into the processes governing heterogeneous chemistry in the atmosphere. Both model parameters and theoretical understanding could benefit from such applications.

Bibliography

Adams, P. J., J. H. Seinfeld, and D. M. Koch. *Global concentrations of tropospheric sulfate, nitrate, and ammonium aerosol simulated in a general circulation model.* J. Geophys. Res.-Atmos., 104(D11): 13791–13823, 1999.

Adler, G., A. A. Riziq, C. Erlick, and Y. Rudich. *Effect of intrinsic organic carbon on the optical properties of fresh diesel soot.* Proc. Natl. Acad. Sci. U. S. A., 107(15): 6699–6704, 2010. doi:10.1073/pnas.0903311106.

Aklilu, Y. A. and D. V. Michelangeli. *Box model investigation of the effect of soot particles on ozone downwind from an urban area through heterogeneous reactions.* Environ. Sci. Technol., 38(21): 5540–5547, 2004. doi:10.1021/es035079x.

Ammann, M., M. Kalberer, D. T. Jost, L. Tobler, E. Rossler, D. Piguet, H. W. Gaggeler, and U. Baltensperger. *Heterogeneous production of nitrous acid on soot in polluted air masses.* Nature, 395(6698): 157–160, 1998.

Ammann, M. and U. Pöschl. *Kinetic model framework for aerosol and cloud surface chemistry and gas-particle interactions - Part 2: Exemplary practical applications and numerical simulations.* Atmos. Chem. Phys., 7(23): 6025–6045, 2007.

Andreae, M. O. *A New Look at Aging Aerosols.* Science, 326(5959): 1493–1494, 2009. doi:10.1126/science.1183158.

Arens, F., L. Gutzwiller, U. Baltensperger, H. W. Gaggeler, and M. Ammann. *Heterogeneous reaction of NO2 on diesel soot particles.* Environ. Sci. Technol., 35(11): 2191–2199, 2001.

Atkinson, R. W., H. R. Anderson, J. Sunyer, J. Ayres, M. Baccini, J. M. Vonk, A. Boumghar, F. Forastiere, B. Forsberg, G. Touloumi, J. Schwartz, and K. Katsouyanni. *Acute effects of particulate air pollution on respiratory admissions - Results from APHEA 2 project.* Am. J. Respir. Crit. Care Med., 164(10): 1860–1866, 2001.

Aubin, D. G. and J. P. D. Abbatt. *Interaction of NO2 with hydrocarbon soot: Focus on HONO yield, surface modification, and mechanism.* J. Phys. Chem. A, 111(28): 6263–6273, 2007. doi:10.1021/jp068884h.

Aumont, B., S. Madronich, M. Ammann, M. Kalberer, U. Baltensperger, D. Hauglustaine, and F. Brocheton. *On the NO2 plus soot reaction in the atmosphere.* J. Geophys. Res.-Atmos., 104(D1): 1729–1736, 1999.

Azri, C., C. Mabrouk, and K. Medhioub. *Diurnal Evolutions of Nitrogen Oxides (NOx), Ozone (O-3), and PM10 Particles at a Busy Traffic Cross-Road in the City of Tunis.* Environ. Prog. Sustain. Energy, 28(1): 143–154, 2009. doi:10.1002/ep.10315.

Bedjanian, Y., S. Lelièvre, and G. Le Bras. *Experimental study of the interaction of HO2 radicals with soot surface.* Phys. Chem. Chem. Phys., 7(2): 334–341, 2005. doi:10.1039/b414217a.

Bedjanian, Y., M. L. Nguyen, and A. Guilloteau. *Desorption of Polycyclic Aromatic Hydrocarbons from Soot Surface: Five- and Six-Ring (C-22, C-24) PAHs.* J. Phys. Chem. A, 114(10): 3533–3539, 2010. doi:10.1021/jp912110b.

Bernstein, J. A., N. Alexis, C. Barnes, I. L. Bernstein, J. A. Bernstein, A. Nel, D. Peden, D. Diaz-Sanchez, S. M. Tarlo, and P. B. Williams. *Health effects of air pollution.* J. Allergy Clin. Immunol., 114(5): 1116–1123, 2004. doi: 10.1016/j.jaci.2004.08.030.

Bertram, A. K., A. V. Ivanov, M. Hunter, L. T. Molina, and M. J. Molina. *The reaction probability of OH on organic surfaces of tropospheric interest.* J. Phys. Chem. A, 105(41): 9415–9421, 2001. doi:10.1021/jp0114034.

Bey, I., D. J. Jacob, R. M. Yantosca, J. A. Logan, B. D. Field, A. M. Fiore, Q. B. Li, H. G. Y. Liu, L. J. Mickley, and M. G. Schultz. *Global modeling of tropospheric chemistry with assimilated meteorology: Model description and evaluation.* J. Geophys. Res.-Atmos., 106(D19): 23073–23095, 2001.

Binkowski, F. S. and U. Shankar. *The Regional Particulate Matter Model .1. Model description and preliminary results.* J. Geophys. Res.-Atmos., 100(D12): 26191–26209, 1995.

Cain, J. P., P. L. Gassman, H. Wang, and A. Laskin. *Micro-FTIR study of soot chemical composition-evidence of aliphatic hydrocarbons on nascent soot surfaces.* Phys. Chem. Chem. Phys., 12(20): 5206–5218, 2010. doi: 10.1039/b924344e.

Colbeck, I. and M. Lazaridis. *Aerosols and environmental pollution.* Naturwissenschaften, 97(2): 117–131, 2010. doi:10.1007/s00114-009-0594-x.

Crutzen, P. J. and F. Arnold. *Nitric-acid cloud formation in the cold antarctic stratosphere - a major cause for the springtime ozone hole.* Nature, 324(6098): 651–655, 1986.

Dachs, J. and S. J. Eisenreich. *Adsorption onto aerosol soot carbon dominates gas-particle partitioning of polycyclic aromatic hydrocarbons.* Environ. Sci. Technol., 34(17): 3690–3697, 2000. doi:10.1021/es991201+.

Durant, J. L., W. F. Busby, A. L. Lafleur, B. W. Penman, and C. L. Crespi. *Human cell mutagenicity of oxygenated, nitrated and unsubstituted polycyclic aromatic hydrocarbons associated with urban aerosols.* Mutat. Res.-Genet. Toxicol., 371(3-4): 123–157, 1996.

Dusanter, S., D. Vimal, P. S. Stevens, R. Volkamer, L. T. Molina, A. Baker, S. Meinardi, D. Blake, P. Sheehy, A. Merten, R. Zhang, J. Zheng, E. C. Fortner, W. Junkermann, M. Dubey, T. Rahn, B. Eichinger, P. Lewandowski, J. Prueger, and H. Holder. *Measurements of OH and HO2 concentrations during the MCMA-2006 field campaign - Part 2: Model comparison and radical budget.* Atmos. Chem. Phys., 9(18): 6655–6675, 2009.

El Haddad, I., N. Marchand, J. Dron, B. Temime-Roussel, E. Quivet, H. Wortham, J. L. Jaffrezo, C. Baduel, D. Voisin, J. L. Besombes, and G. Gille. *Comprehensive primary particulate organic characterization of vehicular exhaust emissions in France.* Atmos. Environ., 43(39): 6190–6198, 2009. doi:10.1016/j.atmosenv.2009.09.001.

Emmerson, K. M., N. Carslaw, L. J. Carpenter, D. E. Heard, J. D. Lee, and M. J. Pilling. *Urban atmospheric chemistry during the PUMA campaign 1: Comparison of modelled OH and HO2 concentrations with measurements.* J. Atmos. Chem., 52(2): 143–164, 2005. doi:10.1007/s10874-005-1322-3.

Evans, M. J. and D. J. Jacob. *Impact of new laboratory studies of N2O5 hydrolysis on global model budgets of tropospheric nitrogen oxides, ozone, and OH.* Geophys. Res. Lett., 32(9), 2005. doi:10.1029/2005GL022469.

Finlayson-Pitts, B. J. *Reactions at surfaces in the atmosphere: integration of experiments and theory as necessary (but not necessarily sufficient) for predicting the physical chemistry of aerosols.* Phys. Chem. Chem. Phys., 11(36): 7760–7779, 2009. doi:10.1039/b906540g.

Finlayson-Pitts, B. J. and J. N. Pitts. *Tropospheric air pollution: Ozone, airborne toxics, polycyclic aromatic hydrocarbons, and particles.* Science, 276(5315): 1045–1052, 1997.

Finlayson-Pitts, B. J. and J. N. Pitts. *Chemistry of the upper and lower atmosphere.* Academic Press, 525 B Street, Suite 1900, San Diego, CA 92101-4495, 1st edn., 2000.

Forster, P., V. Ramaswamy, P. Artaxo, T. Berntsen, R. Betts, D. Fahey, J. Haywood, J. Lean, D. Lowe, G. Myhre, J. Nganga, R. Prinn, G. Raga, M. Schulz, R. Van Dorland, and IPCC 2007. *Climate Change 2007: The Physical Science Basis. Contribution of Working Group I to the Fourth Assessment Report of the Intergovernmental Panel on Climate Change.* Cambridge University Press, Cambridge, UK and New York, NY, USA, 2007.

Fuchs, N. A. and A. G. Sutugin. *High-dispersed aerosols.* In G. M. Hidy and J. R. Brock (Editors), *Topics in current aerosol research.* Pergamon, New York, 1971.

Gerecke, A., A. Thielmann, L. Gutzwiller, and M. J. Rossi. *The chemical kinetics of HONO formation resulting from heterogeneous interaction of NO2 with flame soot.* Geophys. Res. Lett., 25(13): 2453–2456, 1998.

Gross, S. and A. K. Bertram. *Reactive uptake of NO3, N2O5, NO2, HNO3, and O-3 on three types of polycyclic aromatic hydrocarbon surfaces.* J. Phys. Chem. A, 112(14): 3104–3113, 2008. doi:10.1021/jp7107544.

Guilloteau, A., Y. Bedjanian, M. L. Nguyen, and A. Tomas. *Desorption of Polycyclic Aromatic Hydrocarbons from a Soot Surface: Three- to Five-Ring PAHs.* J. Phys. Chem. A, 114(2): 942–948, 2010. doi:10.1021/jp908862c.

Guilloteau, A., M. L. Nguyen, Y. Bedjanian, and G. Le Bras. *Desorption of Polycyclic Aromatic Hydrocarbons from Soot Surface: Pyrene and Fluoranthene.* J. Phys. Chem. A, 112(42): 10552–10559, 2008. doi: 10.1021/jp803043s.

Hansen, J., M. Sato, R. Ruedy, L. Nazarenko, A. Lacis, G. Schmidt, G. Russell, I. Aleinov, M. Bauer, S. Bauer, N. Bell, B. Cairns, V. Canuto, M. Chandler, Y. Cheng, A. Del Genio, G. Faluvegi, E. Fleming, A. Friend, T. Hall, C. Jackman, M. Kelley, N. Kiang, D. Koch, J. Lean, J. Lerner, K. Lo,

S. Menon, R. Miller, P. Minnis, T. Novakov, V. Oinas, J. Perlwitz, J. Perlwitz, D. Rind, A. Romanou, D. Shindell, P. Stone, S. Sun, N. Tausnev, D. Thresher, B. Wielicki, T. Wong, M. Yao, and S. Zhang. *Efficacy of climate forcings*. J. Geophys. Res.-Atmos., 110(D18), 2005. doi: 10.1029/2005JD005776.

Harner, T. and T. F. Bidleman. *Octanol-air partition coefficient for describing particle/gas partitioning of aromatic compounds in urban air*. Environ. Sci. Technol., 32(10): 1494–1502, 1998.

Homann, K.-H. *Fullerenes and soot formation - New pathways to large particles in flames*. Angew. Chem.-Int. Edit., 37(18): 2435–2451, 1998.

Ivanov, A. V., S. Trakhtenberg, A. K. Bertram, Y. M. Gershenzon, and M. J. Molina. *OH, HO2, and ozone gaseous diffusion coefficients*. J. Phys. Chem. A, 111(9): 1632–1637, 2007. doi:10.1021/jp066558w.

Jacobson, M. Z. *Development and application of a new air pollution modeling system .2. Aerosol module structure and design*. Atmos. Environ., 31(2): 131–144, 1997.

Jimenez, J. L., M. R. Canagaratna, N. M. Donahue, A. S. H. Prevot, Q. Zhang, J. H. Kroll, P. F. DeCarlo, J. D. Allan, H. Coe, N. L. Ng, A. C. Aiken, K. S. Docherty, I. M. Ulbrich, A. P. Grieshop, A. L. Robinson, J. Duplissy, J. D. Smith, K. R. Wilson, V. A. Lanz, C. Hueglin, Y. L. Sun, J. Tian, A. Laaksonen, T. Raatikainen, J. Rautiainen, P. Vaattovaara, M. Ehn, M. Kulmala, J. M. Tomlinson, D. R. Collins, M. J. Cubison, E. J. Dunlea, J. A. Huffman, T. B. Onasch, M. R. Alfarra, P. I. Williams, K. Bower, Y. Kondo, J. Schneider, F. Drewnick, S. Borrmann, S. Weimer, K. Demerjian, D. Salcedo, L. Cottrell, R. Griffin, A. Takami, T. Miyoshi, S. Hatakeyama, A. Shimono, J. Y. Sun, Y. M. Zhang, K. Dzepina, J. R. Kimmel, D. Sueper, J. T. Jayne, S. C. Herndon, A. M. Trimborn, L. R. Williams, E. C. Wood, A. M. Middlebrook, C. E. Kolb, U. Baltensperger, and D. R. Worsnop. *Evolution of Organic Aerosols in the Atmosphere*. Science, 326(5959): 1525–1529, 2009. doi:10.1126/science.1180353.

Kanakidou, M., J. H. Seinfeld, S. N. Pandis, I. Barnes, F. J. Dentener, M. C. Facchini, R. Van Dingenen, B. Ervens, A. Nenes, C. J. Nielsen, E. Swietlicki, J. Putaud, Y. Balkanski, S. Fuzzi, J. Horth, G. K. Moortgat, R. Winterhalter, C. E. L. Myhre, K. Tsigaridis, E. Vignati, E. G. Stephanou, and J. Wilson. *Organic aerosol and global climate modelling: a review*. Atmos. Chem. Phys., 5: 1053–1123, 2005.

Kashiwakura, K. and K. Sakamoto. *Emission Characteristics and Cancer Risks of Polycyclic Aromatic Hydrocarbon Emissions from Diesel-fueled Vehicles Complying with Recent Regulations.* J. Health Sci., 56(2): 200–207, 2010.

Khalizov, A. F., M. Cruz-Quinones, and R. Zhang. *Heterogeneous Reaction of NO2 on Fresh and Coated Soot Surfaces.* J. Phys. Chem. A, 2010.

Khoder, M. I. *Diurnal, seasonal and weekdays-weekends variations of ground level ozone concentrations in an urban area in greater Cairo.* Environ. Monit. Assess., 149(1-4): 349–362, 2009. doi:10.1007/s10661-008-0208-7.

Kleffmann, J., K. H. Becker, M. Lackhoff, and P. Wiesen. *Heterogeneous conversion of NO2 on carbonaceous surfaces.* PCCP Phys. Chem. Chem. Phys., 1(24): 5443–5450, 1999.

Knopf, D. A., B. Wang, A. Laskin, R. C. Moffet, and M. K. Gilles. *Heterogeneous nucleation of ice on anthropogenic organic particles collected in Mexico City.* Geophys. Res. Lett., 37, 2010. doi:10.1029/2010GL043362.

Kotamarthi, V. R., J. S. Gaffney, N. A. Marley, and P. V. Doskey. *Heterogeneous NOx chemistry in the polluted PBL.* Atmos. Environ., 35(26): 4489–4498, 2001.

Kotzick, R., U. Panne, and R. Niessner. *Changes in condensation properties of ultrafine carbon particles subjected to oxidation by ozone.* J. Aerosol. Sci., 28(5): 725–735, 1997.

Kwamena, N. O. A., J. A. Thornton, and J. P. D. Abbatt. *Kinetics of surface-bound benzo[a]pyrene and ozone on solid organic and salt aerosols.* J. Phys. Chem. A, 108(52): 11626–11634, 2004. doi:10.1021/jp046161x.

Matthias, V., A. Aulinger, and M. Quante. *CMAQ simulations of the benzo(a)pyrene distribution over Europe for 2000 and 2001.* Atmos. Environ., 43(26): 4078–4086, 2009. doi:10.1016/j.atmosenv.2009.04.058.

Molina, M. J., T. L. Tso, L. T. Molina, and F. C. Y. Wang. *Antarctic stratospheric chemistry of chlorine nitrate, hydrogen-chloride and ice - release of active chlorine.* Science, 238(4831): 1253–1257, 1987.

Müller, J. F. *Geographical distribution and seasonal variation of surface emissions and deposition velocities of atmospheric trace gases.* J. Geophys. Res.-Atmos., 97(D4): 3787–3804, 1992.

National Research Council, Committee on Tropospheric Ozone. *Rethinking the Ozone Problem in Urban and Regional Air Pollution*. National Academy Press, 2101 Constitution Ave., N.W., Washington, D.C. 20418, 1st edn., 1991.

Nguyen, M. L., Y. Bedjanian, and A. Guilloteau. *Kinetics of the reactions of soot surface-bound polycyclic aromatic hydrocarbons with NO2*. J. Atmos. Chem., 62(2): 139–150, 2009. doi:10.1007/s10874-010-9144-3.

Nienow, A. M. and J. T. Roberts. *Heterogeneous chemistry of carbon aerosols*. Annu. Rev. Phys. Chem., 57: 105–128, 2006. doi:10.1146/annurev.physchem.57.032905.104525.

Nishino, J. *Adsorption of water Vapor and carbon dioxide at carboxylic functional groups on the surface of coal*. Fuel, 80(5): 757–764, 2001.

Pakbin, P., Z. Ning, J. J. Schauer, and C. Sioutas. *Characterization of Particle Bound Organic Carbon from Diesel Vehicles Equipped with Advanced Emission Control Technologies*. Environ. Sci. Technol., 43(13): 4679–4686, 2009. doi:10.1021/es8030825.

Pandey, S. K., K.-H. Kim, S.-Y. Chung, S.-J. Cho, M.-Y. Kim, and Z.-H. Shon. *Long-term study of NOx behavior at urban roadside and background locations in Seoul, Korea*. Atmos. Environ., 42(4): 607–622, 2008. doi:10.1016/j.atmosenv.2007.10.015.

Parrish, D. D., C. H. Hahn, D. W. Fahey, E. J. Williams, M. J. Bollinger, G. Hubler, M. P. Buhr, P. C. Murphy, M. Trainer, E. Y. Hsie, S. C. Liu, and F. C. Fehsenfeld. *Systematic variations in the concentration of NOx (NO plus NO2) at Niwot-Ridge, Colorado*. J. Geophys. Res.-Atmos., 95(D2): 1817–1836, 1990.

Phillips, D. H. *Fifty years of benzo[a]pyrene*. Nature, 303(5917): 468–472, 1983.

Pöschl, U. *Formation and decomposition of hazardous chemical components contained in atmospheric aerosol particles*. J. Aerosol Med.-Depos. Clear. Eff. Lung, 15(2): 203–212, 2002.

Pöschl, U. *Atmospheric aerosols: Composition, transformation, climate and health effects*. Angew. Chem.-Int. Edit., 44(46): 7520–7540, 2005. doi:10.1002/anie.200501122.

Pöschl, U., T. Letzel, C. Schauer, and R. Niessner. *Interaction of ozone and water vapor with spark discharge soot aerosol particles coated with benzo[a]pyrene: O-3 and H2O adsorption, benzo[a]pyrene degradation, and atmospheric implications.* J. Phys. Chem. A, 105(16): 4029–4041, 2001.

Pöschl, U., Y. Rudich, and M. Ammann. *Kinetic model framework for aerosol and cloud surface chemistry and gas-particle interactions - Part 1: General equations, parameters, and terminology.* Atmos. Chem. Phys., 7(23): 5989–6023, 2007.

Pósfai, M., J. R. Anderson, P. R. Buseck, and H. Sievering. *Soot and sulfate aerosol particles in the remote marine troposphere.* J. Geophys. Res.-Atmos., 104(D17): 21685–21693, 1999.

Pruppacher, H. R. and J. D. Klett. *Microphysics of Clouds and Precipitation.* Kluwer Academic Publishers, P.O. Box 17, 3300 AA Dordrecht, The Netherlands, 2nd edn., 1997.

Ramanathan, V., P. J. Crutzen, J. T. Kiehl, and D. Rosenfeld. *Atmosphere - Aerosols, climate, and the hydrological cycle.* Science, 294(5549): 2119–2124, 2001.

Riemer, N., M. West, R. A. Zaveri, and R. C. Easter. *Simulating the evolution of soot mixing state with a particle-resolved aerosol model.* J. Geophys. Res.-Atmos., 114, 2009. doi:10.1029/2008JD011073.

Rogaski, C. A., D. M. Golden, and L. R. Williams. *Reactive uptake and hydration experiments on amorphous carbon treated with NO2, SO2, O-3, HNO3, and H2SO4.* Geophys. Res. Lett., 24(4): 381–384, 1997.

Rothenberg, G. *Catalysis.* Wiley-VCH Verlag GmbH & Co. KGaA, Weinheim, 1st edn., 2008.

Rudich, Y. *Laboratory perspectives on the chemical transformations of organic matter in atmospheric particles.* Chem. Rev., 103(12): 5097–5124, 2003. doi:10.1021/cr020508f.

Rudich, Y., N. M. Donahue, and T. F. Mentel. *Aging of organic aerosol: Bridging the gap between laboratory and field studies.* Annu. Rev. Phys. Chem., 58: 321–352, 2007. doi:10.1146/annurev.physchem.58.032806.104432.

Rudich, Y., R. K. Talukdar, and A. R. Ravishankara. *Reactive uptake of NO3 on pure water and ionic solutions.* J. Geophys. Res.-Atmos., 101(D15): 21023–21031, 1996.

Saathoff, H., K. H. Naumann, N. Riemer, S. Kamm, O. Mohler, U. Schurath, H. Vogel, and B. Vogel. *The loss of NO2, HNO3, NO3/N2O5, and HO2/HOONO2 on soot aerosol: A chamber and modeling study.* Geophys. Res. Lett., 28(10): 1957–1960, 2001.

Seinfeld, J. H. and S. N. Pandis. *Atmospheric chemistry and physics.* John Wiley & Sons, Inc., 111 River Street, Hoboken, NJ 07030, 2nd edn., 2006.

Shiraiwa, M., R. M. Garland, and U. Pöschl. *Kinetic double-layer model of aerosol surface chemistry and gas-particle interactions (K2-SURF): Degradation of polycyclic aromatic hydrocarbons exposed to O-3, NO2, H2O, OH and NO3.* Atmos. Chem. Phys., 9(24): 9571–9586, 2009.

Solomon, S., R. R. Garcia, F. S. Rowland, and D. J. Wuebbels. *On the depletion of Antarctic ozone.* Nature, 321(6072): 755–758, 1986.

Springmann, M., D. A. Knopf, and N. Riemer. *Detailed heterogeneous chemistry in an urban plume box model: reversible co-adsorption of O-3, NO2, and H2O on soot coated with benzo[a]pyrene.* Atmos. Chem. Phys., 9(19): 7461–7479, 2009.

Stier, P., J. Feichter, S. Kinne, S. Kloster, E. Vignati, J. Wilson, L. Ganzeveld, I. Tegen, M. Werner, Y. Balkanski, M. Schulz, O. Boucher, A. Minikin, and A. Petzold. *The aerosol-climate model ECHAM5-HAM.* Atmos. Chem. Phys., 5: 1125–1156, 2005.

Stockwell, W. R., P. Middleton, J. S. Chang, and X. Y. Tang. *The 2nd generation regional acid deposition model chemical mechanism for regional air quality modeling.* J. Geophys. Res.-Atmos., 95(D10): 16343–16367, 1990.

Tabor, K., L. Gutzwiller, and M. J. Rossi. *Heterogeneous chemical kinetics of NO2 on amorphous carbon at ambient temperature.* J. Phys. Chem., 98(24): 6172–6186, 1994.

Tie, X., G. Brasseur, L. Emmons, L. Horowitz, and D. Kinnison. *Effects of aerosols on tropospheric oxidants: A global model study.* J. Geophys. Res.-Atmos., 106(D19): 22931–22964, 2001.

U.S. EPA. *Air quality criteria for ozone and related photochemical oxidants (2006 final).* Tech. rep., U.S. Environmental Protection Agency, Washington, DC, EPA/600/R-05/004aF-cF, 2006.

U.S. EPA. *Integrated science assessment for particulate matter (final report)*. Tech. rep., U.S. Environmental Protection Agency, Washington, DC, EPA/600/R-08/139F, 2009a.

U.S. EPA. *Provisional assessment of recent studies on health and ecological effects of ozone exposure*. Tech. rep., U.S. Environmental Protection Agency, Washington, DC, EPA/600/R-09/101, 2009b.

Vander Wal, R. L. and A. J. Tomasek. *Soot oxidation: dependence upon initial nanostructure*. Combust. Flame, 134(1-2): 1–9, 2003. doi:10.1016/S0010-2180(03)00084-1.

Vogel, B., H. Vogel, and F. Fiedler. In: *Ozone in the Troposphere and Stratosphere, Part 1*. Tech. rep., NASA. Goddard Space Flight Center, United States, 1994.

Wilson, J., C. Cuvelier, and F. Raes. *A modeling study of global mixed aerosol fields*. J. Geophys. Res.-Atmos., 106(D24): 34081–34108, 2001.

Zanobetti, A. and J. Schwartz. *The Effect of Fine and Coarse Particulate Air Pollution on Mortality: A National Analysis*. Environ. Health Perspect., 117(6): 898–903, 2009. doi:10.1289/ehp.0800108.

Zaveri, R. A., R. C. Easter, J. D. Fast, and L. K. Peters. *Model for Simulating Aerosol Interactions and Chemistry (MOSAIC)*. J. Geophys. Res.-Atmos., 113(D13), 2008. doi:10.1029/2007JD008782.

Zaveri, R. A., R. C. Easter, and L. K. Peters. *A computationally efficient multicomponent equilibrium solver for aerosols (MESA)*. J. Geophys. Res.-Atmos., 110(D24), 2005a. doi:10.1029/2004JD005618.

Zaveri, R. A., R. C. Easter, and A. S. Wexler. *A new method for multicomponent activity coefficients of electrolytes in aqueous atmospheric aerosols*. J. Geophys. Res.-Atmos., 110(D2), 2005b. doi:10.1029/2004JD004681.

Zaveri, R. A. and L. K. Peters. *A new lumped structure photochemical mechanism for large-scale applications*. J. Geophys. Res.-Atmos., 104(D23): 30387–30415, 1999.

Zhang, L., A. Wiebe, R. Vet, C. Mihele, J. M. O'Brien, S. Iqbal, and Z. Liang. *Measurements of reactive oxidized nitrogen at eight Canadian rural sites*. Atmos. Environ., 42(34): 8065–8078, 2008. doi:10.1016/j.atmosenv.2008.06.034.

Appendix: PartMC-MOSAIC Code

PartMC-MOSAIC, in the version used for this study, consists of more than 100 separate code files. Hence, it is not practical to reproduce the complete code here, or even to give a comprehensive overview of its structure. Instead, we refer the reader to `http://lagrange.mechse.illinois.edu/mwest/partmc/`, where PartMC is available under the GNU General Public License (GPL), and to Rahul A. Zaveri (Atmospheric Science and Global Change Division, Pacific Northwest National Laboratory, Richland, Washington, USA), from whom the MOSAIC code can be obtained upon request.

To show some of the changes that were made to the code of PartMC-MOSAIC for the purpose of this thesis, i.e., to include heterogeneous kinetics based on the PRA framework, we reproduce four selected files here. This choice reflects only the major changes that actually modify the behavior of PartMC-MOSAIC.

A.1 gaschemistry.f90

```
! This file calls the subroutines necessary for the calculation of gas
! phase changes. The treatment of heterogeneous kinetics has been
! included in this module of MOSAIC.


      subroutine GasChemistry(t_in, t_out)
      use module_data_mosaic_kind, only: r8
      use module_data_mosaic_main, only: o2, cair_mlc, h2, h2o, RH, &
         te, pr_atm, iscenario, avogad, dt_sec
      use module_data_mosaic_gas, only: mw_gas, io3, ino2, vel_gas, &
         uptake_gas, ino3, ih2o
      use module_data_mosaic_aero, only: gamma, nbin_a, aer, ipah_a

      implicit none

      real(r8) :: t_in, t_out
      integer nss_spec, ns_spec, ntot, ibin
      real(r8) :: WaterVapor, sigma_pah, store_pah(nbin_a), &
         RH_from_WaterVapor
      real(r8), allocatable :: stot(:)
```

```
o2  = 0.21*cair_mlc
h2  = 0.58*1.e-6*cair_mlc
h2o = WaterVapor(RH, cair_mlc, te, pr_atm)

sigma_pah = 8.d-15    ! PAH (and Y-species) molecular cross section

! set # of quasi-static surface layer species (nss_spec) and # of
! sorption layer species (ns_spec) for selected scenario
nss_spec = 0
ns_spec = 0
if (iscenario .ne. 0) call SetScenario(nss_spec,ns_spec)

! select iregime and calculates ntot
call SelectGasRegime(ntot,nss_spec,ns_spec)

call PeroxyRateConstants

call SetGasIndices       ! set gas indices for selected iregime

allocate(stot(ntot))
stot = 0d0
allocate(gamma(3, nbin_a))
gamma = 0.d0
do ibin = 1, nbin_a
   store_pah(ibin) = aer(ipah_a, 3, ibin) * avogad * 1d-15
end do

call GasRateConstants

if (iscenario .ne. 0) then
   ! "initialize" adsorbing gas concentrations if necessary
   call init_ads_gas_conc(ns_spec, dt_sec, sigma_pah)
end if

! map cnn and aer into stot for selected iregime
call MapGasSpecies(ntot,stot,0)

call GasIntegrator(ntot,stot,t_in,t_out)

if (iscenario .ne. 0) then
   call y2_approx(store_pah, ntot, stot, dt_sec, sigma_pah)
end if

call MapGasSpecies(ntot,stot,1)  ! map stot back into cnn and aer

! calculate sorption layer concentrations and gas phase feedback
if (iscenario .ne. 0) call steady_state(ns_spec, dt_sec)

RH = RH_from_WaterVapor(h2o, cair_mlc, te, pr_atm)

deallocate(stot)
deallocate(gamma)


return
end subroutine GasChemistry
```

A.2 gasrateconstants_het.f90

```
!***************************************************************
! subroutine GasRateConstants_Het: generates thermal rate coefficients
!                   for the selected mechanism
! nomenclature:
! rk_het     = reaction rate constants for heterogeneous rxns (1/s)
!
! author: Rahul A. Zaveri
! date   : June 2006
!
! This file was extended by J. C. Kaiser in 2009/10 to set rate
! constants for adsorption and desorption of O3, NO2, and H2O,
! for several surface layer reactions and for gas-surface-reactions of
! OH and NO3 with particle-bound substances based on the PRA framework
! (Poeschl et al., 2007; Ammann and Poeschl, 2007). Each particle in the
! simulated population is treated individually.
!
!---------------------------------------------------------------------

      subroutine GasRateConstants_Het
      use module_data_mosaic_kind, only: r8
      use module_data_mosaic_main, only: pr_atm, steadystate, &
         te, dt_sec, iscenario
      use module_data_mosaic_gas, only: ngas_max, mw_gas, uptake_gas, &
         D_gas, ihet_gas, vel_gas, rk_het, &
         io3, in2o5, ihno3, ino3, iho2, ino2, ino, iro2, iso2, ih2o, &
         ioh
      use module_data_mosaic_aero, only: naer_s, nbin_a, k_slr, &
         num_a, naer, naer_ss, gamma, i_gsr_1, i_gsr_2, t_des

      implicit none

      logical first
      save first
      data first/.true./
      integer i, ibin, igas, ispec
      integer counter, map_ads_to_gas(naer_s)
      real(r8) :: conv_fac(nbin_a), ads_rate_coeff, surf_area, &
         gamma_slr, Cg, gas_phase_diff_corr_fac


      if(first)then
        first=.false.

        do igas = 1, ngas_max
          mw_gas(igas)     = 1.0 ! molecular weight
          uptake_gas(igas) = 1.0 ! reaction probablity or
                                 ! accomodation coefficient
          D_gas(igas)      = 0.1 ! gas-phase diffusivity in air [cm^2/s]
          ihet_gas(igas)   = 0   ! flag to turn on/off reaction
        enddo

        ihet_gas(ih2o) = 0

        mw_gas(io3)   = 48.0
        mw_gas(in2o5) = 108.0
        mw_gas(ihno3) = 63.0
        mw_gas(ino3)  = 62.0
        mw_gas(iho2)  = 33.0
```

```
      mw_gas(ino2)  = 46.0
      mw_gas(ino)   = 30.0
      mw_gas(iro2)  = 75.0  ! assumed as C3H7O2
      mw_gas(iso2)  = 64.0
      mw_gas(ih2o)  = 18.0
      mw_gas(ioh)   = 17.0

      ! accomodation coefficients of adsorbate-free particles
      uptake_gas(io3)   = 1.0d-3   ! O3 on soot (Shiraiwa et al., 2009)
      uptake_gas(in2o5) = 0.1   ! N2O5 --> 2HNO3
      uptake_gas(ihno3) = 0.1   ! HNO3 --> NO2
      uptake_gas(iho2)  = 0.1   ! HO2 --> 0.5H2O2
      uptake_gas(ino2)  = 6.4d-2   ! NO2 on soot (Tabor et al., 1994)
      uptake_gas(ino)   = 0.1   ! NO --> ?
      uptake_gas(iro2)  = 0.1   ! RO2 -->
      uptake_gas(iso2)  = 0.1   ! SO2 --> H2SO4
      uptake_gas(ih2o)  = 4.d-4   ! H2O on soot (Rogaski et al., 1997)

      ! gas surface reaction probabilities
      uptake_gas(ioh)   = 3.2d-1   ! OH-PYR (Bertram et al., 2001)
      uptake_gas(ino3)  = 7.9d-1   ! NO3-PYR (Gross and Bertram, 2008)

      ! diffusion coefficients for OH and NO3
      D_gas(ioh)  = 217.d0 / (pr_atm * 1013.25d0)   ! Ivanov et al., 2007
      D_gas(ino3) = 107.d0 / (pr_atm * 1013.25d0)   ! Rudich et al., 1996

      ! surface layer reaction rate constants [cm^2/s]
      k_slr(1) = 2.7d-17   ! Shiraiwa et al., 2009 based on
                           ! Poeschl et al., 2001
      k_slr(2) = 2.7d-19   ! (as above + Ammann and Poeschl, 2007)
      k_slr(3) = 2.7d-21   ! (as above)
      k_slr(4) = 7.d-18    ! Ammann and Poeschl, 2007
      k_slr(5) = 7.5d-21   ! Ammann and Poeschl, 2007
      k_slr(6) = 5.d-17    ! Shiraiwa et al., 2009
      k_slr(7) = 5.d-15    ! Shiraiwa et al., 2009

      ! on/off flags for calculation of gas uptake or GSRs via ODEs
      go to (8,7,6,5,4,3,2,1), iscenario + 1

1     continue

2     ihet_gas(ino3) = 1
      if (iscenario .ne. 7) go to 5

3     ihet_gas(ioh)  = 1
      if (iscenario .ne. 7) go to 5

4     continue   ! no additional effect of the gas phase on the particles

5     ihet_gas(ih2o) = 1 - steadystate

6     ihet_gas(ino2) = 1 - steadystate

7     ihet_gas(io3)  = 1 - steadystate

      ! former MOSAIC flags, not used at the moment:
8     ihet_gas(in2o5) = 0   ! N2O5 --> 2HNO3
      ihet_gas(ihno3) = 0   ! HNO3 --> NO2
      ihet_gas(iho2)  = 0   ! HO2 --> 0.5H2O2
      ihet_gas(ino)   = 0   ! NO --> ?
```

```
  ihet_gas(iro2)  = 0    ! RO2 -->
  ihet_gas(iso2)  = 0    ! SO2 --> H2SO4

end if

! mean molecular speeds will be required in subroutines
! ads_rate_coeff, gas_phase_diff_corr_fac and
! steady_state_sorp_spec_conc:
do igas = 1, ngas_max + 1
   vel_gas(igas) = 1.455d4 * sqrt(te/mw_gas(igas))
end do

if (iscenario .eq. 0) then
   ! do what MOSAIC used to do before heterogeneous
   ! kinetics were implemented
   do igas = 1, ngas_max
      rk_het(igas) = 0.d0
      do ibin = 1, nbin_a
         ! first order mtc [1/s]
        rk_het(igas) = rk_het(igas) &
          + ihet_gas(igas) * ads_rate_coeff(igas, ibin)
      end do
   end do
   return
end if

call SetHetReactionIndices

! update these values because ih2o might have changed its value
if (iscenario .gt. 2) then
   ihet_gas(ih2o) = 1 - steadystate
   uptake_gas(ih2o) = 4.d-4
   mw_gas(ih2o) = 18.0
end if

! map indices
map_ads_to_gas(1) = io3
map_ads_to_gas(2) = ino2
map_ads_to_gas(3) = ih2o
map_ads_to_gas(4) = ioh
map_ads_to_gas(5) = ino3

! conversion factors from volume concentration
! to surface concentration
do ibin = 1, nbin_a
   conv_fac(ibin) = 1.d0 / (surf_area(ibin) * num_a(ibin))
end do

if (steadystate .eq. 1) then
   ! store uptake coefficients for gas phase feedback
   do i = 1, 3
      ispec = naer + naer_ss + i
      do ibin = 1, nbin_a
         gamma(i, ibin) = gamma_slr(ispec, ibin)
      end do
   end do
end if

counter = 0
```

```
! adsorption rate coefficients per particle,
! indices i_ads_o3 through i_gsr_2 + nbin_a - 1
do i = 1, naer_s
  igas = map_ads_to_gas(i)
  do ibin = 1, nbin_a
    counter = counter + 1
    ! first order mtc [1/s]
    rk_het(counter) = ihet_gas(igas) * ads_rate_coeff(igas, ibin)
  end do
end do

! correction of gas surface reaction rate coefficients,
! indices i_gsr_1 through i_gsr_1 + nbin_a - 1,
! ATTENTION: assumes molecular cross section of PAH to be 8e-15
! FIXME: change 8.d-15 to sigma_pah
if ((iscenario .eq. 5) .or. (iscenario .eq. 7)) then
   do ibin = 1, nbin_a
      Cg = gas_phase_diff_corr_fac(ioh, ibin)
      rk_het(i_gsr_1+ibin-1) = rk_het(i_gsr_1+ibin-1) * Cg &
         * 8.d-15 * conv_fac(ibin)
   end do
end if

! correction of gas surface reaction rate coefficients,
! indices i_gsr_2 through i_gsr_2 + nbin_a - 1,
! ATTENTION: assumes molecular cross section of PAH to be 8e-15
! FIXME: change 8.d-15 to sigma_pah
if ((iscenario .eq. 6) .or. (iscenario .eq. 7)) then
   do ibin = 1, nbin_a
      Cg = gas_phase_diff_corr_fac(ino3, ibin)
      rk_het(i_gsr_2+ibin-1) = rk_het(i_gsr_2+ibin-1) * Cg &
         * 8.d-15 * conv_fac(ibin)
   end do
end if

! desorption rate coefficients per particle,
! indices i_des_o3 through i_des_no3 + nbin_a - 1
do i = 1, naer_s
   igas = map_ads_to_gas(i)
   do ibin = 1, nbin_a
      counter = counter + 1
      rk_het(counter) = 1.d0 / t_des(i)
   end do
end do

! Langmuir-Hinshelwood type reaction rate coefficients,
! convert from [cm^2/s] on particle surface to [cm^3/s] with
! respect to comp. vol,
! indices i_slr_1 through i_slr_7 + nbin_a - 1
do ibin = 1, nbin_a
   counter = counter + 1
   rk_het(counter) = k_slr(1) * conv_fac(ibin)
   rk_het(counter+nbin_a) = k_slr(2) * conv_fac(ibin)
   rk_het(counter+2*nbin_a) = k_slr(3) * conv_fac(ibin)
   rk_het(counter+3*nbin_a) = k_slr(4) * conv_fac(ibin)
   rk_het(counter+4*nbin_a) = k_slr(5) * conv_fac(ibin)
   rk_het(counter+5*nbin_a) = k_slr(6) * conv_fac(ibin)
   rk_het(counter+6*nbin_a) = k_slr(7) * conv_fac(ibin)
end do
```

```
      return
      end subroutine GasRateConstants_Het
```

A.3 ode_het.f90

```
! In this file, gain and loss terms of the differential equations for
! gas species involved in heterogeneous processes are set for each
! particle individually, and depending on the choice of scenario. These
! terms are used by the numerical integration routine DLSODES to
! calculate gas phase and particle composition evolution.


!***********************************************************************
      subroutine ode_het
      use module_data_mosaic_main
      use module_data_mosaic_gas
      use module_data_mosaic_aero, only: nbin_a, &
         i_gsr_2, i_gsr_1, i_slr_6, i_des_no3, i_slr_7, i_ads_h2o, &
         i_des_h2o, i_ads_no2, i_des_no2, i_slr_5, i_slr_4, i_ads_o3, &
         i_des_o3, i_slr_1, i_slr_2, i_slr_3, &
         ipah_s, iy8_s, iy7_s, io3_ad, ino2_ad, ino3_ad, iy6_s, &
         ih2o_ad, iy5_s, iy2_s, iy3_s, io3_ad, iy4_s

      implicit none

      integer igas, ibin


      if (iscenario .eq. 0) then
         do igas = 1, ngas_max
           p_het(igas) = 0.0
           d_het(igas) = r_het(igas)
         end do
         p_het(ihno3)  = 2.*r_het(in2o5)
         p_het(ino)    = r_het(ino3)
         p_het(ih2so4) = r_het(iso2)
         return
      end if

      go to (7,6,5,4,3,2,1), iscenario

1     continue

2     do ibin = 1, nbin_a
         ! chemical gas phase loss of NO3
         d_het(ino3) = d_het(ino3) + r_het(i_gsr_2+ibin-1)
         ! chemical loss of PAH
         d_het(ipah_s+ibin-1) = d_het(ipah_s+ibin-1) &
            + r_het(i_gsr_2+ibin-1)
         ! production of Y8
         p_het(iy8_s+ibin-1) = p_het(iy8_s+ibin-1) &
            + r_het(i_gsr_2+ibin-1)
      end do
      if (iscenario .ne. 7) go to 5
```

```
3     do ibin = 1, nbin_a
         ! chemical gas phase loss of OH
         d_het(ioh) = d_het(ioh) + r_het(i_gsr_1+ibin-1)
         ! chemical loss of PAH
         d_het(ipah_s+ibin-1) = d_het(ipah_s+ibin-1) &
            + r_het(i_gsr_1+ibin-1)
         ! production of Y7
         p_het(iy7_s+ibin-1) = p_het(iy7_s+ibin-1) &
            + r_het(i_gsr_1+ibin-1)
      end do
      if (iscenario .ne. 7) go to 5

4     do ibin = 1, nbin_a

         if (steadystate .eq. 0) then
            ! chemical loss of adsorbed O3 and NO2
            d_het(io3_ad+ibin-1) = d_het(io3_ad+ibin-1) &
               + r_het(i_slr_6+ibin-1)
            d_het(ino2_ad+ibin-1) = d_het(ino2_ad+ibin-1) &
               + r_het(i_slr_6+ibin-1)
            ! ...produces NO3 (and O2?)
            p_het(ino3_ad+ibin-1) = p_het(ino3_ad+ibin-1) &
               + r_het(i_slr_6+ibin-1)
            ! ...which desorbs or reacts with PAH
            d_het(ino3_ad+ibin-1) = d_het(ino3_ad+ibin-1) &
               + r_het(i_des_no3+ibin-1) &
               + r_het(i_slr_7+ibin-1)
         end if

         d_het(ipah_s+ibin-1) = d_het(ipah_s+ibin-1) &
            + r_het(i_slr_7+ibin-1)
         ! production of Y6
         p_het(iy6_s+ibin-1) = p_het(iy6_s+ibin-1) &
            + r_het(i_slr_7+ibin-1)
         ! gas phase gain due to desorption of NO3
         p_het(ino3) = p_het(ino3) + r_het(i_des_no3+ibin-1)

      end do

5     if (steadystate .ne. 0) go to 6
      do ibin = 1, nbin_a
         ! gas phase loss of adsorbing water vapor
         d_het(ih2o) = d_het(ih2o) + r_het(i_ads_h2o+ibin-1)
         ! gas phase gain due to desorption of water vapor
         p_het(ih2o) = p_het(ih2o) + r_het(i_des_h2o+ibin-1)
         ! gain of adsorbing water vapor on particles
         p_het(ih2o_ad+ibin-1) = p_het(ih2o_ad+ibin-1) &
            + r_het(i_ads_h2o+ibin-1)
         ! desorption and chemical loss of water vapor from particles
         d_het(ih2o_ad+ibin-1) = d_het(ih2o_ad+ibin-1) &
            + r_het(i_des_h2o+ibin-1)
      end do

6     do ibin = 1, nbin_a

         if (steadystate .eq. 0) then
            ! gas phase loss of adsorbing NO2
            d_het(ino2) = d_het(ino2) + r_het(i_ads_no2+ibin-1)
            ! gas phase gain due to desorption of NO2
            p_het(ino2) = p_het(ino2) + r_het(i_des_no2+ibin-1)
```

```
            ! gain of adsorbing NO2 on particles
            p_het(ino2_ad+ibin-1) = p_het(ino2_ad+ibin-1) &
               + r_het(i_ads_no2+ibin-1)
            ! desorption from particles
            d_het(ino2_ad+ibin-1) = d_het(ino2_ad+ibin-1) &
               + r_het(i_des_no2+ibin-1)
            ! chemical loss of adsorbed NO2
            d_het(ino2_ad+ibin-1) = d_het(ino2_ad+ibin-1) &
               + r_het(i_slr_4+ibin-1) &
               + r_het(i_slr_5+ibin-1)
         end if

         ! gas phase gain due to desorption of produced HONO, currently
         ! treated as instantly desorbing
         p_het(ihono) = p_het(ihono) + r_het(i_slr_5+ibin-1)
         ! reactions involving quasi-static surface layer species
         p_het(iy5_s+ibin-1) = p_het(iy5_s+ibin-1) &
            + r_het(i_slr_4+ibin-1)
         d_het(iy2_s+ibin-1) = d_het(iy2_s+ibin-1) &
            + r_het(i_slr_4+ibin-1)
         d_het(iy3_s+ibin-1) = d_het(iy3_s+ibin-1) &
            + r_het(i_slr_5+ibin-1)

      end do

7     do ibin = 1, nbin_a

         if (steadystate .eq. 0) then
            ! gas phase loss of adsorbing O3
            d_het(io3) = d_het(io3) + r_het(i_ads_o3+ibin-1)
            ! gas phase gain due to desorption of O3
            p_het(io3) = p_het(io3) + r_het(i_des_o3+ibin-1)
            ! gain of adsorbing ozone on particles
            p_het(io3_ad+ibin-1) = p_het(io3_ad+ibin-1) &
               + r_het(i_ads_o3+ibin-1)
            ! desorption from particles
            d_het(io3_ad+ibin-1) = d_het(io3_ad+ibin-1) &
               + r_het(i_des_o3+ibin-1)
            ! chemical loss of adsorbed ozone
            d_het(io3_ad+ibin-1) = d_het(io3_ad+ibin-1) &
               + r_het(i_slr_1+ibin-1) &
               + r_het(i_slr_2+ibin-1) &
               + r_het(i_slr_3+ibin-1)
         end if

         ! reactions involving quasi-static surface layer species
         p_het(iy2_s+ibin-1)  = p_het(iy2_s+ibin-1) &
            + r_het(i_slr_1+ibin-1)
         p_het(iy3_s+ibin-1)  = p_het(iy3_s+ibin-1) &
            + r_het(i_slr_2+ibin-1)
         p_het(iy4_s+ibin-1)  = p_het(iy4_s+ibin-1) &
            + r_het(i_slr_3+ibin-1)
         d_het(ipah_s+ibin-1) = d_het(ipah_s+ibin-1) &
            + r_het(i_slr_1+ibin-1)
         d_het(iy2_s+ibin-1)  = d_het(iy2_s+ibin-1) &
            + r_het(i_slr_2+ibin-1)
         d_het(iy3_s+ibin-1)  = d_het(iy3_s+ibin-1) &
            + r_het(i_slr_3+ibin-1)

      end do
```

```
      return
      end subroutine ode_het
```

A.4 hetchemistry.f90

```
! This file contains a collection of functions and subroutines for the
! computation of heterogeneous kinetics within MOSAIC.
! (written by J. C. Kaiser, 2009/10)


!> computes adsorption rate coefficient of gas igas on particle ibin
      function ads_rate_coeff(igas, ibin)
      use module_data_mosaic_kind, only: r8
      use module_data_mosaic_gas, only:  uptake_gas, k_gas, vel_gas
      use module_data_mosaic_aero, only: num_a

      implicit none

      real(r8) :: ads_rate_coeff
      ! func. arguments:
      integer :: igas, ibin
      ! local variables:
      real(r8) :: accom, surf_cov, surf_area

      ! dynamic accommodation coefficient
      accom = uptake_gas(igas) * (1.d0 - surf_cov(ibin))

      ! mass transfer coefficient [cm/s]
      k_gas(igas) = vel_gas(igas) * accom / 4.d0

      ads_rate_coeff = k_gas(igas) * surf_area(ibin) * num_a(ibin)  ! [1/s]
      ads_rate_coeff = max(0.d0, ads_rate_coeff)   ! [1/s]

      return
      end function ads_rate_coeff


!-----------------------------------------------------------------------

!> computes surface concentration of ispec on particle ibin
      function surf_conc(ispec, ibin)
      use module_data_mosaic_kind, only: r8
      use module_data_mosaic_main, only: avogad
      use module_data_mosaic_aero, only: aer, num_a

      implicit none

      real(r8) :: surf_conc
      ! func. arguments:
      integer :: ispec, ibin
      ! local variables:
      real(r8) :: num_molec, surf_area

      ! convert nmol/m^3 to # of molecules
      num_molec = aer(ispec, 3, ibin) * avogad * 1d-15 / num_a(ibin)
```

```
      surf_conc = num_molec / surf_area(ibin) ! [molec/cm^2]

      return
      end function surf_conc

!-----------------------------------------------------------------------

!> computes sorption layer coverage of particle ibin
      function surf_cov(ibin)
      use module_data_mosaic_kind, only: r8
      use module_data_mosaic_aero, only: naer_s, naer, &
         naer_ss, cross_sect

      implicit none

      real(r8) :: surf_cov
      ! func. argument:
      integer :: ibin
      ! local variables:
      integer :: i, isorp
      real(r8) :: surf_conc

      surf_cov = 0.d0

      do i = 1, naer_s
         isorp = naer + naer_ss + i
         surf_cov = surf_cov + surf_conc(isorp, ibin) * cross_sect(i)
      enddo


      return
      end function surf_cov

!-----------------------------------------------------------------------

!> computes surface area of particle ibin
      function surf_area(ibin)
      use module_data_mosaic_kind, only: r8
      use module_data_mosaic_main, only: pi

      implicit none

      real(r8) :: surf_area
      ! func. argument:
      integer :: ibin
      ! local variables:
      real(r8) :: particle_volume, var, d_part

      var = particle_volume(ibin) * 3.d0 / 4.d0 / pi
      d_part = 2.d0 * (var)**(1.d0 / 3.d0)  ! particle diameter [cm]
      surf_area = pi * d_part**2   ! [cm^2]

      return
      end function surf_area

!-----------------------------------------------------------------------
```

```
!> computes core volume of particle ibin
      function particle_volume(ibin)
      use module_data_mosaic_kind, only: r8
      use module_data_mosaic_aero, only: naer, mw_aer_mac, num_a, &
         dens_aer_mac, aer

      implicit none

      real(r8) :: particle_volume
      ! func. argument:
      integer :: ibin
      ! local variables:
      integer :: ispec
      real(r8) :: vol_part, vol_spec, conv_fac(naer)

      ! compute aerosol conversion factors
      ! (nmol(species)/m^3(air) to cm^3(species))
      do ispec = 1, naer
         conv_fac(ispec) = 1.D-15 * mw_aer_mac(ispec) / num_a(ibin) &
            / dens_aer_mac(ispec)
      enddo

      vol_part = 0d0
      do ispec = 1, naer
         ! volume of species ispec in particle [cm^3]
         vol_spec = aer(ispec, 3, ibin) * conv_fac(ispec)
         vol_part = vol_part + vol_spec   ! volume of particle [cm^3]
      enddo

      particle_volume = vol_part

      return
      end function particle_volume


!-----------------------------------------------------------------------

!> supplies the algebraic functions to be zeroed under steady state
!  assumption to the solver nleq1e. Input x must be in
!  [molec/cm^3(air)], output f will be in [molec/cm^3(air)/s].
      subroutine fcn(n, x, ibin, f, ifail)
      use module_data_mosaic_kind, only: r8
      use module_data_mosaic_main, only: iscenario, h2o, cnn
      use module_data_mosaic_gas,  only: vel_gas, uptake_gas, &
         ih2o, ino2, io3
      use module_data_mosaic_aero, only: cross_sect, k_slr, t_des, &
         ino3_ads, iy2_a, iy3_a, ipah_a

      implicit none

      ! subr. arguments:
      integer :: n, ibin
      real(r8) :: x(n), f(n)
      logical ifail
      ! local variables:
      real(r8) :: jcoll(n), theta, accom(n), surf_conc
      integer :: i

      f = 0.d0
```

```
      ! determine surface coverage (might have to be done separately
      ! for the individual scenarios eventually)
      theta = 0.d0
      do i = 1, n
         theta = theta + cross_sect(i) * x(i)
      end do
      if ((iscenario .eq. 4) .or. (iscenario .eq. 7)) then
         theta = theta - cross_sect(4) * x(4)
         theta = theta + cross_sect(5) * x(4)
      end if

      go to (7,6,5,4,3,2,1), iscenario

1     continue

2     if (iscenario .ne. 7) go to 5   ! no extra terms required

3     if (iscenario .ne. 7) go to 5   ! no extra terms required

4     if (n .gt. 3) then
         f(4) = k_slr(6) * x(1) * x(2) &
            - k_slr(7) * surf_conc(ipah_a, ibin) * x(4) &
            - x(4) / t_des(5)
      end if
      f(2) = -1.d0 * k_slr(6) * x(1) * x(2)
      f(1) = -1.d0 * k_slr(6) * x(1) * x(2)

5     jcoll(3) = vel_gas(ih2o) * h2o / 4.d0
      accom(3) = uptake_gas(ih2o) * (1.d0 - theta)
      f(3) = accom(3) * jcoll(3) - x(3) / t_des(3)

6     jcoll(2) = vel_gas(ino2) * cnn(ino2) / 4.d0
      accom(2) = uptake_gas(ino2) * (1.d0 - theta)
      f(2) = f(2) + accom(2) * jcoll(2) - x(2) / t_des(2) &
         - x(2) * (k_slr(4) * surf_conc(iy2_a, ibin) &
            + k_slr(5) * surf_conc(iy3_a, ibin))

7     jcoll(1) = vel_gas(io3) * cnn(io3) / 4.d0
      accom(1) = uptake_gas(io3) * (1.d0 - theta)
      f(1) = f(1) + accom(1) * jcoll(1) - x(1) / t_des(1) &
         - x(1) * (k_slr(1) * surf_conc(ipah_a, ibin) &
            + k_slr(2) * surf_conc(iy2_a, ibin) &
            + k_slr(3) * surf_conc(iy3_a, ibin))

      return
      end subroutine fcn


!-----------------------------------------------------------------------

!> supplies the Jacobian matrix of the system of algebraic equations
!  under steady state assumption to the solver nleq1e.
      subroutine jac_nleq1(n, ldjac, x, ibin, dfdx, ifail)
      use module_data_mosaic_kind, only: r8
      use module_data_mosaic_main, only: iscenario, cnn, h2o
      use module_data_mosaic_gas, only: vel_gas, uptake_gas, &
         io3, ino2, ih2o
      use module_data_mosaic_aero, only: k_slr, cross_sect, t_des, &
         iy2_a, iy3_a, ipah_a
```

```
      implicit none

      ! subr. arguments:
      integer :: n, ldjac, ibin
      real(r8) :: x(n), dfdx(ldjac,n)
      logical ifail
      ! local variables:
      real(r8) :: jcoll(n), jads_o(n), surf_conc

      dfdx = 0.d0

      go to (7,6,5,4,3,2,1), iscenario

1     continue

2     if (iscenario .ne. 7) go to 5   ! no extra variables required

3     if (iscenario .ne. 7) go to 5   ! no extra variables required

4     jcoll(1) = vel_gas(io3) * cnn(io3) / 4.d0
      jcoll(2) = vel_gas(ino2) * cnn(ino2) / 4.d0
      jcoll(3) = vel_gas(ih2o) * h2o / 4.d0
      jads_o(1) = uptake_gas(io3) * jcoll(1)
      jads_o(2) = uptake_gas(ino2) * jcoll(2)
      jads_o(3) = uptake_gas(ih2o) * jcoll(3)
      dfdx(1,1) = -1.d0 * k_slr(6) * x(2)
      dfdx(1,2) = -1.d0 * k_slr(6) * x(1)
      dfdx(1,4) = -1.d0 * cross_sect(5) * jads_o(1)
      dfdx(2,1) = -1.d0 * k_slr(6) * x(2)
      dfdx(2,2) = -1.d0 * k_slr(6) * x(1)
      dfdx(2,4) = -1.d0 * cross_sect(5) * jads_o(2)
      dfdx(3,4) = -1.d0 * cross_sect(5) * jads_o(3)
      dfdx(4,1) = k_slr(6) * x(2)
      dfdx(4,2) = k_slr(6) * x(1)
      dfdx(4,3) = 0.d0
      dfdx(4,4) = -1.d0 * k_slr(7) * surf_conc(ipah_a, ibin) &
        - 1.d0 / t_des(5)

5     jcoll(1) = vel_gas(io3) * cnn(io3) / 4.d0
      jcoll(2) = vel_gas(ino2) * cnn(ino2) / 4.d0
      jcoll(3) = vel_gas(ih2o) * h2o / 4.d0
      jads_o(1) = uptake_gas(io3) * jcoll(1)
      jads_o(2) = uptake_gas(ino2) * jcoll(2)
      jads_o(3) = uptake_gas(ih2o) * jcoll(3)
      dfdx(1,3) = -1.d0 * cross_sect(3) * jads_o(1)
      dfdx(2,3) = -1.d0 * cross_sect(3) * jads_o(2)
      dfdx(3,1) = -1.d0 * cross_sect(1) * jads_o(3)
      dfdx(3,2) = -1.d0 * cross_sect(2) * jads_o(3)
      dfdx(3,3) = -1.d0 * cross_sect(3) * jads_o(3) &
        - 1.d0 / t_des(3)

6     jcoll(1) = vel_gas(io3) * cnn(io3) / 4.d0
      jcoll(2) = vel_gas(ino2) * cnn(ino2) / 4.d0
      jads_o(1) = uptake_gas(io3) * jcoll(1)
      jads_o(2) = uptake_gas(ino2) * jcoll(2)
      dfdx(1,2) = dfdx(1,2) - cross_sect(2) * jads_o(1)
      dfdx(2,1) = dfdx(2,1) - cross_sect(1) * jads_o(2)
      dfdx(2,2) = dfdx(2,2) - cross_sect(2) * jads_o(2) &
        - 1.d0 / t_des(2) &
```

```
        - k_slr(4) * surf_conc(iy2_a, ibin) &
        - k_slr(5) * surf_conc(iy3_a, ibin)

7     jcoll(1) = vel_gas(io3) * cnn(io3) / 4.d0
      jads_o(1) = uptake_gas(io3) * jcoll(1)
      dfdx(1,1) = dfdx(1,1) - cross_sect(1) * jads_o(1) &
        - 1.d0 / t_des(1) &
        - k_slr(1) * surf_conc(ipah_a, ibin) &
        - k_slr(2) * surf_conc(iy2_a, ibin) &
        - k_slr(3) * surf_conc(iy3_a, ibin)

      return
      end subroutine jac_nleq1


!-----------------------------------------------------------------------

!> computes surface concentrations of sorption layer species and adjusts
!  gas phase under assumption of steady state
      subroutine steady_state_sorp_spec_conc(timestep, ibin)
      use module_data_mosaic_kind, only: r8
      use module_data_mosaic_main, only: iscenario, avogad, cnn, h2o
      use module_data_mosaic_gas,  only: io3, ino2, vel_gas, ih2o
      use module_data_mosaic_aero, only: nbin_a, aer, num_a, &
        io3_ads, ino2_ads, ih2o_ads, ino3_ads, gamma

      implicit none

      ! subr. arguments:
      real(r8) :: timestep
      integer :: ibin
      ! local variables:
      real(r8) :: rtol_nleq1, conv_fac(nbin_a), surf_area, &
        map_ads_to_gas(2), loss_fac
      real(r8), allocatable :: conc(:)
      integer :: n, dummy, i, ierr, igas

      ! determine number of sorption layer species n
      call SetScenario(dummy, n)

      ! concentrations of sorption layer species
      allocate(conc(n))

      do i = 1, n
        ! initial "guess" to be supplied to NLEQ1E
        conc(i) = 1.d13
      end do
      if (n .gt. 3) conc(4) = 1.d11

      ! set NLEQ1E input parameters
      rtol_nleq1 = 1.d-3   ! desired relative tolerance
      ierr = 0   ! should still be 0 upon successful return

      ! solve system of algebraic equations given by setting all
      ! derivatives of sorption layer species concentrations to zero
      call NLEQ1E(n, conc, ibin, rtol_nleq1, ierr)
      if (ierr .gt. 0) write(6,'(a,i2)') 'Stopped in subroutine', &
        ' steady_state_sorp_spec_conc because NLEQ1 exited with', &
        ' status IERR =', ierr, '.'
```

```
      ! conversion from [molec/cm^2] to [nmol/m^3(air)]
      conv_fac(ibin) = surf_area(ibin) * num_a(ibin) * 1d15 / avogad

      ! convert new surface concentrations and write to aer
      aer(io3_ads, 3, ibin) = conc(1) * conv_fac(ibin)
      if (n .gt. 1) aer(ino2_ads, 3, ibin) = conc(2) &
         * conv_fac(ibin)
      if (n .gt. 2) aer(ih2o_ads, 3, ibin) = conc(3) &
         * conv_fac(ibin)
      if (n .gt. 3) aer(ino3_ads, 3, ibin) = conc(4) &
         * conv_fac(ibin)

      deallocate(conc)

      return
      end subroutine steady_state_sorp_spec_conc


!-----------------------------------------------------------------------

!> computes gas phase diffusion correction factor of gas igas towards
!  particle ibin
      function gas_phase_diff_corr_fac(igas, ibin)
      use module_data_mosaic_kind, only: r8
      use module_data_mosaic_main, only: pi
      use module_data_mosaic_gas,  only: vel_gas, mw_gas, &
         D_gas, uptake_gas

      implicit none

      real(r8) :: gas_phase_diff_corr_fac
      ! func. arguments:
      integer :: igas, ibin
      ! local variables:
      real(r8) :: var, particle_volume, d_part, knudsen

      ! compute particle diameter [cm]
      var = 3.d0 * particle_volume(ibin) / (4.d0 * pi)
      d_part = 2.d0 * (var)**(1.d0 / 3.d0)

      ! Knudsen number
      knudsen = 6.d0 * D_gas(igas) / (vel_gas(igas) * d_part)

      ! compute gas phase diffusion correction factor
      var = (0.75d0 + 0.28d0 * knudsen) / (knudsen * (1.d0 + knudsen))
      gas_phase_diff_corr_fac = 1.d0 / (1.d0 + uptake_gas(igas) * var)

      return
      end function gas_phase_diff_corr_fac


!-----------------------------------------------------------------------

!> computes uptake coefficients for O3, NO2 and H2O
      function gamma_slr(ispec, ibin)
      use module_data_mosaic_kind, only: r8
      use module_data_mosaic_main, only: te, cnn, h2o
      use module_data_mosaic_gas,  only: io3, ino2, ih2o, uptake_gas, &
         vel_gas
      use module_data_mosaic_aero, only: naer_ss, naer, t_des
```

```
      implicit none

      real(r8) :: gamma_slr
      ! func. arguments:
      integer :: ispec, ibin
      ! local variables:
      integer :: igas
      real(r8) :: map_ads_to_gas(3), store, accom, surf_cov, jdes, &
         surf_conc, jcoll

      ! map indices
      map_ads_to_gas(1) = io3
      map_ads_to_gas(2) = ino2
      map_ads_to_gas(3) = ih2o

      ! set concentration of water vapor to pre-timestep value
      store = cnn(ih2o)
      cnn(ih2o) = h2o

      igas = map_ads_to_gas(ispec - naer_ss - naer)

      ! accomodation coefficient, corrected by sorption layer coverage
      accom = uptake_gas(igas) * (1.d0 - surf_cov(ibin))

      ! desorption and collision fluxes [cm^-2 s^-1]
      jdes = surf_conc(ispec, ibin) / t_des(ispec - naer_ss - naer)
      jcoll = vel_gas(igas) * cnn(igas) / 4.d0

      ! compute gas phase diffusion correction factor
      gamma_slr = accom - jdes / jcoll

      ! restore updated water vapor concentration
      cnn(ih2o) = store

      return
      end function gamma_slr


!-----------------------------------------------------------------------

!> computes initial surface concentrations of adsorbing gas species and
!  adjusts gas phase under assumption of steady state
      subroutine init_ads_gas_conc(n, timestep, sigma_pah)
      use module_data_mosaic_kind, only: r8
      use module_data_mosaic_main, only: steadystate, cnn, avogad, h2o
      use module_data_mosaic_gas,  only: io3, ino2
      use module_data_mosaic_aero, only: nbin_a, ipah_a, aer, io3_ads, &
         ino2_ads, ih2o_ads

      implicit none

      ! subr. arguments:
      real(r8) :: timestep, sigma_pah
      integer :: n
      ! local variables:
      real(r8) :: surf_conc
      integer :: ibin
      logical :: init
```

```
      if (steadystate .eq. 0) return

      ! whether or not to "initialize" the particle
      init = .false.

      do ibin = 1, nbin_a

         if ((1.d0 / sigma_pah - surf_conc(ipah_a, ibin)) &
               .lt. (1.d-10 / sigma_pah)) then

            ! particle is newly emitted
            init = .true.

            ! do one steady state timestep for adsorbing gases
            call steady_state_sorp_spec_conc(timestep, ibin)

            ! gas phase adjustments
            cnn(io3) = cnn(io3) - aer(io3_ads, 3, ibin) * avogad * 1d-15
            if (n .gt. 1) then
               cnn(ino2) = cnn(ino2) &
                  - aer(ino2_ads, 3, ibin) * avogad * 1d-15
            end if
            if (n .gt. 2) then
               h2o = h2o - aer(ih2o_ads, 3, ibin) * avogad * 1d-15
            end if

         end if

      end do

      ! adjust uptake coefficients etc.
      if (init) call GasRateConstants

      return
      end subroutine init_ads_gas_conc


!-----------------------------------------------------------------------

!> calls steady_state_sorp_spec_conc and computes gas phase feedback in
!  case of steady state assumptions based on uptake coefficients
      subroutine steady_state(n, timestep)
      use module_data_mosaic_kind, only: r8
      use module_data_mosaic_main, only: steadystate, cnn, h2o
      use module_data_mosaic_gas,  only: vel_gas, io3, ino2, ih2o
      use module_data_mosaic_aero, only: nbin_a, num_a, gamma

      implicit none

      ! subr. arguments:
      real(r8) :: timestep
      integer :: n
      ! local variables:
      real(r8) :: conv_fac(nbin_a), surf_area, loss_fac
      integer :: ibin

      if (steadystate .eq. 0) return

      do ibin = 1, nbin_a
         ! do a steady state timestep
```

```
      call steady_state_sorp_spec_conc(timestep, ibin)
      ! conversion from [molec/cm^2] to [molec/cm^3]
      conv_fac(ibin) = surf_area(ibin) * num_a(ibin)
    end do
    ! gas phase adjustments
    loss_fac = sum(gamma(1,:) * conv_fac) * vel_gas(io3) / 4.d0
    cnn(io3) = cnn(io3) - loss_fac * cnn(io3) * timestep
    if (n .gt. 1) then
      loss_fac = sum(gamma(2,:) * conv_fac) * vel_gas(ino2) / 4.d0
      cnn(ino2) = cnn(ino2) - loss_fac * cnn(ino2) * timestep
    end if
    if (n .gt. 2) then
      loss_fac = sum(gamma(3,:) * conv_fac) * vel_gas(ih2o) / 4.d0
      h2o = h2o - loss_fac * h2o * timestep
    end if

    return
    end subroutine steady_state


!-----------------------------------------------------------------------

!> approximates [Y2] and subsequent species if PAH depletion by GSR with
!  gas phase NO3 is > 80% of initial [PAH] in one timestep
    subroutine y2_approx(old_pah, ntot, stot, timestep, sigma_pah)
    use module_data_mosaic_kind, only: r8
    use module_data_mosaic_main, only: iscenario, steadystate, cnn, &
      h2o
    use module_data_mosaic_gas,  only: vel_gas, ino3, uptake_gas, io3
    use module_data_mosaic_aero, only: nbin_a, ipah_s, num_a, k_slr, &
      io3_ad, ipah_a, t_des, iy2_s, iy3_s, iy4_s, iy5_s

    implicit none

    ! subr. arguments:
    real(r8) :: old_pah(nbin_a), stot(ntot), timestep, sigma_pah
    integer :: ntot
    ! local variables:
    real(r8) :: conv_fac, surf_area, prefac, surf_conc, jcoll, &
      kappa, surf_cov, lambda, y2_surf, ratio
    integer :: ibin

    if (iscenario .ne. 7) return
    if (steadystate .eq. 0) return

    do ibin = 1, nbin_a

      ! conversion from surface concentration to volume concentration
      conv_fac = surf_area(ibin) * num_a(ibin)

      if (((old_pah(ibin) - stot(ipah_s+ibin-1)) / conv_fac) &
          .gt. 0.8 / sigma_pah) then

        ! calculate integral of a parameterization for Y2 production

        ! aer should still have pre-time step values
        prefac = k_slr(1) * (stot(io3_ad+ibin-1) / conv_fac) &
          * surf_conc(ipah_a,ibin)

        ! cnn should still have pre-time step values
```

```
        jcoll = vel_gas(ino3) * cnn(ino3) / 4.d0
        kappa = uptake_gas(ino3) * sigma_pah &
           * (1 - surf_cov(ibin)) * jcoll

        ! cnn should still have pre-time step values
        jcoll = vel_gas(io3) * cnn(io3) / 4.d0
        lambda = uptake_gas(io3) * jcoll / (stot(io3_ad+ibin-1) &
           / conv_fac) - 1.d0 / t_des(1)

        y2_surf = prefac * &
           ((1.d0 - exp(-kappa * timestep)) / kappa &
           + (exp(-(lambda + kappa) * timestep) - 1.d0) &
              / (lambda + kappa))

        ratio = y2_surf * conv_fac / stot(iy2_s+ibin-1)

        stot(iy2_s+ibin-1) = y2_surf * conv_fac

        ! adjust subsequent species, too
        stot(iy3_s+ibin-1) = stot(iy3_s+ibin-1) * ratio
        stot(iy4_s+ibin-1) = stot(iy4_s+ibin-1) * ratio
        stot(iy5_s+ibin-1) = stot(iy5_s+ibin-1) * ratio

     end if

  end do

  return
  end subroutine y2_approx
```